UNIVERSITÀ DEGLI STUDI
DI GENOVA

Scuola di Scienze Matematiche
Fisiche e Naturali

Corso di Laurea Magistrale in
SCIENZE CHIMICHE

Tesi di Laurea Magistrale

Study And Application of a Radical Solventylation Reaction based on a Photoinduced Hydrogen Atom Transfer (HAT) Process

Primo Relatore
Prof. Basso Andrea

Primo Correlatore
Lambruschini Chiara

Secondo Correlatore
Prof.ssa Castellano Maila

Candidato
Valentina Ricciardiello

Anno accademico 2023/2024

ACKNOWLEDGMENTS

TABLE OF CONTENTS

Abstract

Il processo di trasferimento di un atomo di idrogeno (HAT, acronimo in inglese di Hydrogen Atom Transfer) rappresenta una reazione fondamentale sia nell'ambito biologico che in quello della chimica organica, assumendo un'importanza significativa nella chimica dei radicali. La generazione di radicali arilici a partire da azosolfoni mediante l'irradiazione con luce visibile costituisce un substrato versatile, grazie alla sua elevata reattività e alla sua natura ambifilica che permette la reazione con diverse tipologie di solventi mediante un processo HAT.

Questo approccio consente con successo la funzionalizzazione versatile di una serie di olefine, utilizzando radicali a base di carbonio derivati da composti come acetone, acetonitrile, cloroformio, diclorometano, acetato di metile e formiato di metile, sostanze comunemente presenti in laboratorio e a basso costo. Il tutto avviene in condizioni prive di fotocatalizzatori e metalli. Nella condizione di questa tipologia di reazione, risulta essenziale mantenere un'elevata diluzione al fine di mitigare l'aggiunta diretta di radicali arilici ai substrati olefinici.

Lo studio inizia con la reazione tra un azosolfone e un'olefina, nota come trappola radicalica. Questa reazione è stata ottimizzata e testata con diversi solventi, producendo il prodotto principale con una buona resa. Tuttavia, si è verificata la persistenza di un sottoprodotto solfonilato. Comprendendo il meccanismo alla base di questo sottoprodotto, sono stati progettati diversi substrati di azosolfoni per ottenere solo il prodotto desiderato, eliminando il sottoprodotto solfinato. Nonostante rese basse del sottoprodotto, questa reattività indesiderata ha persistito.

Nella fase successiva dello studio, abbiamo esplorato la reattività di altre tre trappole radicaliche con diversi solventi, ottenendo una serie di prodotti, alcuni dei quali inediti in letteratura. In tutte le prove, è stata osservata la formazione del sottoprodotto con varie rese, ma sono emersi risultati promettenti in termini di resa del prodotto, quando il cloroformio è stato utilizzato come solvente.

1. Introduction

This thesis explores the field of photochemical reactions and their meticulously deciphered mechanisms. The research has been conducted at the BOG'S (BioOrganic Chemistry at Genova) research group, situated within the Department of Chemistry and Industrial Chemistry at the University of Genova.

BOG research group actively engages in various domains of organic chemistry, with a primary focus on synthesizing diverse libraries of drug-like molecules. This has been achieved through the application of Multicomponent Reactions (MCRs), Organocatalysis, and Biocatalysis. Notably, there has been a surge of interest in the field of photochemistry, guided by the expertise of Professor Andrea Basso. This has led to numerous publications in recent years, showcasing dedication to advancing the field.

1.1 A Brief Introduction to Photochemistry

Contemplating life without light presents a formidable challenge. The Earth owes its oxygen-rich atmosphere to the fundamental natural process of photosynthesis. Furthermore, sunlight plays a crucial role in human health, aiding the production of essential Vitamin D for bone and kidney health, and enabling the photochemical reactions in our eyes, granting us the ability to perceive our surroundings[1].

In addition, the protective ozone layer, essential in shielding us from harmful UV radiation capable of inducing DNA mutations, is formed through the photolysis of molecular oxygen. The exploration of this intricate process, vital to life, carries a profound historical legacy. Rooted in the examination of chemical modifications resulting from the interaction of light, numerous scientists from diverse backgrounds have significantly contributed to unraveling the intricacies of this phenomenon. Their collective efforts have paved the way for our current understanding of the scientific field known as photochemistry[2].

One of the earliest-known photoreactions involving an organic compound is attributed to santonin, an anthelmintic historically used to treat parasitic worm infections. As far back as 1834, Hermarin Trommsdorff reported the intriguing observation that exposure to sunlight turns santonin yellow and causes its crystals to burst[3]. Subsequently, in the summer of 1885, Camician and Silber embarked on a series of sunlight-based photochemistry experiments. Their ensuing discoveries and numerous publications played an important role in shaping this field. Their influential contributions have rightly earned them recognition as pioneers and founders of photochemistry, a branch of chemistry now integral to solar energy conversion and green chemistry[4].

Photochemistry is defined as the scientific discipline that investigates chemical transformations induced by the interaction of one or more reagents with electromagnetic radiation. The phenomenon of energy transfer through matter or space is referred as radiation and it manifests in various forms, including light, heat, x-rays and even sound. Electromagnetic radiation, displaying both wave and particle characteristics, aligns with the principles of wave-particle duality theory.

The wave behavior of electromagnetic radiation is characterized by its propagation in a wave-like manner, involving the periodic disturbance of electric and magnetic fields oscillating on planes perpendicular to each other as shown in Figure 1[5]. This oscillation occurs at a constant speed, and the direction of propagation is perpendicular to the plane defined by the oscillations of the two fields. Describing this wave characteristic of the electromagnetic radiation involves the relationship between wavelength (λ) and frequency (ν) given by the equation (1):

$$c = \lambda\nu \tag{1}$$

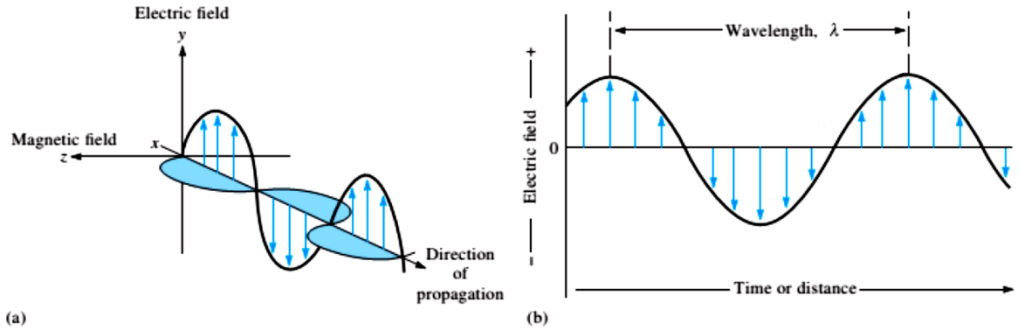

FIGURE 1.1 Electromagnetic Radiation

Where *c* represents the propagation velocity (speed of light, 2.99×108 m/s) in a vacuum and *c*/*n* in a medium with a refractive index *n*. As shown in Figure 1, wavelength (λ) is the distance between two analogous points of a single wave cycle or to the maximum points, while frequency (ν) is the inverse of the period, measured in hertz (Hz). Due to the constant velocity, a decrease in frequency corresponds to an increase in wavelength in an inversely proportional manner. All forms of electromagnetic radiation are categorized based on their characteristic wavelengths, typically expressed in nanometers or by frequency in Hz, the categorization based on these parameters is called electromagnetic spectrum.

The particle behavior of electromagnetic radiation is described by the concept of a photon—a fundamental particle or quantum of light. When a photon is absorbed by a molecule, it imparts its energy to the molecule. The energy of the photon, measured in Joules, is directly proportional to its frequency (ν) given in Hz and by Planck's constant (*h*) with a value of 6.626×10−34 J·s, expressed by the equation (2)[6].

$$E = h\nu \quad (2)$$

Under specific conditions, this energy is capable of being absorbed by molecules, and such interactions between matter and light is studied by the field of photochemistry. The Grotthuss-Draper Law, a fundamental principle and the first law of photochemistry, establishes that light absorption is a crucial prerequisite for initiating any photochemical reaction. Generally, either one of the substrates or a photocatalyst must undergo light absorption to the occurrence of the reaction[7].

The initiation of any photochemical reaction commences with the absorption of a single photon by a molecule, a phenomenon described by the Stark–Einstein law, where one photon activates one molecule[7]. This absorption event leads to the creation of an excited state, elevating one electron of the absorbing molecule to a higher energy level. Conjugation of double bonds in the molecular system, along with the presence of auxiliary functional groups (auxochromes), dictates the absorption process. This molecular system influences the intensity (hyperchromic and hypochromic effects) and wavelength of the absorption band (bathochromic and ipsochromic effects, or red and blue shifts, respectively).

To absorb light, the energy of the incident photon must match the energy difference between the molecule's fundamental state and an excited state. The minimal energy needed for the electronic excitation of organic molecules is usually around 30-40 kcal/mol, corresponding to the red visible light range (700-800 nm). In contrast, the maximum limit of energy used in organic photochemistry is about 140 kcal/mol, corresponding to ultraviolet light range (100-400 nm). This ultraviolet wavelength carries more energy, approximately 140 kcal/mol, enabling the breaking of molecular bonds, in comparison to the 80 kcal/mol energy required to break a carbon-carbon bond.

Upon photon absorption, these compounds undergo promotion of an electron to an antibonding $\pi*$ orbital, resulting an excited electronic state. These states can manifest as a Singlet Excited State (S) if electrons retain opposite spins, or a Triplet Excited State (T) in case of spin inversion, theoretically possible but spin forbidden. Alternatively, a Rydberg State occurs when an electron transitions from the valence shell to a higher one.

The electronic excitation involves a transition from the Highest Occupied Molecular Orbital (HOMO) to the Lowest Unoccupied Molecular Orbital (LUMO). Throughout this event, the nucleus retains its initial ground state geometry, with electron rearrangement constituting a vertical transition as per the Frank-Condon Principle.

The absorption phenomenon unfolds rapidly (10^{-15} s). Subsequently, the molecule tends to return to its ground state S_0, releasing excess energy through various pathways depicted in the Perrin-Jablonski diagram Figure 1.2[8], primarily involving internal

conversion and vibrational relaxation. This process includes thermal energy transfer through vibrational relaxation, a non-radiative phenomenon. After reaching a minimum vibrational energy for the excited state S_1, two pathways may emerge. Fluorescence occurs if the energy is released in a single de-excitation to S_0 event by emitting a photon. If an intersystem crossing (ISC) occurs due to the excited electron undergoing a spin inversion, leading to a triplet state, de-excitation from the triplet state T_1 to S_0 can occur through a non-radiative process or by emitting light, known as phosphorescence.

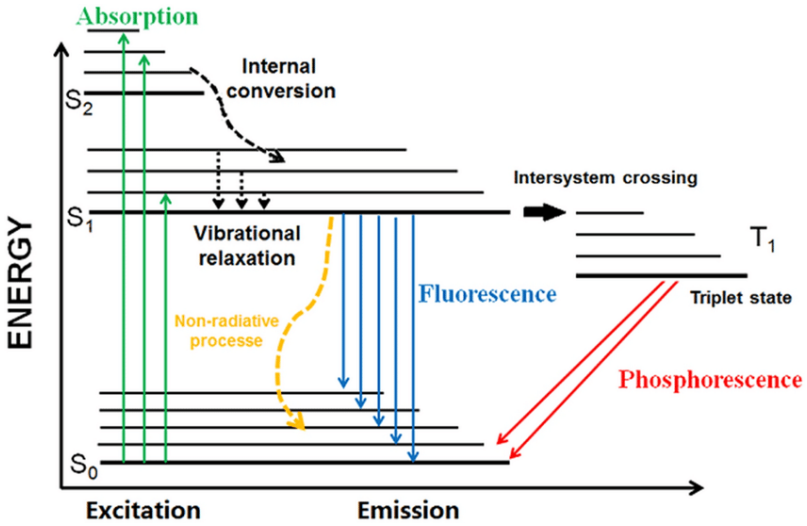

FIGURE 1.2 Jablonski diagram

In the absence of a chromophore functional group, most organic substances are inherently colorless, meaning they do not absorb in the visible light spectrum. Instead, they absorb in the more energetic ultraviolet region (200-400 nm), necessitating more energetic and sophisticated equipment.

Permitted transitions for organic molecules include σ-σ*, π-π*, n-σ*, and n-π* as shown in Figure 1.3. Direct photochemistry is predominantly characterized by π-π* and n-π* transitions, occurring in the UV-visible region, where these transitions are more probable due to the lower energy difference between the ground state and the excited state.

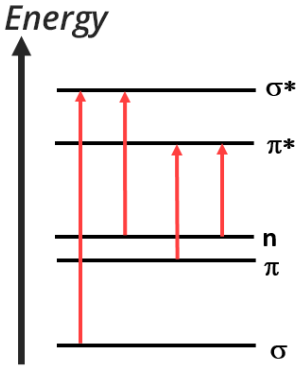

FIGURE 1.3 Permitted Transitions for Organic Molecules

Recent studies have explored colored organic compounds' use, absorbing in the UV-visible region, for induced visible light chemical transformations. This process is possible by introducing Dyedauxiliary groups, capable of imparting color and reactivity to an organic molecule, generating a visible-light-absorbing molecule with photolyzable bonds leading to a desired reactivity. Arylazo compounds, generates reactive species like aryl radicals under the UV-visible region, making them a promising structure for this purpose. The process is achievable with cost-effective and simple apparatus, utilizing low-energy-demand visible light sources like Light-Emitting Diodes (LEDs). This chemical process involves using a colored compound (arylazocompounds) to absorb radiation in the visible light range, promoting the formation of reactive intermediates (aryl radicals) that interact with other organic compounds present in the reaction environment, typically unreactive in this wavelength range. In aryl diazosulfone compounds, this is achieved through the transition of an electron from a bonding π orbital to an antibonding π∗ orbital at 450 nm and the transition of an electron from a nonbonding n electron pair to an antibonding π∗ orbital at 366 nm[9].

Direct photochemistry stands out as a powerful method for activating systems, enabling innovative chemical transformations. Unlike thermal reactions (Figure 1.4 Left) where heat is the energy source where reagent R transforms into product P through intermediates I and transition states, with a catalyst lowering the energy barriers. In photochemical reactions (Figure 1.4 Right), photons serve as the energy source. Upon absorption, they generate electronically excited states, leading to the formation of reactive intermediates. This facilitates high-yield and selective generation of desired products. Photochemical reactions offer the potential to produce compounds that are challenging to obtain through thermal processes, offering the opportunity to create high molecular complexity in a single step[10].

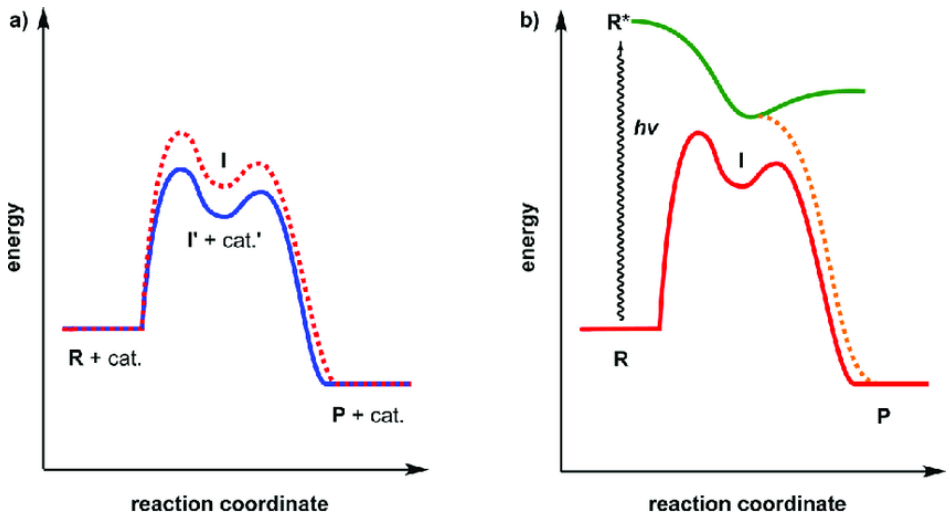

FIGURE 1.4 Reaction Pathway. Left Thermal Reaction. Right Photochemical Reaction

1.2 Visible Light-Driven Photocatalytic-Free Reactions

The field of photochemistry embraces a wide array of activation modes achieved through employing energy derived from photons as they are called "the 21st century reagent"[7]. Despite the utilization of various wavelengths in synthetic organic photochemistry, visible light is considered safer from a green chemistry perspective. Visible light emerges as a renewable, sustainable, and non-harmful energy source in this context. Chemical processes conducted in this region are not only of great interest but also exhibit high functional group tolerance.

This energy is selectively absorbed by carefully designed species, among the diverse methods in photochemistry, one prominent and frequently employed approach involves the use of photon-absorbing catalysts, known as photocatalysts. These catalysts, includes transition metal complexes, organic dyes, and inorganic semiconductors, efficiently absorb energy from visible light photons, initiating subsequent organic transformations[11].

Upon excitation under visible light, photocatalysts facilitates specific reaction pathways involving substrates, reagents, or secondary catalysts. exposure to visible light at wavelengths where typical organic molecules do not absorb selectively excites the photocatalyst. For example, the resulting excited state of a photoredox catalysist exhibits dual characteristics, serving as both a potent oxidant and a potent reductant simultaneously. This electronic duality stands in contrast to conventional redox reaction where the reaction medium is typically either oxidative or reductive (but not both). This characteristic grant access to a distinctive reaction environment in organic chemistry. This catalytic method significantly contributes to the development of innovative synthetic strategies for bond formations, particularly in the generation of carbon-carbon and carbon-heteroatom bonds in organic chemistry, advancing and refining synthetic methodologies[11].

While catalysts are integral to numerous chemical transformations, the exploration of catalyst-free conditions, especially in industrial and pharmaceutical processes, has attracted considerable interest. Catalyst-free visible-light-driven reactions can progress through two main pathways: (1) the absorption of light by at least one substrate, activating a single-electron transfer pathway, leading to radical substrates; and (2) the formation of an electron donor-acceptor complex (EDA complex) without the use of a photocatalyst[12]. Catalyst-free reactions under visible light have start to receive attention, recent studies have demonstrated promising results, indicating the potential of this approach in synthetic organic chemistry.

This research aims to functionalize a number of substituted olefins using recent advances in visible-light-driven reactions employing aryl azosulfone as a dyedauxiliary group, leading to the generation of aryl radical intermediates. These aryl radicals display highly reactive and amphiphilic characteristics, initiating a hydrogen atom transfer (HAT)

reaction with the solvent to form a solvent radical. The resulting carbon-centered radical from the solvent subsequently reacts with the olefin, yielding a cyclized and valuable building block. This building block finds application in the synthesis of esermethole, a precursor to physostigmine, a clinical treatment for glaucoma.

The protocol has been optimized and tested with various solvents, such as acetone, acetonitrile, dichloromethane, chloroform, methyl formate, and methyl acetate, resulting in the main product with a good yield. However, the persistent of a sulfonylated byproduct has been observed. To address this, different azosulfone substrates were designed to selectively obtain the desired product, eliminating the sulfonylated byproduct. Despite encountering low yields of the byproduct, this undesired reactivity has persisted.

This protocol exhibits versatility, operating under relatively mild conditions and exclusively in the absence of metals and photocatalysts. This distinguishes it from other protocols dependent on metals and photocatalysts, making it a promising approach for organic synthesis.

2. Theoretical Background and State of the Art

2.1 HAT: A Novel Approach in Photochemistry

Hydrogen atom transfer (HAT) represents a fundamental chemical process characterized by the coordinated migration of a proton and an electron ($H^+ + e^- \equiv H\bullet$). This concerted motion occurs within a single kinetic step, originating from the same reactants and leading to the same product, as illustrated in equation (3) [13]:

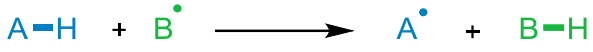

(3)

HAT is a common and essential chemical reaction that has been the focus of research for over a century, highlighting the extensive depth of exploration in this field. Extensive research has emphasized the significant role of HAT in both chemical synthesis and biologically relevant redox reactions. Its influence extends across a wide range of processes, including hydrocarbon combustion, atmospheric chemistry, and enzymatic catalysis. A profound understanding of these fundamental principles is crucial for advancing research in these interconnected fields[14].

For instance, in the field of biology, a significant proportion of chemical oxidative reactions originate with a HAT reaction. Among the enzymes known to employ this remarkable capability is heme cytochromes P450, which plays an essential role in a wide array of organisms, including mammals, plants, insects, bacteria, and fungi[15,16]. These metalloenzymes harness a high-valent iron oxo active species named Compound I (Cpd I). This versatile species is at the heart of various metabolic processes, from neutralizing foreign compounds (xenobiotics) to synthesizing essential brain chemicals like serotonin and dopamine. The study of these enzymatic processes has served as a captivating case study, garnering extensive attention from diverse research groups for many years. This research not only underscores the extraordinary progress of nature's chemical transformations but also delves into the broader implications and applications of these phenomena in the realm of biological and medical science[17,18].

HAT is categorized as a subset of proton-coupled electron transfer (PCET) processes, which includes a diverse range of reactions involving the transfer of one electron and one proton. These reactions can manifest either in a concerted manner (cPCET), where electrons and protons move simultaneously yet separately, or in a sequential fashion (PCET), involving distinct initial transfers of electrons or protons. PCET processes carry significant implications across various biological processes and applications in fuel cells, solar cells, chemical sensors, and electrochemical devices. Furthermore, they constitute integral components of diverse energy conversion processes, playing crucial roles in vital functions such as photosynthesis and respiration[19,20].

HAT reactions are increasingly gaining significance in the field of organic chemistry due to their straightforward and mild approach to activating C-H bonds[21]. This type of bond activation, especially concerning C(sp^3)-H bonds, is a significant challenge in synthetic chemistry since the C-H bond is the most common feature in organic molecules[22]. Selective activation of these types of bonds with versatile methodologies could revolutionize the strategies for assembling carbon-based building blocks. A clearer insight into this activation process by cleaving the C-H bond can be gained from Scheme 2.1, where we can observe that HAT reactions involve the coordinated transfer of an electron and a proton from the substrate, representing the hydrogen donor, to a receiving species (a hydrogen abstractor) in a single kinetic step[22].

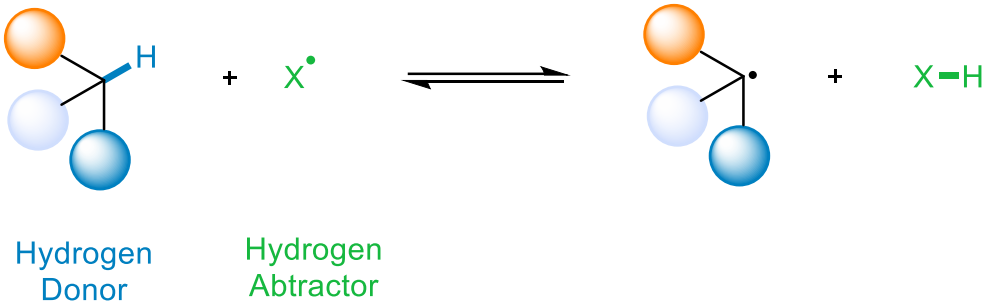

SCHEME 2.1 "Homolytic Cleavage of a C−H Bond via a Hydrogen Atom Transfer step"

Conventional strategies for activating C-H groups encompass the utilization of enolates exploiting the acidity of hydrogens in proximity to electron-withdrawing groups to craft versatile nucleophiles for forging C-C bonds. This approach tends to carry limitations that significantly constrain the scope of applicable substrates.

Furthermore, when we examine aliphatic C-H bonds, often labelled as "un-functional groups," they are distinctive due to their well-established reputation for their lack of reactivity. This is attributed to their low polarity and the strong single bond between Carbon and Hydrogen, necessitating the development of sophisticated methodologies to make them adaptable for functionalization. Therefore, the pursuit of precise and selective techniques for modifying C-H bonds becomes increasingly indispensable, with the potential to become one of the most universally applicable and important processes in the field of organic synthesis[23].

In contemporary methodologies, an alternative strategy that plays a central role nowadays is the use of activating or directing groups. These functional groups serve a dual purpose, both in facilitating specific reaction pathways and in enhancing selectivity and overall efficiency[24]. Despite attempts to use temporary directing groups like transition metal-based systems which are functions temporarily bound to substrates to drive selectivity, the direct modification of aliphatic C−H bonds in organic molecules remains a pursuit that continues to challenge modern chemistry[23].

The dynamic field of research presented in this thesis remains exceptionally active, driven by its potential to facilitate late-stage functionalization and endorse atom-economic synthesis, all without the requirement for pre-functionalization or the installation of directing groups. The implications of such research are profound, especially within the domains of medicinal chemistry[25] and the synthesis of both natural and synthetic compounds.

2.1.1 Thermodynamic Aspect: BDE

Numerous research groups are actively engaged in the development of models to elucidate HAT processes and predict their reaction rates. One such model is grounded in Marcus theory, utilizing free energies and inherent energy barriers. This model ingeniously combines the Bell-Evans-Polanyi[26] equation with the Marcus equations as exemplified in the comprehensive work of Mayer[27]. Mayer's research has solidly affirmed the validity of equations for hydrogen atom abstraction reactions across a wide range of experimental rate constants. However, it's essential to note that this achievement demands substantial computational efforts and does not consider polar effects.

Simultaneously, the Jerusalem research group has aimed to create a model that can estimate critical variables using readily available data, simplifying the calculation process[18]. This approach involves the valence bond (VB) diagram, which has proven effective in evaluating hydrogen atom abstraction barriers and deriving significant trends from easily accessible data, including bond energies[14].

The VB model provides a comprehensive perspective on various aspects of chemical reactivity, organic reactions, and state reactivity. Its applications extend to diverse fields, including homogeneous catalysis. Notably, The Jerusalem research group, has recently expanded the VB model to address reactions involving P450 enzymes and Cpd I. This extension encompasses processes such as hydrogen abstraction, arene activation, and sulfoxidation[18,28].

HAT can provide a considerably great degree of flexibility at activating C-H bonds, as their thermodynamic viability is closely tied to the bond dissociation energies (BDEs) of the C-H bond to be cleaved. Consequently, reactivity can be effectively predicted and understood. The reaction coordinate for a HAT reaction is illustrated in Figure 2.1. As evident, the viability of the process is dictated by the BDEs of the implicated bonds.

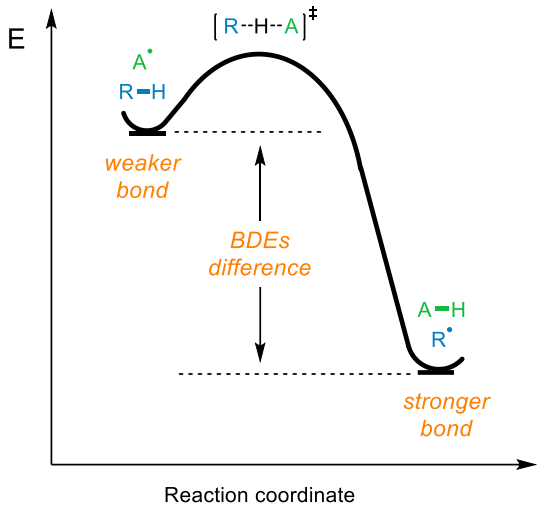

FIGURE 2.1 Reaction Coordinate for a HAT Reaction

A lower BDE and a more stable resulting radical render a bond easier to break. However, it's important to note that this is a general rule and applies only under specific conditions. Often, additional factors must be carefully considered to explain differences in selectivity observed when working with specific substrates. BDE values are presented in kcal/mol, and in Figure 2.2, there is a depiction of the most representative compounds. Figure 2.2 is taken from Capaldo L, Ravelli D, and Fagnogni's paper and all credits goes to the authors[22].

Upon closer examination of the compounds in Figure 2.2, we can identify the compounds with the lowest BDE, indicating weaker C-H bonds. These compounds include cyclohexene, phenyl acetonitrile, thiophenol, and diphenylmethane, forming a more stable radical. Conversely, stronger compounds with a higher BDE such as benzene, water, and acetylene possess stronger C-H bonds, resulting in less stable radicals. In summary the stronger the C-H bond, the less stable the resulting radical[29].

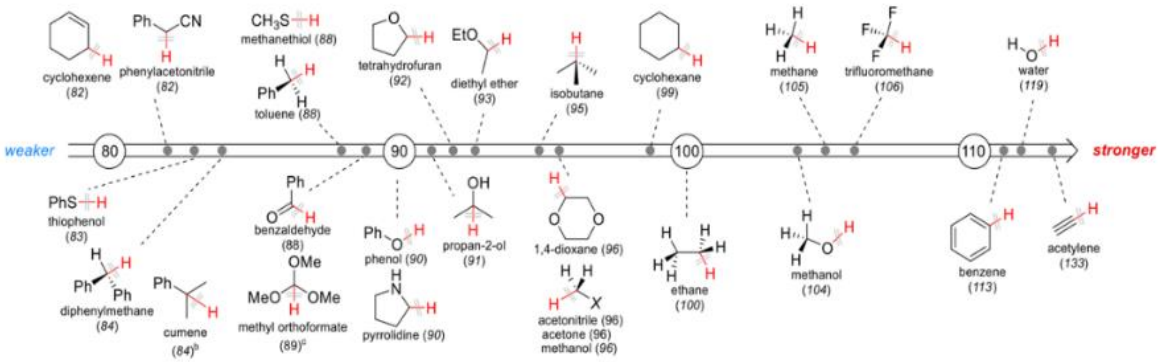

FIGURE 2.2 Bond dissociation energies (BDEs) in kcal/mol of the X−H bonds (in red) in representative compounds

The cleavage of C-H bonds is influenced by a wide range of factors. These factors include bond strength for example in hydrocarbons, where the relative stability of the resulting organo-radical dictates the preference for cleaving tertiary C-H bonds over secondary or primary ones. Other factors include hyperconjugation, conjugation (significantly impacting HAT selectivity), strain release, steric and torsional effects, polar effects, and stereoelectronic effects. The specific influence of these factors depends clearly on the hydrogen donor but also the characteristics of the hydrogen abstractor are important to determining the HAT course, for example steric hindrance plays a significant role. This can lead to a 'substrate-dependent' phenomenon, where the molecular geometry dictates the activation of specific reaction sites, driven primarily by straightforward steric and torsional effects.

2.1.2 Kinetic Aspects: Radical Philicity and Polarity Effects

2.1.2.1 Radical Philicity

The concept of Radical Philicity plays a crucial role in shaping the outcomes of various organic reactions, and its impact is particularly profound in the field of selective HAT chemistry. Comprehending radical philicity is a dominant factor in the development and fine-tuning of novel radical-based transformations.

Ever since the introduction of the concepts of "electrophile" and "nucleophile" by Ingold[30], associated with electron-deficient and electron-rich species respectively, there have been numerous endeavors to categorize atoms, molecules, and charged entities using empirical scales of electrophilicity and nucleophilicity. While these classifications are well established for many chemical species, it has been relatively difficult to classify radicals in terms of electrophilicity and nucleophilicity.

In the field of organic chemistry, radical intermediates often feature an incomplete octet of electrons, making them technically "electron-deficient". However, in contemporary terminology, the term "electron-deficient" is associated with electrophilicity. This linguistic distinction may lead to the misconception that all radicals act as electrophiles, which is not accurate. In fact, those involved in radical chemistry have long recognized that many radicals exhibit nucleophilic behavior, and in some cases, this nucleophilicity is quite pronounced[31].

It is worth noting that the nature of a radical has a noticeable influence on its reactivity towards specific sites in a substrate. In essence, an electrophilic radical tends to target electron-rich sites in the substrate, whereas a nucleophilic radical exhibits a preference for electron-poor sites. De Proft and his team have developed an index system to rank radicals based on their philicity. The rank obtained is absolute and is based on theoretical electrophilicity that doesn't depend on any input from reaction data. These results were then compared with those obtained through Principal Component Analysis (PCA), which incorporated a mix of experimental and theoretical reaction data. Remarkably, both methods produced highly consistent results[32]. Figure 2.3 portrays the established nucleophilicity scale for the 35 radicals investigated by De Proft. It offers a side-by-side comparison with the global electrophilicity scale. Notably, fluorine exhibits the highest electrophilic character, while *tert-butyl* displays one of the highest nucleophilicity character. Figure 2.3 is taken from F. De Proft, Vleeschouwer and Geerlings paper and all credits go to the authors [32].

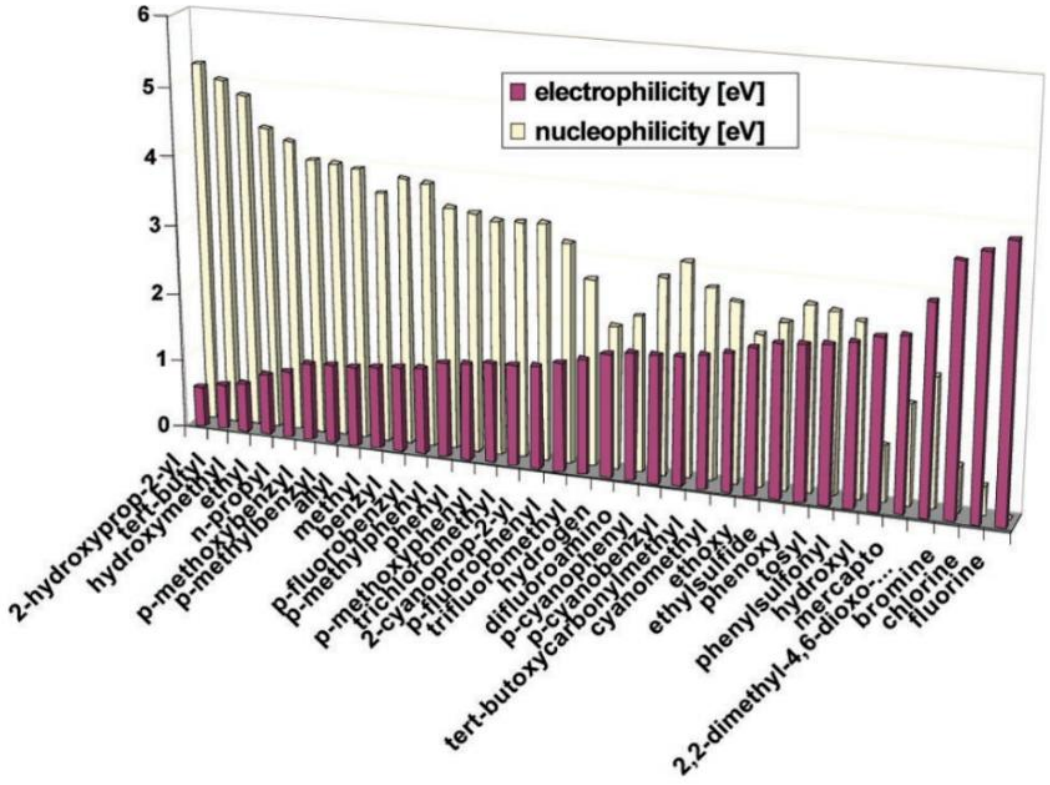

FIGURE 2.3 "Electrophilicity versus Nucleophilicity"

An efficient and practical qualitative method for predicting radical philicity that can be applied in the laboratory without relying on theoretical data and long calculations has been introduced by R. Welis and colleagues[31]. This approach involves a series of steps:

1. Evaluate comparative analysis between a radical and its corresponding anion (the reduced form) and cation (the oxidized form).

2. Evaluate which of these species is more stable and commonly found as an intermediate in organic chemistry.
3. Conclude whether the radical exhibits an electrophilic or nucleophilic character:

    - If the anion is more stable, it suggests that the radical is predisposed to undergo Single Electron Transfer (SET) reduction more readily than oxidation, signifying its electron deficiency and the desire to gain an electron, leading to an electrophilic character.

    - If the cation is more stable, it implies a preference for SET oxidation, indicating that the radical is electron-rich and inclined to lose an electron, demonstrating a nucleophilic character.

In the scheme 2.2, several examples illustrate this behavior more clearly. Beginning with the *t-butoxyl* species, we know that a negative charge on an oxygen atom is stable compared to a positive one. Therefore, the more stable charged form is an anion, implying that its radical will tend to gain an electron, exhibiting electrophilic characteristics. In the second example, we have a *tert-butyl* species, and as we know, it's more stable charged species is a cation. Consequently, its radical will tend to lose an electron, demonstrating a nucleophilic character. In the final example, we consider the trimethylsilyl group, whose more stable charged species is also a cation. This implies that its radical will display a nucleophilic character.

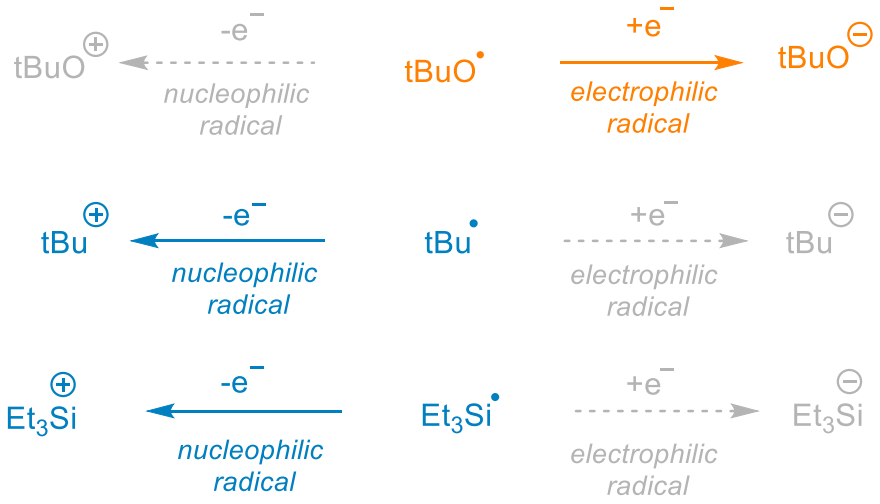

SCHEME 2.2 Qualitative Method for Predicting Radical Philicity

In some cases, certain species exhibit ambiphilic characteristics, indicating that they possess both nucleophilic and electrophilic properties. This versatility makes them valuable as synthetic intermediates. Aryl radicals serve as an exemplary instance of this ambiphilic nature. The concept of radical philicity assumes a significant importance in the second part of this chapter, 'Aryl Radicals in Organic Chemistry', where we explore the intricate generations and transformations of aryl radicals in depth.

In Figure 2.4, C(sp^3)-centered radicals are depicted, showcasing a propensity towards nucleophilicity as the energy of the singly occupied molecular orbital (SOMO) is higher. Moreover, these radicals can express electrophilic characteristics, frequently requiring multiple electron-withdrawing groups to confer electrophilic behavior upon an inherently nucleophilic alkyl radical. In contrast, aryl radicals typically demonstrate limited influence from other functional groups and exhibits an ambiphilic reactivity, as mentioned.

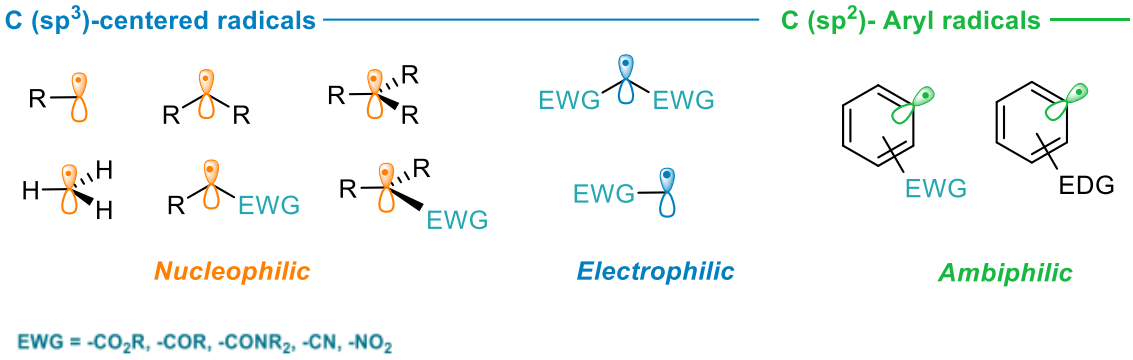

FIGURE 2.4 Radical Philicity

2.1.2.2 Polarity Effects

One of the key factors significantly impacting the outcome and selectivity of HAT reactions is the polarity effects, which can either align (match) or misalign (mismatched) with the identity of the C-H bond to be cleaved (hydrogen donor) and the hydrogen abstractor.

In a HAT reaction, polar effects can be described as the presence or absence of partial charge on a specific hydrogen atom. This partial charge is influenced by the atom's surrounding environment and nearby substituents. Nucleophilic radicals tend to abstract hydrogen atoms with a partial positive charge (δ+), often referred to as "protic" hydrogen atoms. In contrast, electrophilic radicals are more inclined to abstract hydrogen atoms with a partial negative charge (δ−), often termed "hydridic" hydrogen atoms. This understanding provides a useful tool for predicting the outcome of a radical HAT event[31].

For instance, when working with electrophilic species like alkoxy radicals or their related electrophilic derivatives, there is a clear preference for abstracting hydridic (nucleophilic) C-H bonds rather than electron-poor (electrophilic) ones of similar strength. This preference is directly linked to the electronic characteristics of the available radical intermediate. Consequently, the presence of electron-withdrawing or electron-donating groups significantly influences the polarity of C-H bonds in the substrate. This

enables for example the utilization of solvents containing electrophilic C−H bonds that are relatively labile e.g., acetonitrile and acetone when a nucleophilic hydrogen abstractor is involved during the reaction[22] see Figure 2.1.

Let's study a case derived from research conducted by Fagnogni and Ryu[33] that demonstrates how the presence of an electron-withdrawing group can impact the chemical outcome of a HAT reaction. Consider their investigation involving cyclopentanone, where the α C-H bond is typically weaker than the β C-H bond based on BDE values. However, intriguingly, the β C-H bond is cleaved due to polar effects in all the cases studied.

This phenomenon is a result of the use of an electronegative oxygen-centered radical as hydrogen abstractor. When the hydrogen from the α C-H bond is abstracted by the oxygen-based catalyst, the transition state (TS) strives to balance the positively charged (δ+) carbon atom, resulting in a polar TS (Figure 2.5, TS-a). This effect introduces a positive charge in the α C, disrupting its normal polarity. Consequently, the preferential cleavage occurs at the β C-H bond, following its usual polarity (Figure 2.5, TS-b). To gain a deeper insight into the polar effects during the HAT reaction, the transition states are provided. The catalyst used in these studies was tetrabutylammonium decatungstate (TBADT). In this study, cyclopentanone was subjected to the reaction with electron-deficient alkenes, which resulted in the complete regioselective formation of β-alkylated cyclopentanones. This approach exemplifies a selective conversion of sp^3 C–H bonds into C–C bonds.

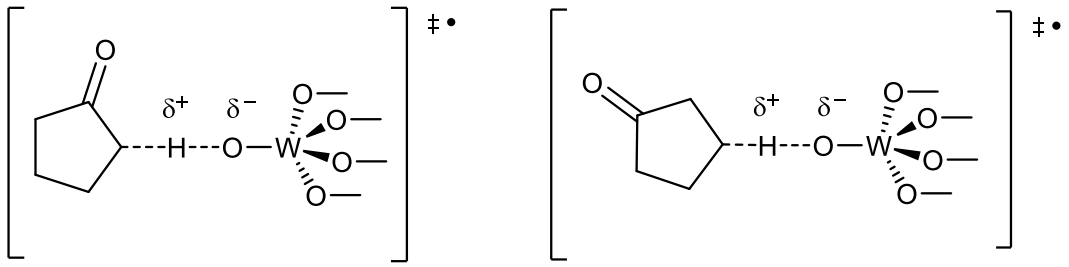

FIGURE 2.5 Transition State of Cyclopentanone and TBADT during a HAT

A critical aspect of HAT reactions involves evaluating whether reactant polarities are either matched or mismatched. One of the remarkable advantages of polarity matching lies in its ability to facilitate hydrogen abstraction events, overcoming the constraints imposed by thermodynamic driving forces within the HAT step and the BDE of available C-H bonds. This principle becomes evident through the example showcased by Fagnogni and Ryu, focusing on the case of the selective alkylation of cyclopentanone.

The determining factor is the ionic matching between the HAT catalyst and the hydrogen atom undergoing exchange. This phenomenon has been extensively studied by MacMillan's team, with their research centering on the quinuclidinium radical cation as a valuable HAT electrophilic catalyst. This catalyst selectively alkylates hydridic C–H bonds while leaving weaker C–H bonds unaltered, as illustrated in Figure 2.6. This selectivity is facilitated by the lower kinetic barrier associated with electrophilic radicals that engage in selective hydrogen abstraction at the most hydridic C–H bonds, thus representing a polarity match. This innovative approach enables targeted functionalization, moving beyond the conventional model solely based on BDEs. The figure was taken from MacMillan and team paper and all credits goes to the authors[34].

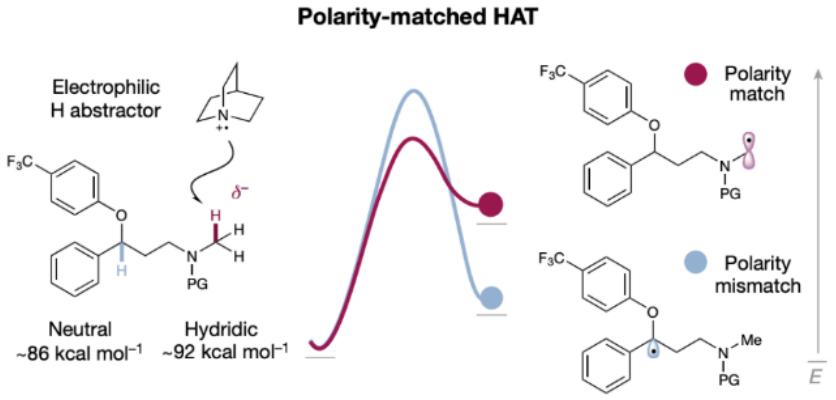

FIGURE 2.6 Polarity Matching Between Quinuclidinium Radical and Two Distinct Hydrogen Atoms

We can visualize all general scenarios in Scheme 2.3, establishing a framework for assessing polarity matches that makes possible the radical process, in particular the HAT reaction favorable and polarity mismatches that disfavored it.

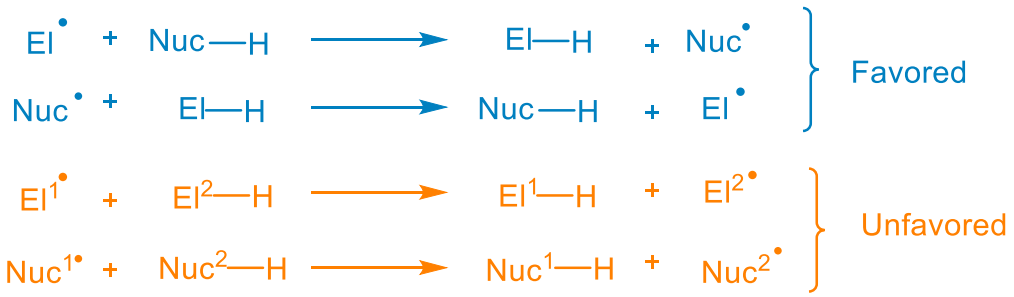

SCHEME 2.3 General Scenarios for Attribuiting Polarity Matched or Mismatched in a HAT reaction.

An interesting approach that enhances the flexibility of these transformations in HAT processes is known as Polarity Reversal Catalysis (PRC). In this technique, an additional co-catalyst is introduced into the solution to facilitate polarity mismatched HAT reaction, transforming them into polarity-matched reactions. Specifically, by introducing a catalyst

that replaces the polarity mismatched step with two polarity matched steps, it becomes possible to achieve a favorable overall reaction featuring two kinetically favored processes.

For example, Roberts and his colleagues[35] applied this method to the reduction of alkyl halides with silanes. Without the inclusion of a PRC catalyst, the reaction would proceed slowly because the nucleophilic alkyl radical must engage in a HAT with the electron-rich hydrogen (hydric hydrogen) atom of the silane, resulting in an unfavorable polarity mismatch. However, in the presence of PRC, the nucleophilic alkyl radical can execute a polarity-matched abstraction on the protic hydrogen of the thiol catalyst. Subsequently, the sulfur-centered radical carries out a second matched abstraction on the silane, resulting in a significantly more favorable process and improving the yield of the product obtained. This technique is illustrated in Scheme 2.4.

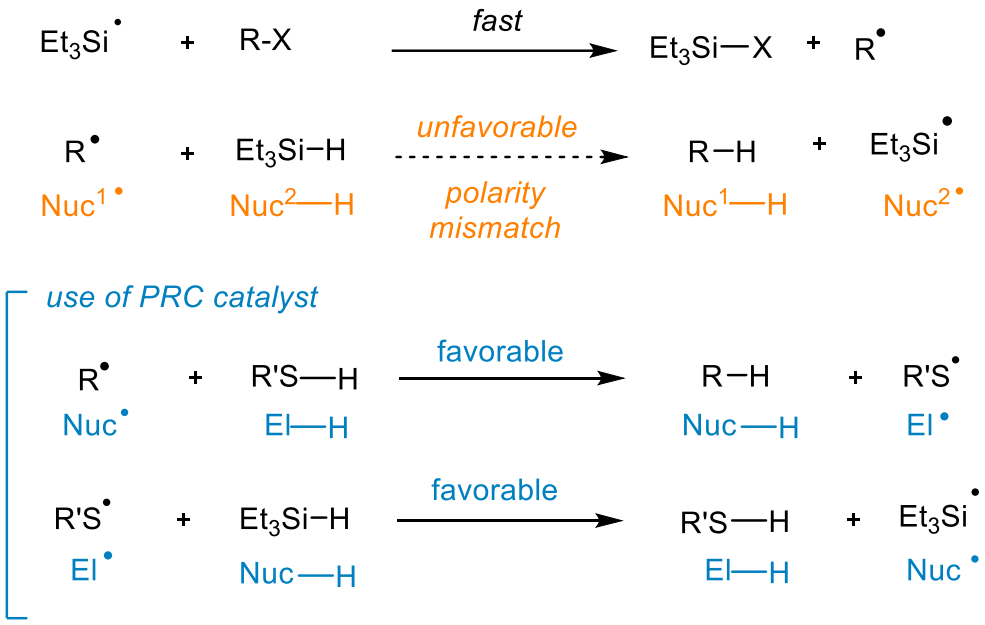

SCHEME 2.4 An example of an application of a PRC catalyst

2.2 Aryl Radicals in Organic Chemistry

2.2.1 Evolution of Aryl Radical Chemistry

The field of aryl radical chemistry has an impressive history extending back over a century. Its inception is credited to the pioneering work of Peter Griess in 1866[36], who elucidated the formation of iodobenzene from phenyldiazonium salts and molecular iodine. Over the subsequent 150 years, aryl radical chemistry has solidified its position as a foundational discipline within the domain of organic chemistry.

In this evolution, four distinguished name reactions have played an important role, undergoing continuous refinement and emerging as cornerstones of innovation. Sandmeyer's 1884 transformation of aryl diazonium salts into haloarenes, enabling the efficient synthesis of haloarenes using readily accessible starting materials[37].

In 1896, Pschorr introduced an intramolecular cyclization method that facilitated the construction of cyclic structures, expanding the repertoire of synthetic tools available to organic chemists[38]. The Gomberg-Bachmann synthesis of biaryl compounds, unveiled in 1924[39], followed a mechanism like the Pschorr reaction, thus contributing significantly to the synthesis of biaryl structures, prevalent in diverse organic compounds. The fourth prominent reaction, the Meerwein arylation of olefins, made its debut in the literature in 1939, further enriching the toolkit of aryl radical chemists[40].

Aryl diazonium salts remained the primary source of aryl radicals for an extended period. Their popularity stemmed from their ease of use and ready availability. However, their tendency to yield a diverse array of side reactions curtailed their utility as radical precursors, impeding a deeper exploration of their radical chemistry.

A significant leap in versatility occurred in the late 1960s with the widespread adoption of stannanes for radical reactions. This innovation enabled the generation of aryl radicals through halogen atom transfer (XAT) from haloarenes using tin radicals.

In addition to these classical reactions, a group of innovative and promising methods for aryl radical generation has surfaced. Notably, photoredox catalysis has emerged as a potent technique, facilitating the generation of aryl radicals from a diverse array of precursors. These methodologies have effectively surmounted the limitations associated with aryl halides and arenediazonium salts[41].

2.2.2 Reactivity of Aryl Radicals

Aryl radicals, known for their remarkable reactivity, often engage in reactions that proceed under relatively mild conditions[42]. Aryl radicals possess the capability to facilitate the functionalization of arenes and to tackle more intricate transformations, including C–H functionalization reactions. Their reactivity displays a distinctive feature related to radical philicity, as mentioned in the first part of this chapter, ‘Chapter 2.1.2.1 Radical Philicity’, where they exhibit an ambiphilic behavior.

Organic chemistry primarily revolves around carbon-based structures, making carbon-centered radicals the most prevalent type of radical intermediates in this field. To gain a better understanding of the reactivity of aryl radicals, let's begin with the simplest radicals, known as alkyl radicals. These radicals typically feature a Singly Occupied Molecular Orbital (SOMO) localized in an unhybridized *p* orbital. It's worth noting that

the carbon atom bearing the SOMO is actually sp^2 hybridized, while the radical in effect resides in a *p* orbital as shown in Figure 2.7a.

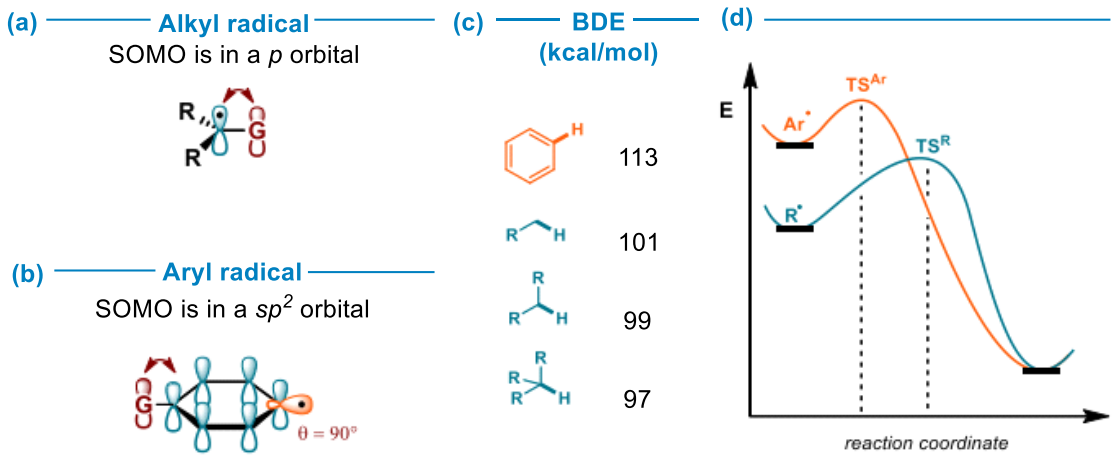

FIGURE 2.7 (a) SOMO of an Alkyl Radical (b) SOMO of an Aryl Radical (c) BDEs values (d) Reaction coordinate for Alkyl and Aryl Radicals

Compared to alkyl radicals, where the SOMO primarily resides in an unhybridized *p* orbital, aryl radicals feature a SOMO in a sp^2 orbital, as shown in Figure 2.7b, characterized by an increased *s* character. *s* orbitals, occupying lower energy levels and being closer to the nucleus, exhibit denser electron distribution in contrast to *p* orbitals. Consequently, electrons in *s* and *sp* hybrid orbitals are positioned closer to the nucleus than those in a *p* orbital. These factors result in *sp* and sp^2 radicals that, generally, display more electrophilic characteristics.

The concept of hybridization also is related to stability. Hybrid orbitals with a higher *s* character form stronger bond, resulting in higher energetic costs to break bonds to *sp*-hybridized or sp^2-hybridized carbon atoms as opposed to sp^3-carbons. A comparison between the BDEs of aromatic C(sp^2)-H bonds (113 kcal/mol) and aliphatic C(sp^3)-H bonds (that can range from 82-106 kcal/mol) are illustrated in Figure 2.7c, underscores the high reactivity of aryl radicals, enabling effective hydrogen atom transfer reactions even from unactivated alkanes.

In cases where the SOMO assumes a sp^n hybrid orbital, these radicals exhibit higher energy levels compared to radicals with an unhybridized *p* orbital SOMO, such as alkyl radicals. Consequently, reactions involving sp^n-hybridized radicals are typically highly exergonic (Figure 2.7d), often progressing through early, reactant-like transition states in contrast to those involving *p*-orbital SOMOs. As a result, sp^n-hybridized radicals exhibit an elevated predisposition toward ambiphilicity, showcasing an inclination for both nucleophilic and electrophilic behavior, setting them apart from the majority of, for example, alkyl radicals, and making them very versatile synthons.

Aryl radicals exhibit a unique structural characteristic in which their SOMO is oriented perpendicular to the π system comprising the aromatic ring. The orthogonal alignment, marked by a 90° dihedral angle between the SOMO and the π system, minimizes their interaction (Figure 2.7b). Consequently, the introduction of electron-donating or electron-withdrawing substituents onto the aromatic ring has theoretically, a minimal impact on the radical's philicity. This behavior contradicts conventional reactivity expectations associated with aromatic rings[31].

2.2.3 Generation of Aryl Radicals

The effective use of aryl radicals is constrained by several significant limitations, primarily associated with the complexities of their generation. The overall efficiency of reactions involving aryl radicals is heavily dependent on the methodology used for their production and the careful choice of suitable precursor compounds. These factors play a crucial role in determining the success on these types of process.

As previously mentioned, photoredox catalysis has emerged as a powerful tool for generating aryl radicals from various precursors. In 2019, Basso conducted a research employing this modern approach, which involved a mechanism utilizing a ruthenium(II)-photoredox catalyst for aryl radical generation from diazonium salts through a SET step.

It is, however, imperative to recognize that this method does have certain limitations. These includes the dependence on a metal catalyst, reflecting in the necessity for a complex ruthenium photoredox catalysis. Furthermore, complications arise from the limited solubility of the aryl precursor, specifically the diazonium salts.

In response to these limitations, the pursuit of an ideal radical precursor was initiated. A precursor that should exhibit photosensitivity to visible-light and demonstrate exceptional solubility in a wide range of organic solvents was target. Moreover, the decomposition of this precursor should yield volatile by-products, thereby simplifying the purification process.

Regarding the pursuit of a photosensitivity to visible-light precursor, light can act as the sole trigger for substrate activation, enabling the generation of reactive intermediates without aggressive reagents or harsh conditions[43]. Furthermore, photons as environmentally friendly "reagents," can activate substrates without leaving residual byproducts, simplifying the purification process. Nevertheless, the difficulty arises when working with colorless organic compounds, requiring the use of specialized equipment[44].

With the rise of low-energy-demand visible-light sources, such as light-emitting diodes (LEDs), there has been a shift in emphasis towards the identification of chemical systems capable of efficiently absorbing photons. Visible-light photocatalysis utilizes the

potential of colored compounds to absorb light energy, transforming them into highly reactive species. These activated species possess the capacity to enable the conversion of colorless substrates enabling a wide range of chemical transformations.

In a simplified context, this type of reactions involves direct photon absorption, achieved by a colored reactant, thereby eliminating the need for a photocatalyst. Although various colored compounds exist, their direct involvement in photochemical reactions is often limited, with exceptions such as diarylazo compounds.

Notably, Stefano Protti and colleagues have pioneered various strategies for introducing a colored and photo-reactive moiety into a solution. In recent years, they have introduced the concept of a " dyedauxiliary group", which they define as a functional group with the dual capability of imparting color and photochemical reactivity to an organic molecule. A more contemporary example of such a dyedauxiliary group is the $-N_2SO_2R$ substituent in hetero-arylazo sulfones[9]. These derivatives exhibit thermal stability and vibrant colors, and they can be easily synthesized from the corresponding anilines[45] or hydrazines[46]. This is a clear example of how photochemistry can offer a valuable contribution to selectivity, efficacy, and sustainability in organic synthesis.

Notably, in 1959 Overberge introduced aryl azosulfone compounds, proposing a decomposition mechanism that involves initial homolytic dissociation, leading to the formation of free-radical intermediates and the subsequent generation of the aryl radical[47]. Additionally, in 1982, Kobayashi introduced the concept of using the $-N_2SO_2R$ substituent performing as a dyedauxiliary group[48].

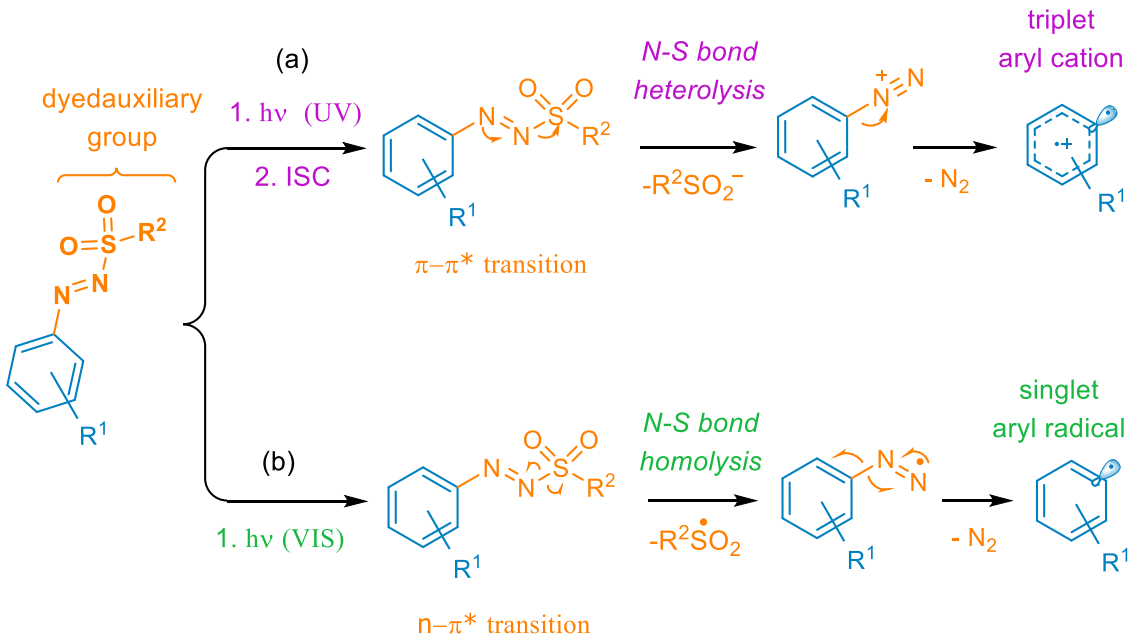

SCHEME 2.5 Aryl Azosulfones Wavelength-dependent generation (a) triplet aryl cations (UV) (b) singlet aryl radical (VIS)

Regarding the photophysics of aryl azosulfones, they display dual absorption peaks, one in the UV range (300−360 nm, with ε values of 10000−20000 M^{-1} cm^{-1}) and another in the visible spectrum (400−450 nm, with ε values of 100−200 $M^{-}1$ cm^{-1}). These peaks have been attributed to a π-π* and an n-π* transition, respectively. Consequently, the observed photoreactivity depends on the excited state that's populated, and this varies with the wavelength of irradiation. Under UV light (the state undergoes intersystem crossing (ISC) to the corresponding triplet state) they undergo heterolysis of the N-S bond, forming aryl cations, Scheme 2.5a. Conversely, when exposed to visible-light, homolysis of the same bond occurs, resulting in the formation of aryl radicals (via singlet state), as shown in Scheme 2.5b. When using a polychromatic light source, such as sunlight, both aryl cations and aryl radicals become accessible[9].

Aryl azosulfones have found successful application in several aryl radical transformations. These include the visible light-driven arylation of xanthines, where the introduction of an aryl group significantly enhanced the biological properties. This family of compounds is widely utilized for its pharmacological properties. Among them, caffeine is renowned for its effectiveness in addressing apnea in newborn babies and as an analgesic, particularly in combination therapies, such as headache treatment[49]. Additionally, dual visible-light/gold-catalyzed Suzuki type coupling of arylazo sulfones with arylboronic acids provides access to a range of hetero-biaryls. Moreover, Gomberg–Bachmann photo-arylation via aryl azosulfones enables the synthesis of various hetero-biaryls with satisfactory yields, all achieved without the need of a photocatalyst or additional additive[9].

Last year, Basso conducted a study in which, instead of relying on ruthenium photoredox catalysis and diazonium salts, he successfully obtained aryl radicals generated through visible light irradiation, utilizing various substituted aryl azosulfones situated within the sulfonyl moiety and the aromatic ring of the aryl group. Subsequently, this innovative methodology was applied to functionalize olefins, resulting in a wide range of diverse products[50]. The central focus of this thesis revolves around the application of this radical-based approach for aryl radical generation.

2.3 The Curious Case of Solventylation of Olefins

In the first part of this chapter, we extensively explored methods to refine HAT reactions. This involved a comprehensive understanding of the radical philicity between the hydrogen donor and the hydrogen abstractor. Additionally, we analyzed the polarity effects resulting from the presence of electron-donating and electron-withdrawing groups, leading to the creation of both matching and mismatched scenarios. We also examined the use of a PCR catalyst to achieve a matched situation. While these factors indeed play a significant role in HAT reactions and have been subjected to extensive examination and analysis, innovative strategies have been introduced to address the diverse limitations inherent in conventional HAT protocols through various research initiatives[51].

Nonetheless, a significant challenge in HAT reactions arises from the solventylation process, a parasitic reaction mediated by the solvent, inadvertently involving reactivity as hydrogen donors[52]. These reactions can be particularly troublesome when operating under dilute conditions[50]. They are notably affected by the polarity of C-H bonds in the substrate. For instance, the choice of solvents containing electrophilic C−H bonds that are relatively labile, such as acetonitrile and acetone, can be problematic when a nucleophilic hydrogen abstractor is involved as a substrate during the reaction[22]. While such secondary reactions are typically considered undesirable in HAT processes, select research groups have begun exploring these pathways as an intriguing alternative.

In the domain of traditional chemistry, there have been various efforts to explore alternative routes for practical applications that involve the use of solvents as substrates during the reaction. For example, economical and readily available acetonitrile was employed under transition-metal-free conditions to synthesize cyanomethylated coumarins with high yield. These resulting compounds could be readily transformed into related coumarin derivatives[53]. Coumarin plays a significant role due to its and its derivatives' anticoagulant effects, achieved by suppressing the production of coagulation factors. Additionally, these compounds may also possess the ability to inhibit platelet aggregation[54].

In a recent study, Zhao and their research team introduced an innovative approach to synthesize chloro- and cyano-containing oxindoles. They used versatile solvents such as acetonitrile and dichloromethane, boronic acid as the aryl radical precursor, and manganese(III) acetate as the oxidant This method not only yielded good to moderate yields but also enabled the direct formation of a C–C bond and the concurrent construction of the oxindole ring[55]. Oxindoles are renowned for their significance in the domains of chemistry, pharmaceuticals, and materials industries, making this approach a promising contribution to the field[56].

In the field of HAT reactions, a noteworthy case by Van der Eycken deserves attention. He introduced an innovative approach utilizing non-activated ketones as both the reaction medium and the hydrogen donor. The key to this method was the used of dicumyl peroxide, employed as the precursor for the cumyloxyl radical, which played the role of a hydrogen abstractor, enabling a selective HAT. This HAT process led to the formation of a radical derived from the ketone. Subsequently, this radical seamlessly added to the C=C bond of N-acrylamide, aided by copper (II) chloride serving as the radical mediator and microwave-assisted.

What distinguishes this last methodology is its environmentally friendly nature and its capacity to yield valuable 3,3-disubstituted oxindoles under gentle reaction conditions. The operational simplicity of this protocol renders it accessible for a diverse array of

functional groups. Consequently, it consistently yields the desired products in moderate to high yields, highlighting the potential this strategy holds[57].

Liu's investigation explores into the utilization of N-acrylamide as a source of the C=C precursor for the radical generated in the HAT reaction, enabling the formation of a novel C-C bond. His experiments involved N-methyl-N-phenylmethacrylamide and saturated hydrocarbons, and the reaction was carried out in the presence of dicumyl peroxide, with copper (I) as catalyst at elevated temperatures. This approach not only demonstrated its effectiveness in producing alkyl-substituted oxindoles but also unveiled an innovative pathway for selectively modifying straightforward alkanes through a free radical cascade process. The achievement of this reaction depends significantly on Cu catalysis[58].

The BOG research group has made significant contributions to this field by exploring an efficient flow methodology for solventylation, which is referred to as 'acetonylation.' This process not only utilizes acetone as a solvent but also employs it as a hydrogen donor in the HAT process, resulting in the formation of the acetonyl radical. This radical assumes a central role, acting as a synthon that facilitates the formation of a new C−C bond[59].

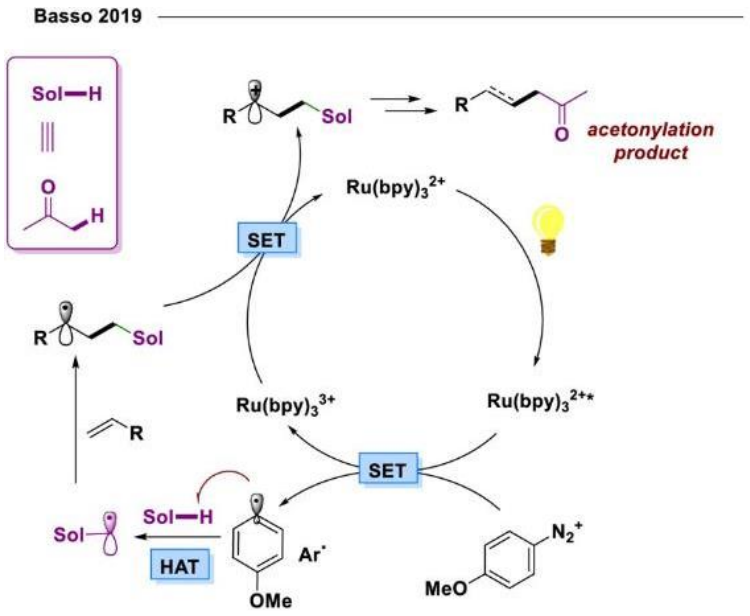

SCHEME 2.6 Ruthenium(II)-Photoredox Catalyst for Aryl Radical Generation

Scheme 2.6 provides a comprehensive overview of the solventylation process including a HAT process and two SET steps. The mechanism illustrated depicts the conversion of the precursor, diazonium salts, into the reactive aryl radical. In particular, this transformation as mentioned, was achieved through utilizing a ruthenium(II)-photoredox catalyst, specifically $Ru(bpy)_3Cl_2$ at 1 mol% and a 450 nm light source. Subsequently, with the successful generation of the ambiphilic aryl radical, the HAT

process initiated, abstracting a hydrogen atom from the solvent, acetone, which was maintained at a concentration of 0.01 M.

The resulting electrophilic radical, the acetonyl radical, subsequently reacted with an olefin, referred also to as a radical trap. This interaction resulted in the formation of a radical intermediate with a newly formed carbon-carbon bond. Through SET oxidation step facilitated by the ruthenium-based catalyst, the acetonylation product was successfully obtained, with the regeneration of the catalyst. This methodology demonstrated its effectiveness by yielding the desired product in good yields, under mild reaction conditions, and offering the flexibility to employ a variety of olefins.

It's worth noting that this methodology mechanism operates at a low concentration, typically 0.01 M of the initial substrate, to prevent undesired reaction between the aryl radical and the olefin substrates. This deliberate choice of low concentration enables efficient HAT between the acetone and the aryl radical, facilitated by the presence of the ruthenium(II)-photoredox catalyst[60]. This transformative approach not only redefines the conventional HAT event but also elevates it to a central step, enhancing the functionalization of olefins.

While these concepts are intriguing in theory and demonstrate robustness and reliability, they face a common constraint primarily arising from the limited solubility of the radical precursors in the HAT process, such as the diazonium salts or, at times, the catalysts required for the mechanism of the reaction. Furthermore, several of these methodologies depend on heavy or transition metal species, imposing restrictions on their versatility. To tackle this challenge, there is a strong desire for a universally applicable and efficient protocol that operates without the need for metals, thus allowing for the straightforward incorporation of various functional groups into the same substrate with unparalleled ease.

To achieve this objective, the pursuit of an optimal radical precursor was initiated and thoroughly explored in Chapter 2.2.3, focusing on the generation of aryl radicals through the introduction of innovative concept involving dyedauxiliary groups, like the $-N_2SO_2R$ substituent in hetero-arylazo sulfones. The intended precursor for these experiments, depicted as **1** in scheme 2.8, exemplifies this compound type. It possesses photosensitivity to visible light, eliminating the need for photoredox catalysis, displays exceptional solubility in a wide variety of organic solvents, and upon decomposition, produces volatile by-products, thus simplifying the purification process.

The chosen olefin for the solventylation process was N-methyl-N-phenylmethacrylamide **2** in scheme 2.7. It was selected as a radical trap due to its intrinsic reactivity towards both nucleophilic and electrophilic radicals. The synthesis of the olefin **2** involved the reaction of aniline with methacryloyl chloride in the presence of triethylamine, resulting in a 70% yield. The solventylation process, as depicted in Scheme 2.8, involves precursor **1** and olefin **2** to produce product **3**, which incorporates the solvent within its structure. This process was conducted under diluted conditions (0.01 M) in an inert argon atmosphere at room temperature and exposed to overnight 450 nm irradiation. Notably, these investigations were carried out under batch conditions, and comparisons with flow conditions revealed no significant differences in yields[60].

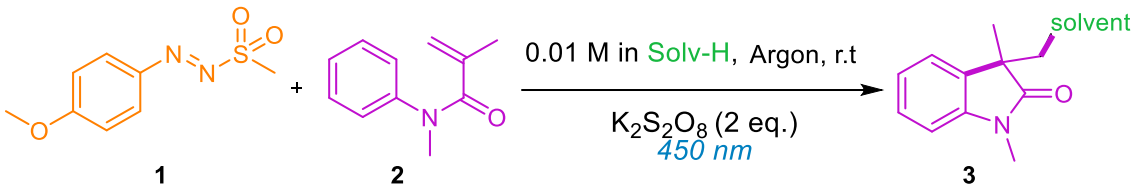

SCHEME 2.7 Solventylation Reaction

Regarding the mechanistic framework of the solventylation process using precursor **1** and olefin **2** under the conditions mentioned, is elucidated in Scheme 2.9. Upon irradiation with high-power blue LEDs at 450 nm, the dyedauxiliary group contained within the aryl azosulfone compound **1** absorbs the light energy, initiating subsequent fragmentation characterized by N-S bond homolysis and the ejection of molecular N_2. This sequence leads to the formation of alongside a sulfur-centered radical **4** and the desired aryl radical **5**.

The aryl radical **5** functions as a hydrogen abstractor in the HAT step, with acetone **6** serving as the hydrogen donor and, also solvent of the reaction, yielding the acetonyl radical **8** and the protonated aryl radical, anisole **6**. Subsequently, the acetonyl radical **8** engages with the chosen olefin **2**, generating the radical intermediate **9**. This radical intermediate **9** undergoes cyclization, leading to the formation of radical intermediate **10**. The sulfur-centered radical **10** plays an important role in the oxidation of radical intermediate **10**, resulting in the generation of the cation intermediate **12** and the azomesylate anion **11**. In the presence of anion **11**, cation intermediate **12** undergoes deprotonation, ultimately yielding the desired product **14** and the side product **13**.

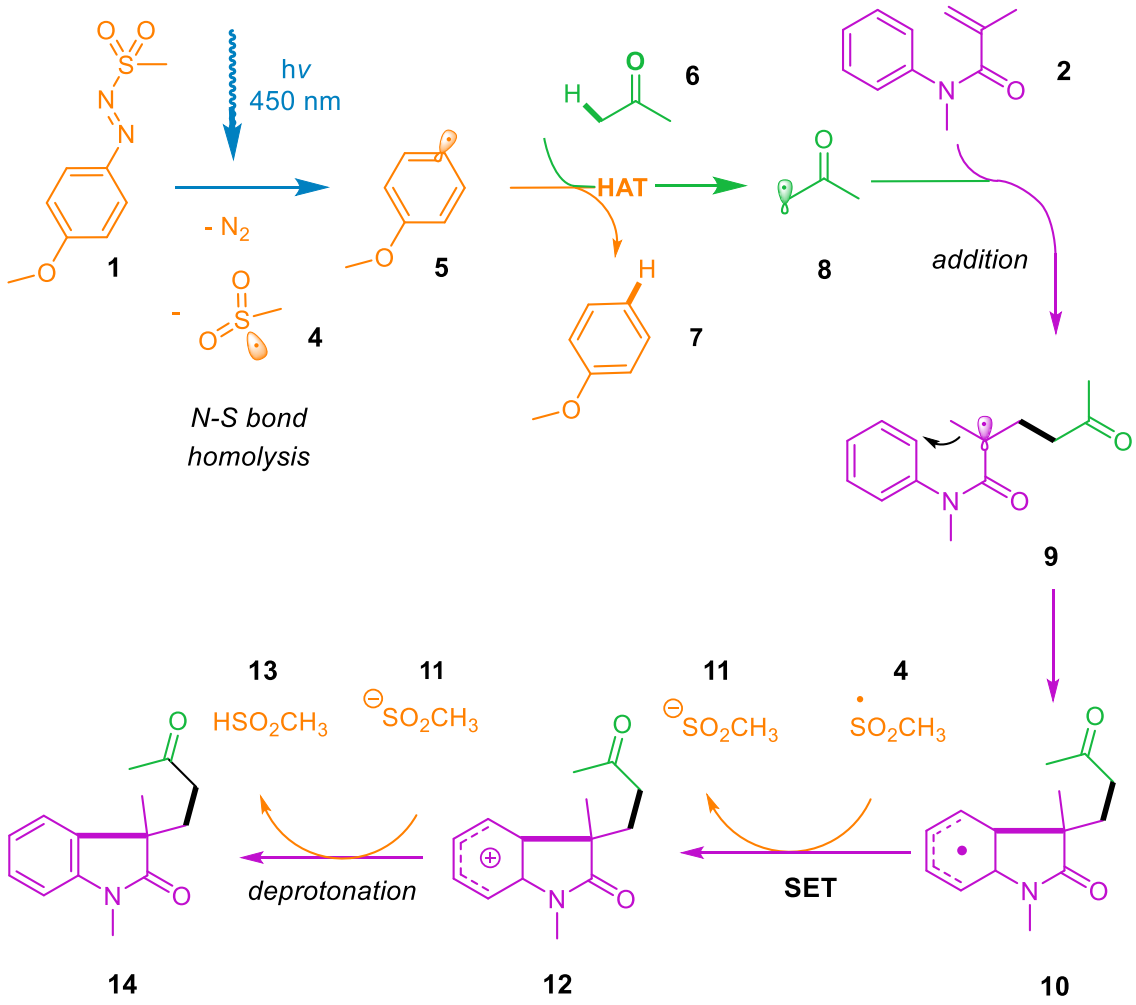

SCHEME 2.8 Mechanism of the Solventylation Process

In Scheme 2.8, we can determine three important steps. The first involves the generation of the aryl radical **5** from the precursor **1**, which we have already discussed. The second crucial process entails the HAT from the solvent, which starts with the generation of the aryl radical **5** and leads to the formation of acetonyl radical **8** with the generation of anisole **7** a volatile compound, which can be readily eliminated using a rotary evaporator. The third critical step leads to the desired product and involves the oxidation of the radical intermediate **10** from the reactive sulfur-centered radical **4**.

In the context of the oxidation step, in contrast with the BOG previous Ru(II)-catalyzed procedure, which necessitated an oxidative transformation (i.e., the turnover step within the photocatalytic cycle, leading to catalyst regeneration) were conducted a thorough investigation of the implementation of various external oxidants, both homogeneous and heterogeneous, to identify optimal conditions for enhancing the solventylation process, in particular the acetonylation reaction, ultimately leading to the formation of the final product **14**. Remarkably, the reaction yield exhibited a significant improvement when potassium persulfate was employed as external oxidant. However, due to the limited solubility of potassium persulfate in most solvents, a phase transfer catalyst was

introduced to facilitate the process. Surprisingly, this addition had a detrimental effect on the reaction's outcome. The working hypothesis, put forth by the PhD student who conducted the experiments, suggests that the increased turbidity of the solution, which scattered more light, and the higher concentration of potassium persulfate in the solution may have created a powerful oxidizing environment, potentially leading to the degradation of the starting materials, thereby accounting for the higher conversion rate. The best results were obtained using 2 equivalents of the external oxidant potassium persulfate.

Despite the initial expectations, as discussed in Chapter 2.2.2 on the Reactivity of Aryl Radicals, the introduction of electron-donating or electron-withdrawing substituents onto the aromatic aryl ring had a limited impact. However, studies conducted by the BOG research group revealed reduced efficiency in HAT reactions when using diazonium salts with withdrawing substituents in the *para* position, such as 4-fluoro and 4-chloro. Computational analyses supported these findings, showing slightly higher transition state (TS) barriers for the HAT event with 4-fluorophenyl and 4-chlorophenyl radicals. As a result, we decided to initiate the study with the corresponding aryl azosulfone **1** (as illustrated in Scheme 2.9), which facilitated the HAT process by generating the 4-methoxyphenyl radical as the hydrogen abstractor. We also explored the inclusion of an electron-withdrawing substituent in the *para* position in the aryl azosulfone, such as the *para-acyl* group, leading to the generation of the 4-acetophenone radical. The experimental outcomes of these investigations are presented in the Results and Discussions chapter.

The BOG research group conducted a study for the application of the solventylation protocol as illustrated in Scheme 2.9. They synthesize the intermediate **16** for the total synthesis of esermethole **16**, a precursor to physostigmine, a clinical treatment for glaucoma[61]. The primary step involved the synthesis of compound **16** through the solventylation process from the radical trap **15** and the aryl azosulfone **1** on a 1 mmol scale (path a), achieved by conducting multiple parallel batches runs with the reported diluted condition 0.01 M, the external oxidant $K_2S_2O_8$ (2 equiv), $MeNO_2$ as solvent, under HP LEDs at 450 nm (0.6 W), and an overnight reaction.

Subsequently, the desired solventylation product **16** was reduced to form amine **17** (Scheme 2.9, path b), which was further modified to produce both enantiomers of esermethole **18** through chiral resolution and two additional synthetic steps[50].

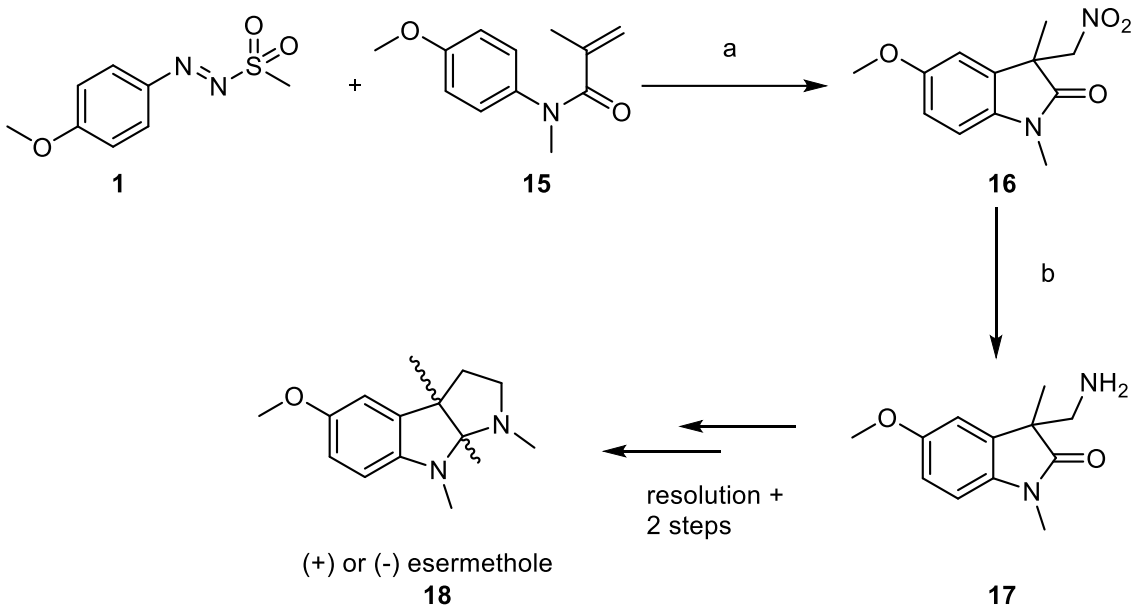

SCHEME 2.9 Application of the Solventylation Protocol in the Synthesis of an Advanced Intermediate for Esermethole

2.4 Research Objectives: Exploring the Solventylation Process

The innovative BOG protocol, exemplified by the general reaction in scheme 2.7 and the mechanism in scheme 2.8, showcases remarkable versatility by enabling the functionalization of diverse olefin substrates with carbon-centered radicals derived from various solvents. Notably, this method distinguishes itself for its environmental friendliness as it obviates the need for metal or photocatalysts. This approach operates independently of copper or ruthenium, microwaves, and high temperatures. It's worth noting that our approach effectively prevents the direct addition of aryl radicals to olefin substrates, particularly under high dilution conditions[50].

One of the standout features of this improved solventylation is the excellent solubility of the radical precursor, allowing for the use of a broader array of solvents, which enhances the method's applicability. Beyond acetone, other solvents were successfully employed, consistently under mild conditions. The reactions consistently yielded good to high yields without the requirement of a ruthenium-based photoredox catalyst. Instead, an oxidant facilitated the SET step, resulting in the formation of the final product and the establishment of a new carbon-carbon bond. These reactions were consistently conducted under diluted conditions (0.01 M) using a 450 nm light source and in a batch-style experimentation.

The elimination of photoredox catalysts not only simplifies the process but also enhances its cost-effectiveness and sustainability, aligning with the principles of green

chemistry and reduced environmental impact. Furthermore, solventylation shows promise in enabling late-stage functionalization and promoting atom-economic synthesis, particularly in medicinal chemistry and the synthesis of various compounds as we studied in the total synthesis of esermethole. The ability to modify molecules without extensive pre-functionalization is a highly sought-after capability, and this consistently occurs under mild conditions in the solventylation process, highlighting its safety profile and straightforward application.

In conclusion, solventylation, without the need for photoredox catalysts, represents a valuable and forward-looking development in organic chemistry. Its combination of sustainability, operational simplicity, adaptability, mild conditions, and improved solubility of the aryl precursor positions it as a method worthy of exploration in various applications. As we continue to advance our understanding of this process, the possibilities for its impact on the field of organic chemistry are promising.

The forthcoming chapter's central focus lies in the results and discussion of the experimentations of the solventylation, where we explore a wide array of substrates to efficiently generate aryl radicals from the precursor, aryl azosulfone. Our goal is to streamline this process and subsequently enable efficient HAT in a variety of solvents, resulting in the creation of diverse new products. Additionally, we conduct experiments with differently substituted radical traps, leading to the discovery of novel products in good yields.

3. Results and Discussions

In the field of organic chemistry, the exploration into the solventylation process, free from dependence on photoredox catalysis, attracts significant attention. Enhancing this investigation demands a profound understanding of its mechanism and reactivity of involved compounds, marked by careful experimentation and continuous optimization. This chapter initiates a comprehensive journey, presenting an analysis of results and discussions derived from a meticulously designed series of experiments aimed at understanding the intricacies of the solventylation process, specifically employing aryl azosulfones.

Starting with Chapter 3.1, where we explore the optimization of the reaction using aryl azosulfone **1** and radical trap **2** and investigate different factors influencing the solventylation process, the research progresses to Chapter 3.2. Here, we explore the synthetic scope of five distinct aryl azosulfones. Utilizing consistently radical trap **2**, our investigations were focused on understanding the reaction conditions, solvent effects, and the synthetic potential inherent in various aryl azosulfones. Chapter 3.3 extends this exploration, investigating the scope of diverse radical traps while consistently employing aryl azosulfone **1**. This effort resulted in the discovery of new products, some of which had not been reported in existing literature.

The outcomes presented in this chapter significantly contribute to our comprehension of the intricate interplay among reactants, solvents, and other factors, such as an argon atmosphere and temperature. These insights, obtained through different experimentations, further enhance our approach in the pursuit of improved synthetic outcomes. As we analyzed results and discussions, we unravel the complexities intrinsic to the solventylation using aryl azosulfones, providing valuable understanding helping us to advance synthetic methodologies in the domain of organic chemistry.

3.1 Optimization of Reaction Conditions for Enhanced Solventylation

The optimization process is based on the protocol employing aryl azosulfone **1**, a vibrant yellow/orange soluble solid, with radical trap **2** and the external oxidant, potassium persulfate, with an argon atmosphere and under 450nm LED light source irradiation. These conditions were examined and established in the previous chapter 2.3. The reaction extended overnight, and unless explicitly stated otherwise, it was conducted at room temperature.

We started by screening diverse solvents for an enhanced solventylation process. This experimentation yielded a spectrum of diverse products, each distinguished by the presence of the solvent used within the product as observed in the general structure **3** represented in Scheme 3.1. The solvents employed were acetone, yielding product **19**, acetonitrile, yielding **20**, and dichloromethane, yielding **21**.

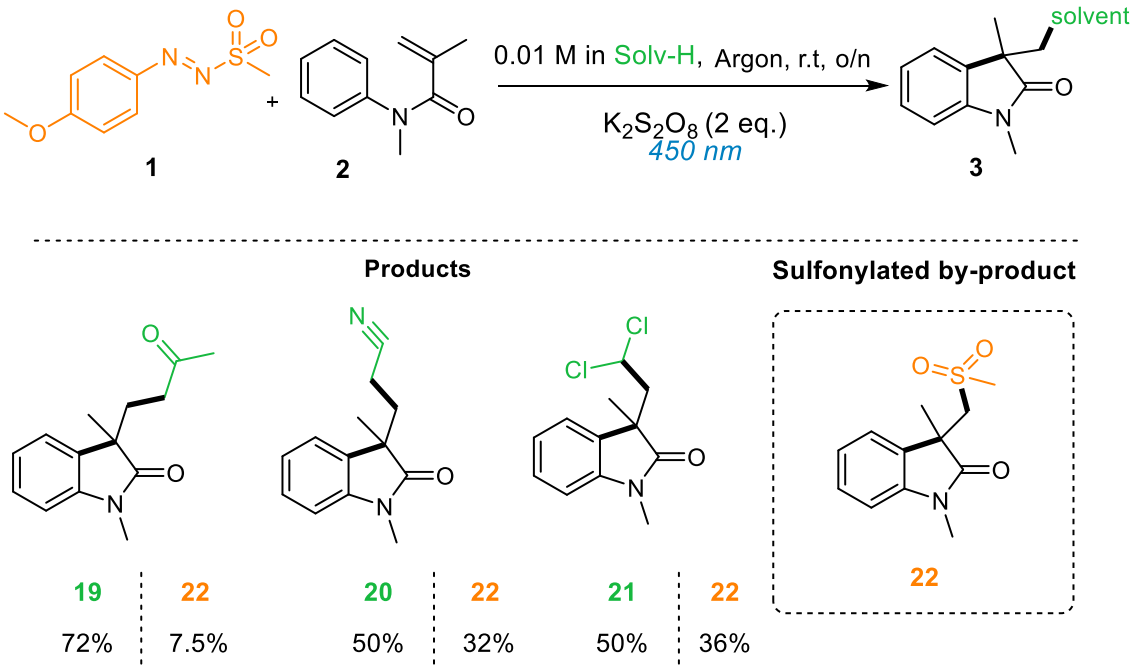

*SCHEME 3.1 Solvent Screening for Aryl DiazoSulfone **1** & Radical Trap **2***

As observed in Scheme 3.1, the highest product yield was achieved in the case of the solventylation using acetone with 72% yield of product **19**, concurrently yielding the lowest sulfonylated by-product **22** at 7.5%. In the reaction employing acetonitrile, a moderate yield of 50% was obtained for the product **20**, yet it exhibited a higher sulfonylated by-product **22** at 32%. A similar trend was observed with dichloromethane in the production of **21**, also resulting in a 50% and yielding the sulfonylated by-product **22** at 36%. This investigation furnished insights into the intricate interplay among reagents and solvents, thereby enhancing our understanding of solventylation processes and their underlying mechanisms.

Interestingly, when acetonitrile was employed as the solvent, we observed a lower yield 50% compared to acetone 72%. Despite the relatively low BDE of the C(sp^3)-H bond in acetonitrile, which should facilitate a smooth HAT (measuring 96.0 kcal/mol, compared to 95.9 kcal/mol for acetone), this may indicate a higher energy barrier for acetonitrile radical addition to the radical trap **2**, thus impeding the overall process of solventylation.

We observed that the formation of the sulfonylated by-product **22**, manifested with varying yields in the solventylation process. In most instances, the primary products and the sulfonylated by-product **22** could be conveniently isolated via FC (Flash Chromatography) purification, facilitated by their significant disparity in polarity. This feature obviates purification complications. Avoiding the generation of the sulfonylated by-product **22** poses a formidable challenge in principle, owing to the inherent stability of the sulfur centered radical **4**, as in scheme 3.2, present within the reaction environment. These radicals exhibit a propensity to engage in addition reactions with both electron-rich and electron-poor olefins[62].

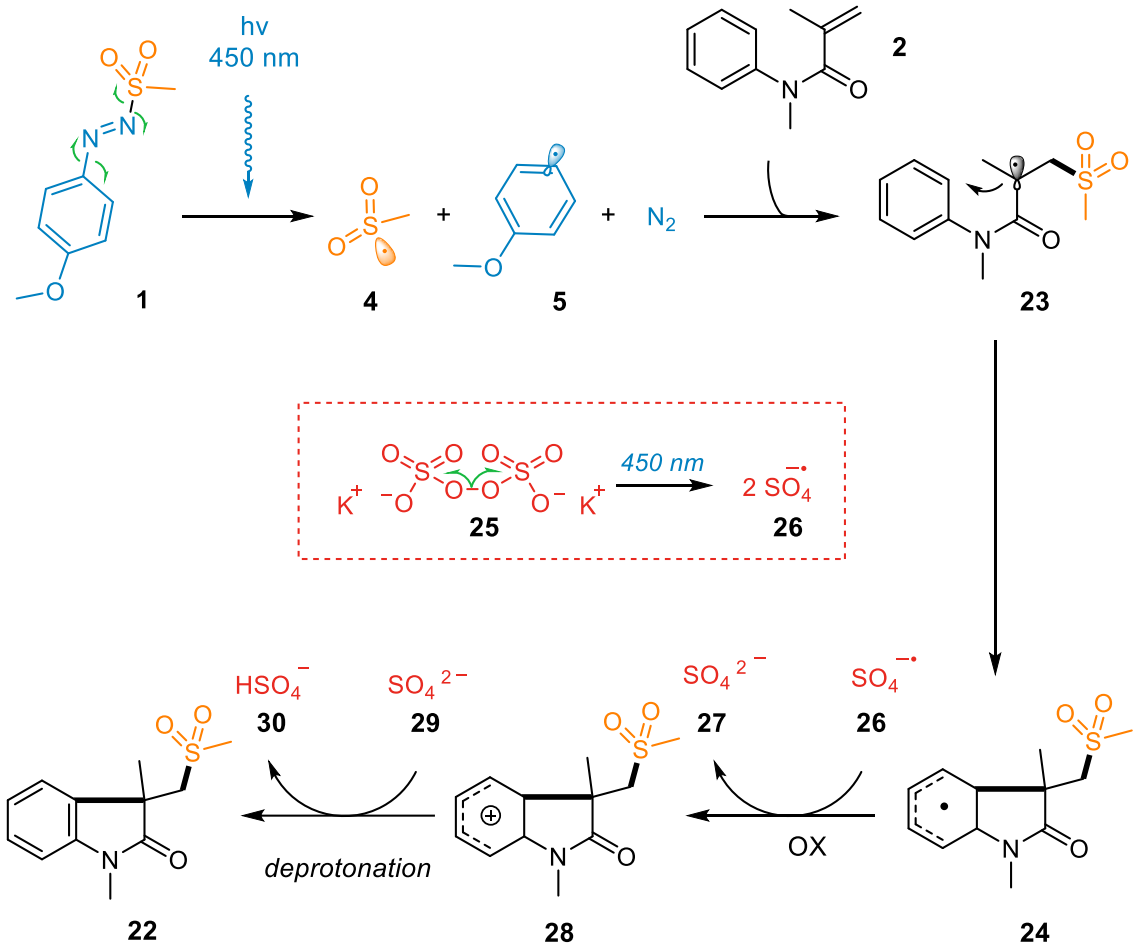

*SCHEME 3.2 Proposed Mechanism for The Generation of The Sulfonylated By-Product **22***

The formation of the sulfonylated by-product **22** is anticipated to proceed through the proposed mechanism outlined in scheme 3.2. Initiated by the exposure of aryl azosulfone **1** to a 450nm LED light source irradiation, N-S bond homolysis occurs, accompanied by the expulsion of molecular N_2, resulting in the generation of the sulfur-centered radical **4**, molecular nitrogen, and the aryl radical **5**. Upon encountering the radical trap **2**, the sulfur-centered radical **4** adds to it, forming the radical intermediate **23**, which subsequently undergoes cyclization to produce the radical intermediate **24**. With the

presence of the external oxidant in the reaction atmosphere, potassium persulfate **25** (depicted in the dashed box), undergoes homolysis of the peroxide bond O-O under 450 nm LED irradiation. This process generates the active sulfate radical **26**, characterized by a significant reduction potential of 2.6 V [636465]. Through a SET oxidation process, the sulfate radical **26** generates the cation **28** and the anion **27**. The latter anion then deprotonates the cation **28**, leading to the undesired sulfonylated by-product **22** and species **29**.

To reduce the formation of the sulfonylated by-product **22**, a series of experiments were conducted using aryl azosulfone **1** and radical trap **2** in acetonitrile (MeCN), aiming to produce product **20** with the incorporation of an additive as illustrated in scheme 3.3. Recognizing the reactivity of the sulfur-centered radical **4** with both electron-poor and electron-rich olefins, ethyl vinyl ether **30**, an electron-rich olefin, was chosen as the additive. The anticipation was that ethyl vinyl ether **30** would engage with the highly reactive sulfur-centered radical **4**, thereby preventing its reaction with olefin **2**. Consequently, this would render the radical trap **2** available for the desired solventylation reaction initiated by the aryl radical **5**, leading to the formation of the desired product **20**. Various quantities of ethyl vinyl ether **30** were explored, starting with 0.5 equivalents, and increasing to 1, 2, 3, and finally, 5 equivalents.

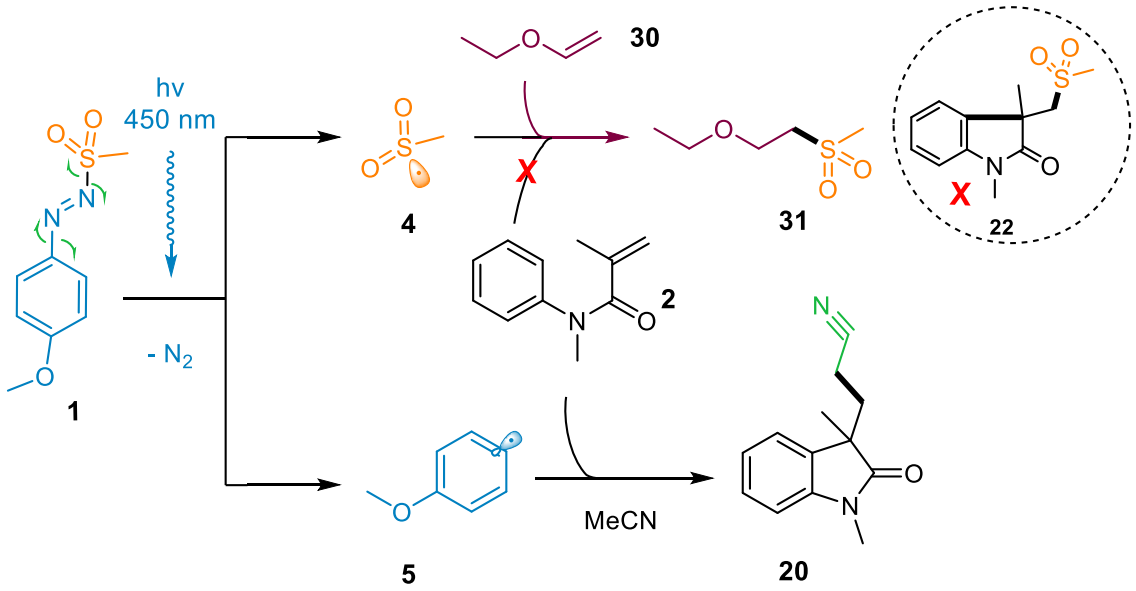

*SCHEME 3.3 Optimizing Solventylation: Ethyl Vinyl Ether **30** as a Reactivity Modulator*

To study the impact of the used of the additive, we analyzed yields and the ratio of product **20**, sulfonylated by-product **22**, and radical trap **2** by quantitative H^1NMR (qH^1NMR) spectroscopy method. Benzyl phenyl sulfide **32** in scheme 3.4, was employed as internal standard for this purpose due to its good solubility and non-overlapping chemical shifts with other relevant signals: δ 4.09 (s, 2H, CH_2) for the internal standard **32**, δ 3.19 (s, 3H, CH_3) for the product **20**, δ 4.97 - 5.04 (m, 2H, CH_2) for the radical trap

2, and δ 3.24 (s, 3H, CH_3) for the sulfonylated by-product **22**. The chemical shifts and corresponding multiplicities of the considered protons are depicted in Scheme 3.4. The experimental procedure involved allowing the reaction to proceed overnight under 450nm LED irradiation. Upon completion, the work-up included filtration through cotton. Following this, 10 mg of the internal standard **32**, accurately weighed using an analytical balance, was introduced into the mixture. Subsequently, the mixture underwent analysis through H^1NMR. Regrettably, this method did not yield reliable results, presumably because the potent oxidant, potassium persulfate, present in the reaction environment, likely oxidized the internal standard to sulfoxide, subtracting it from the reaction environment therefore rendering the quantification process unattainable[66].

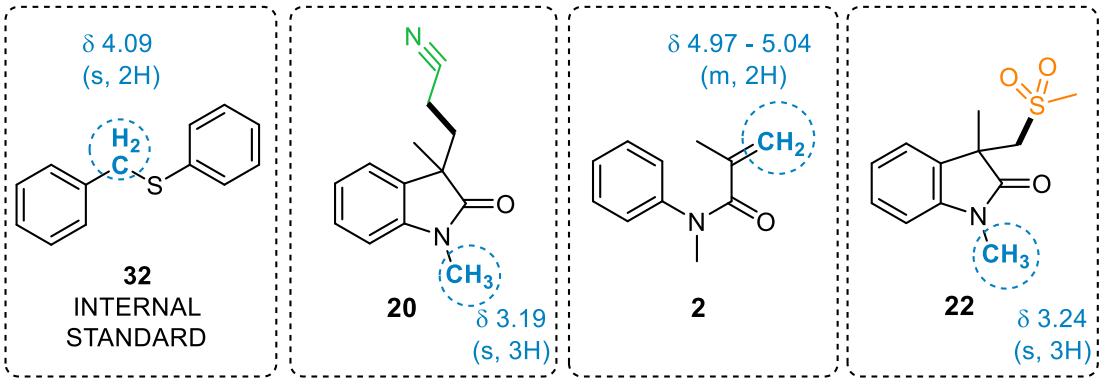

SCHEME 3.4 Quantitative H^1NMR Analysis of Solventylation: Chemical Shifts and Compound Identities

In our pursuit of evaluating the additive's impact on the solventylation process, we conducted a trial using arylazosulfone **1** and radical trap **2** in acetone. The analysis considered the weighted outcomes post-FC purification, revealing a 51% yield for the desired product **19** and an 18% yield for the sulfonylated by-product **22**. Additionally, we observed 28% of unreacted radical trap **2** after purification. This outcome, when compared to the reaction in acetone without the additive, where we achieved a 72% yield for the desired product **19** and a 7.5% yield for the sulfonylated by-product **22**, indicates a negative impact on the reaction outcome.

As we proceed in the process of improving the conditions for an enhanced solventylation process, investigations from experiments conducted using aryl azosulfone **1** and radical trap **2** in acetone, illustrated in scheme 3.5, revealed a substantial impact of the reaction environment, specifically the presence of an argon atmosphere.

Significantly, the reaction conducted in an argon environment demonstrated a substantial 72% yield for product **19**, whereas an identical reaction without argon yielded only 40% for the same product. In the presence of an argon atmosphere, we not only attained a substantial product **19** yield of 72% but also observed a minimal recovery of 7% of unreacted initial quantity of radical trap **2**. This outcome suggests that 93% of the

radical trap actively engaged in the solventylation reaction, leading to the desired product **19** as the major outcome.

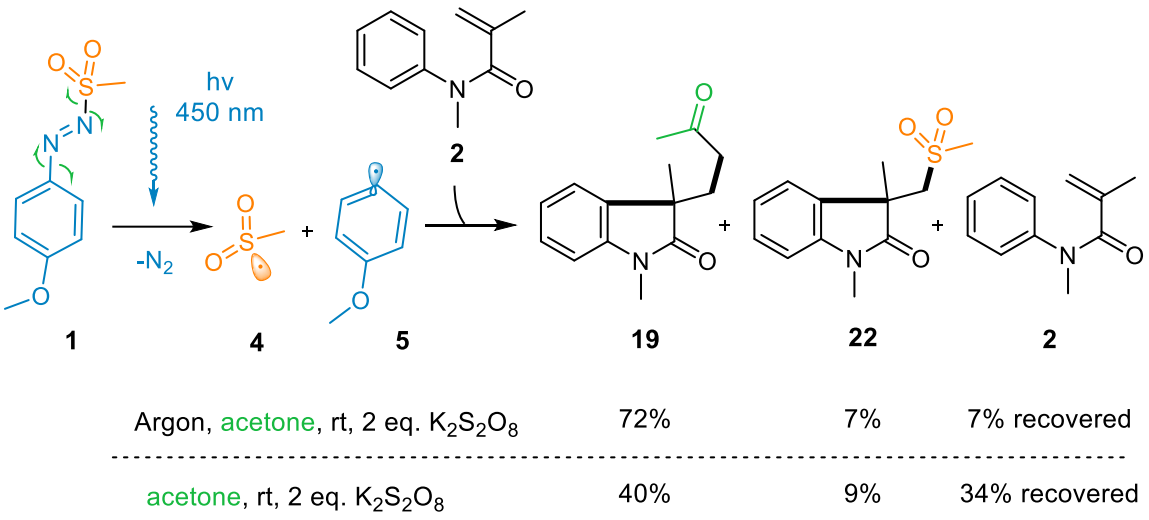

SCHEME 3.5 Impact of an Argon Environment in the Solventylation Process

Conversely, the reaction conducted without argon resulted in a significantly lower product **19** yield of 40%. This disparity is attributed to the amphiphilic reactivity of the aryl radical **5**, which probably tends to interact with the molecular oxygen naturally present in the environment, diverting it from the intended reaction pathway[67]. This interaction led to a higher recovery of the unreacted radical trap **2**, subsequently reduce yields for the desired product **19** and slightly increasing the presence of the undesired sulfonylated by-product **22**. This slight increase may be attributed to a greater availability of radical trap **2** for the reactive sulfonyl radical **4** in the absence of argon. The 34% recovery of radical trap **2** after FC purification indicates that only 66% of the radical trap **2** participated in the reaction. These results are outlined in scheme 3.5.

Having established the importance of an argon atmosphere for the solventylation reaction, we commence a screening process to explore a range of conditions, as outlined in the subsequent series of tests. However, these experiments, initially intended to deepen our understanding of the solventylation process, were excluded from the optimization process due to unattainable results caused by data incompatibility with the qH^{1}NMR method. This issue arose, as mentioned, from the presence of the potent oxidant, potassium persulfate, in the reaction environment, which likely oxidized the internal standard, subtracting it from the reaction environment and rendering the data unattainable.

For the next experiments, it's noteworthy that when referring to 'solids,' it denotes a mixture of compounds, specifically aryl azosulfone **1** and radical trap **2**, existing in a solid state. Likewise, when mentioning an 'additive,' it consistently refers to the additive ethyl vinyl ether **30**. All these experiments were conducted using aryl azosulfone **1** and radical

trap **2** in MeCN leading to the formation of product **20**. Scheme 3.4 illustrates the product **20**, the internal standard **32**, the radical trap **2** and the sulfonylated by-product **22**, along with their corresponding chemical shifts and multiplicity considered for the qH^1NMR method.

We intended to thoroughly investigate the roles played by an argon atmosphere and the impact of oxygen in the reaction mixture. Experiments were conducted introducing varying amounts of oxygen (1, 2, 3, and 4 mL of air) into the reaction mixture before subjecting it to 450nm LED irradiation. Simultaneously, we investigated the effects of degassing the solution with argon and without argon.

A comprehensive series of experiments were developed to analyze various influential factors. The impact of temperature was studied through tests conducted at 0°C and -15°C. At 0°C, six vials were prepared, with the first four involving the degassing of solids with argon. The experiments included setups with no additive and no air, 1 equivalent of additive with no air, no additive with 2 mL of air, and 1 equivalent of additive with 2 mL of air. The remaining two tests omitted the argon degassing, exploring conditions without additive and air, and with 1 equivalent of additive and no air.

Extending our investigation to -15°C, six additional experiments were conducted. These encompassed scenarios with no additive and no air, 1 equivalent of additive with no air, no additive with 2 mL of air, 1 equivalent of additive with 2 mL of air, 0.5 equivalents of additive with no air, and 0.5 equivalents of additive with 2 mL of air. The concentration of the reaction mixture was also studied. Six tests were performed with concentrations of 0.01M, 0.02M, and 0.005M, each with 1 equivalent of additive. Subsequent tests with the same concentrations omitted the additive.

To an improved understanding of the influence of the additive, a set of experiments was initiated at 1.5 equivalents, with and without argon degassing of the solid mixture. In a final set of six vials, the impact of air, without argon degassing, was explored with 2.5 mL of air.

Unfortunately, the results of these experiments, as mentioned, were not reliable due to data incompatibility with the qH^1NMR method. It is important to note that in the solvent screening of aryl azosulfone **1**, the impact of an argon atmosphere illustrated in Table 3.1 in the solvenylation process, and for the subsequent trails in the upcoming chapters, our exclusive reliance was on results obtained from the FC purification process and yields calculated from the weighted outcomes and not from the qH^1NMR method.

In our pursuit of understanding the temperature's impact on the solventylation process, we conducted an experiment employing arylazosulfone **1** and radical trap **2** in acetone at 0 °C. The analysis, considering weighted outcomes post-FC purification, revealed a 61% yield for the desired product **19** and a 12% yield for the sulfonylated by-product **22**.

Additionally, we observed 19% of unreacted radical trap **2** after purification. Comparatively, the reaction in acetone at room temperature yielded a 72% yield for the desired product **19** and a 7.5% yield for the sulfonylated by-product **22**. This suggests that reducing the reaction temperature to 0 °C does not enhance the solventylation process.

3.2 Exploring the Synthetic Scope of Aryl Azosulfones

In this section we explore the synthetic scope of five distinct aryl azosulfones, consistently employing radical trap **2**. Each experiment was studied to improve the solventylation process, with a specific goal of reducing sulfonylated by-products.

Chapter 3.2.1 introduces the first experiments using a phenyl substituent in the sulfone moiety. In Chapter 3.2.2, we extend our investigations to aryl azosulfones featuring a *para*-tolyl substituent, contributing to optimized conditions and a clearer understanding of the solventylation process. Chapter 3.2.3 explores a *tert*-butyl substituent, aiming to minimize undesired by-products. In Chapter 3.2.4, we evaluate an aryl azosulfone with both *tert*-butyl and *para*-acetyl substituents, optimizing conditions for improved yields and reaction selectivity. The final exploration, detailed in Chapter 3.2.5, involves an aryl azosulfone with a phenyl and *para*-acetyl, revealing challenges in different solvents and emphasizing the intricate interplay between substituents. These experiments collectively enrich our understanding of aryl azosulfone behavior, providing valuable insights into factors influencing the solventylation process.

All reactions detailed in this section employed radical trap **2**, 2 equivalents of $K_2S_2O_8$, argon degassing and 450 nm LED irradiation overnight. Unless specified otherwise, we used 1 equivalent of arylazosulfone at room temperature. Reported yields were calculated based on the weighted compounds obtained after FC purification.

3.2.1 Aryl Azosulfone with a Phenyl Substituent in the Sulfone Moiety

Our initial focus turned to aryl azosulfone **32**, as depicted in scheme 3.6, featuring a phenyl group in the sulfone moiety. The rationale behind this choice was the anticipation of a more stable and less reactive sulfur-centered radical, aiming to reduce its interaction with radical trap **2** and, consequently, reducing the formation of sulfonylated by-product **33**.

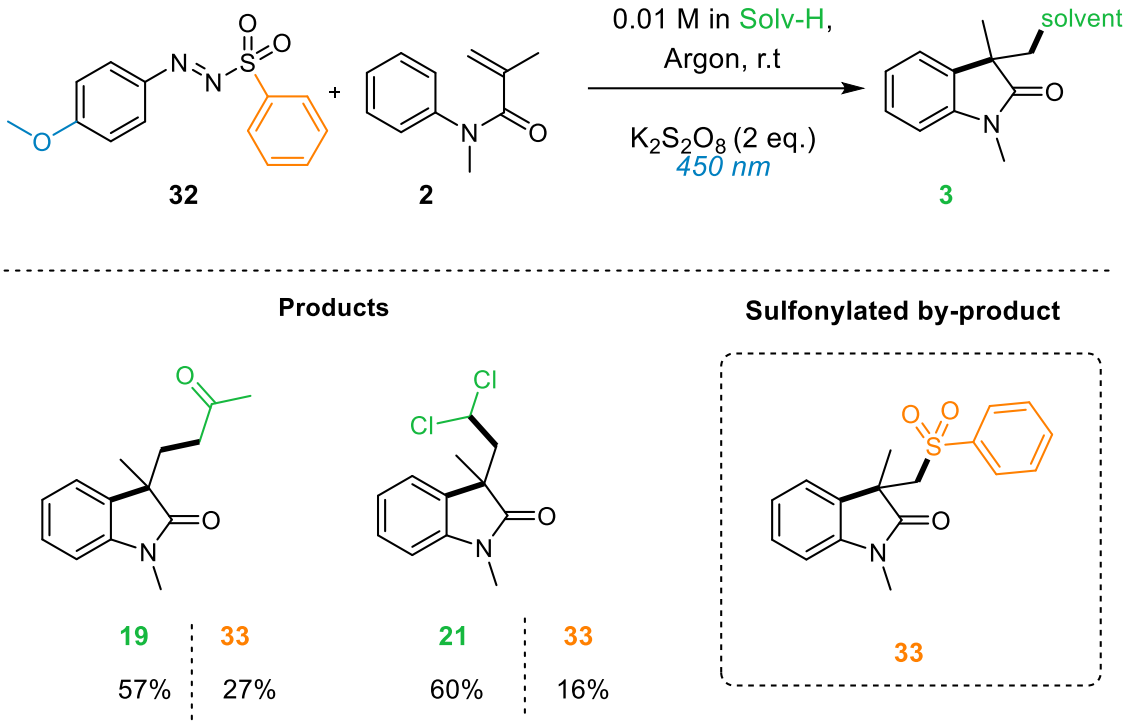

SCHEME 3.6 Scope of Aryl Azosulfone: a Phenyl Substituent in the Sulfone Moiety

Despite these expected advantageous characteristics, when compared to the results obtained with aryl azosulfone **1**, this precursor yielded a lower product yield of 57% in the case of acetone **19** and a slightly improved yield of 60% for the dichloromethane product **21**, scheme 3.6. Although, the use of dichloromethane resulted in a decreased yield of the sulfonylated by-product **33** at 16%, whereas acetone saw an increase in the sulfonylated by-product **33** yield to 27%. These outcomes underscore the delicate balance between radical stability and reaction efficiency as we proceed in our investigation to enhanced results.

3.2.2 Aryl Azosulfone with a para-tolyl Substituent in the Sulfone Moiety

We then expanded our investigations on the impact of the *para*-tolyl substituent in the sulfone moiety, as depicted in scheme 3.7. Dichloromethane (DCM) was selected as the solvent for this experiment. Our objective was to determine whether this modification could enhance the yield of the desired product **21** while reducing the formation of the sulfonylated by-product **35**. The latter is formed through the addition of the *para-tolyl* sulfonyl radical to the radical trap **2**. We hypothesized that the *para-tolyl* sulfonyl radical might exhibit lower reactivity, consequently reducing the formation and subsequently, the yield, of the sulfonylated by-product **35**.

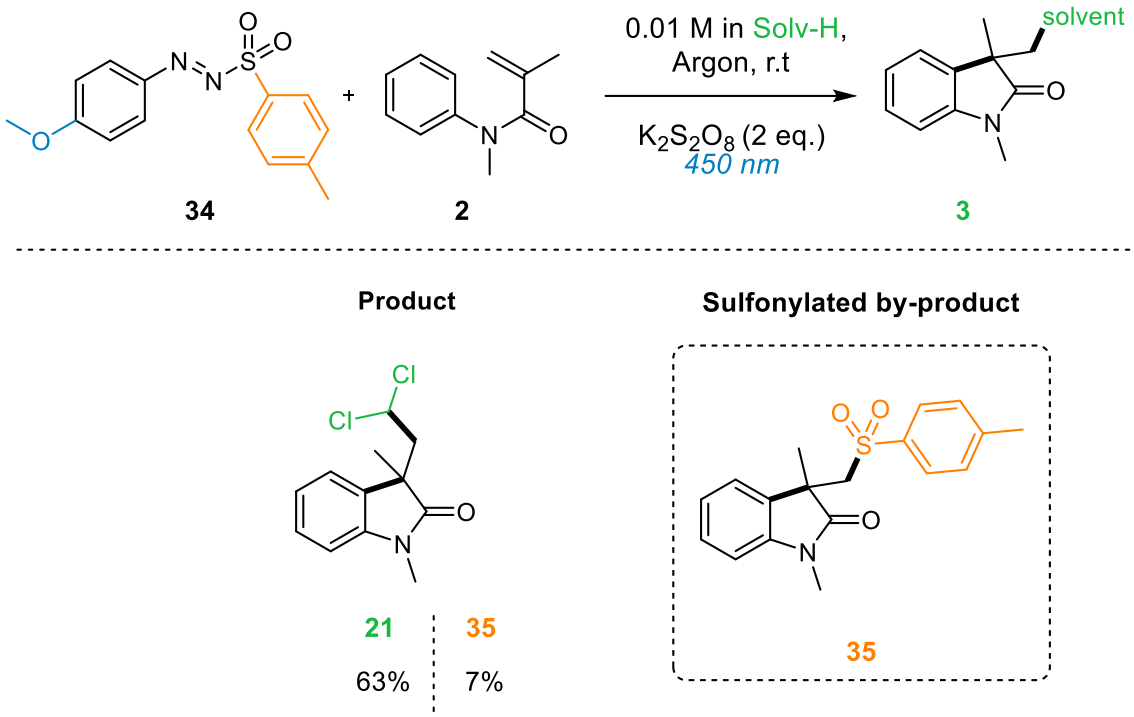

SCHEME 3.7 Scope of Aryl Azosulfone: a p-tolyl Substituent in the Sulfone Moiety

When compared to the results obtained with aryl azosulfone **32** in DCM**,** we observed a slight increase in the yield of product **21** to 63%, and a corresponding decrease in the yield of sulfonylated by-product **35** to 7%, scheme 3.7. These findings suggest that the anticipated decrease in reactivity of the *para*-tolyl sulfonyl radical has likely been achieved. This reduction appears to have effectively mitigated the generation of the undesired sulfonylated by-product **35**, all the while preserving a satisfactory yield of the desired product **21**.

3.2.3 Aryl Azosulfone with a tert-butyl in the Sulfone Moiety

We then decided to focus on a particularly promising experimental approach proposed by a PhD student. This approach involved, the structural modification of the aryl azosulfone experimenting with the sulfone moiety, in this case with a *tert*-butyl substituent. This structural alteration aimed to result in, upon photolysis, a less reactive sulfur-centered radical, thus minimizing the formation of undesired sulfonylated by-products. A more oxidizing radical species was also desired, capable of executing the oxidation step without the need for an external oxidant. However, adjusting the redox properties of the sulfur-centered radical posed challenges, primarily attributable to the restricted synthetic methodologies available for azosulfones.

In scheme 3.8a, we expected the aryl azosulfone **36** with a *tert*-butyl substituent in the sulfone moiety to follow a specific pathway under 450 nm LED irradiation. This pathway

involved the photolysis of the studied aryl azosulfone **36**, leading to fragmentation and the generation of the desired aryl radical **5** along with *tert*-butyl sulfonyl radical **37**. The release of SO_2 during this process resulted in the formation of *tert*-butyl radical **38**. In a strong oxidizing environment, *tert*-butyl radical **38** was supposed to swiftly oxidize into cation **39**. The final goal of this sequence was to produce gaseous isobutene **40**. This well-planned cascade aimed to prevent any interaction of *tert*-butyl sulfonyl radical **37** with the radical trap **2**, thereby avoiding the formation of undesired sulfonylated derivative by-products.

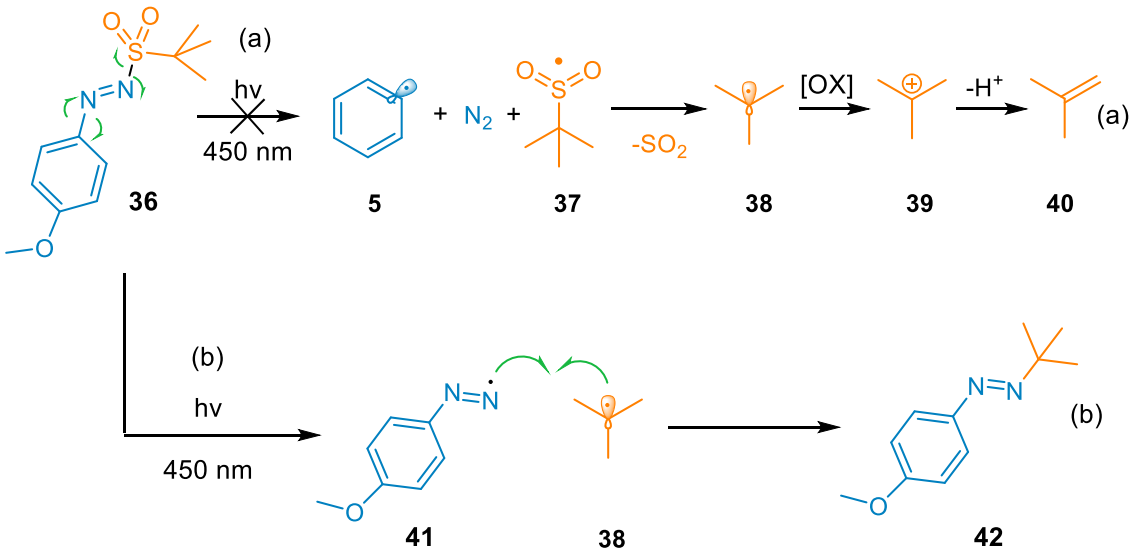

*SCHEME 3.8 The formation of Azoderivative **42** occurred via pathway (b) instead of the anticipated pathway of fragmentation, oxidation, and elimination of the precursor **36** (a)*

In line with our theoretical expectations, we conducted three experiments utilizing aryl azosulfone **36** with acetone as the solvent, as depicted in Scheme **3.9**. The first experiment was conducted at room temperature using 1 equivalent of aryl azosulfone **36**. In the second experiment, the reaction temperature was raised to 35 °C while still using 1 equivalent of aryl azosulfone **36**. The last experiment was carried out at 35 °C, employing 2 equivalents of aryl azosulfone **36**.

The first experiment progress was monitored using Thin Layer Chromatography (TLC), which revealed an unreacted radical trap **2**, absence of the desired product **19**, and the presence of a more polar compound. H^1NMR analyses were performed to confirm the absence of the desired product **19**, unfortunately confirming the presence of a polar compound identified as structure **42**. This compound resulted from SO_2 extrusion from aryl azosulfone **36** and the addition of the tert-butyl radical **38**.

Unexpectedly, under these conditions, aryl azosulfone **36** deviated from the anticipated pathway **a** (as outlined in Scheme **3.8**), instead following path **b**. Unfortunately, the alkylation of radical trap **2** by the acetonyl radical did not occur, and

the desired solventylation product **19** was not obtained. Instead, we obtained by-product **42** with a yield of 30%. Table 3.1, Entry 1

This unexpected reactivity is attributed to the extreme instability of *tert*-butyl radical **38**, likely reacting with diazenyl radical **41** (path b in Scheme 3.8) before the release of molecular nitrogen—a crucial step for the required aryl radical formation in the solventylation process. Unfortunately, this phenomenon follows polarity matching in the radical coupling step, and additionally, the release of nitrogen is the rate-determining step in the aryl azosulfone fragmentation, further favoring the intermediate **41** and, therefore, favoring path b, generating by-product **42**.

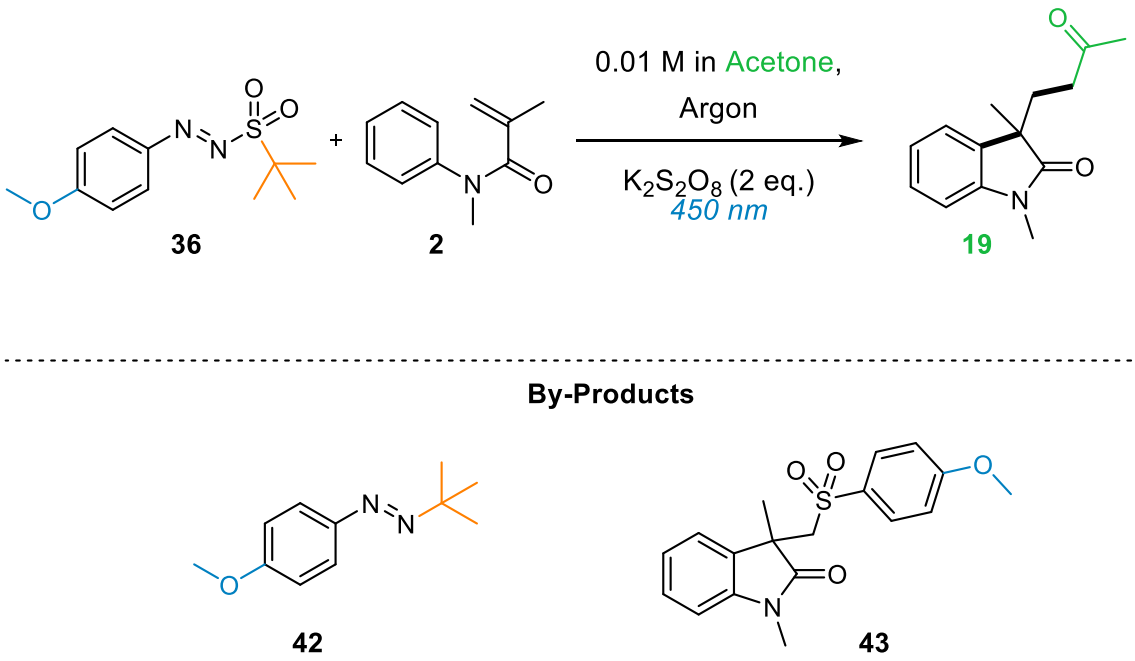

SCHEME 3.9 Scope of Aryl Azosulfone: a t-butyl in the Sulfone Moiety

For the second experiment, we subtly elevated the reaction temperature from room temperature to 35 °C. This modification aimed to enhance the liberation of molecular nitrogen, promoting the generation of the required aryl radical **5** for the subsequent solventylation process. Fortunately, this modification yielded product **19** with a satisfactory yield of 60%. And by-product **43** with a yield of 16%. Additionally, traces of compound **42** were observed in the initial fractions of flash chromatography obtained with a 4% yield (Table 3.1, Entry 2).

After observing positive results at 35 °C, we decided to investigate solventylation at this temperature to further improve the yield. In our usual procedure, we employ one equivalent of aryl azosulfone **36**, but in this experiment, we increased it to two equivalents. Surprisingly, this adjustment didn't lead to the expected improvement in product **19**. Instead, it resulted in a significant increase in the formation of by-product **42**, obtained with a 48% yield, while the yield of product **19** decreased to only 14%.

Additionally, we observed the by-product **43** with a substantial yield of 44%, indicating that a higher quantity of aryl azosulfone **36** at 35 °C intensifies reactivity along unintended pathways. This increased quantity had a detrimental effect on our planned solventylation process, particularly during the HAT step, favoring the formation of by-products **42** and **43**.

A proposed mechanism for generating by-product **43** is depicted in Scheme 3.10. The process initiates with the photolysis of aryl azosulfone **36** at 450 nm LED irradiation, causing fragmentation and generating the desired aryl radical **5**, molecular nitrogen, and sulfur dioxide. Subsequently, instead of reacting as planned with acetone through a HAT reaction, the aryl radical **5** interacts with sulfur dioxide. This interaction leads to the formation of sulfonyl radical intermediate **44**. Following this, sulfonyl radical intermediate **44** reacts with radical trap **2**, generating a sulfonyl-substituted alkyl radical **45**. Subsequent steps result in the cyclized by-product **43**. The structures of **43** was confirmed through H^1NMR and validated using gas chromatography-mass spectrometry (GC-MS).

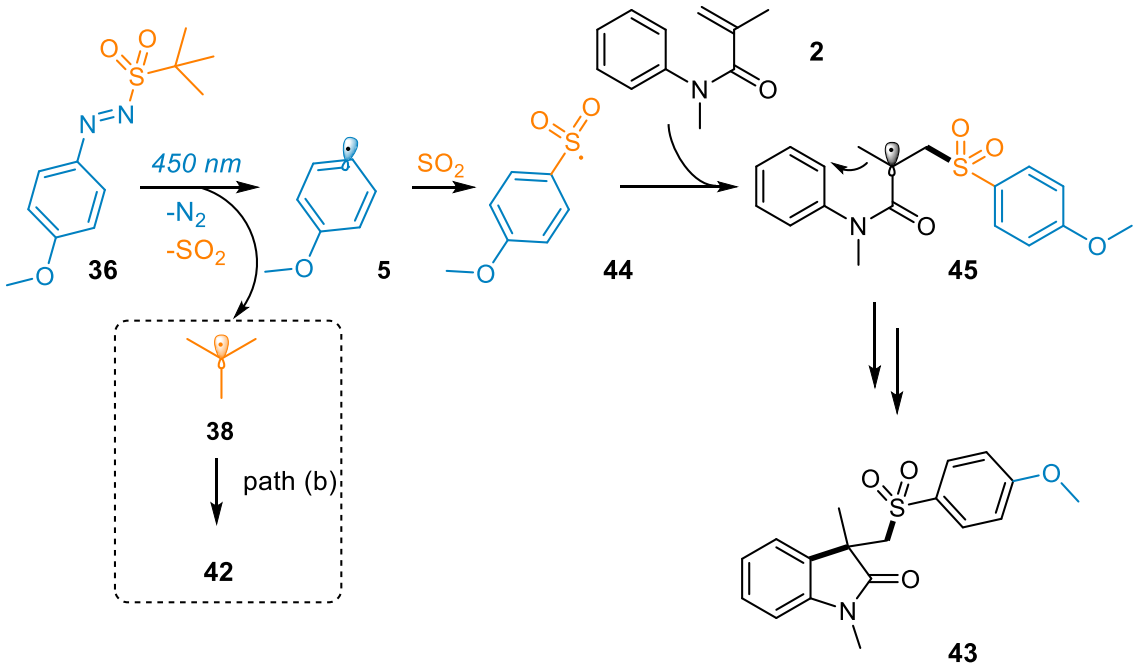

*SCHEME 3.10 Proposed Mechanism for Formation of By-product **43***

Notably, the generation of the *tert*-butyl radical **38** during this process**,** from aryl azosulfone **36**, results in the formation of by-product **42** following path **b**, as previously investigated. Both pathways leading to by-products **42** and **43** are enhanced when the reaction is carried out at 35°C using 2 equivalents of aryl azosulfone **36**. The results of this experiment are presented in Table 3.1, Entry 3.

Entry	Conditions	19 [%]	42 [%]	43 [%]
1	r.t, 1 eq. of **36**	-	30	-
2	35°C, 1 eq. of **36**	60	4	16
3	35°C, 2 eq. of **36**	14	48	44

Table 3.1 Experimental Outcomes with Aryl Azosulfone 36

Employing aryl azosulfone **36** at room temperature and at 35°C, a distinct temperature-dependent trend was observed. The heightened production of the target compound, **19**, is notably observed at 35°C. Notably, an increased quantity of substrate used **36** reveals a negative impact on the reaction yield for product **19**, concurrently facilitating the generation of by-products **42** and **43**. This observation suggests that, under these specific conditions, the methoxy radical **5** exhibits a significant preference for mechanistic pathways leading to the formation of by-products **42** and **43**, deviating from the intended solventylation process.

3.2.4 Aryl Azosulfone with a tert-butyl in the Sulfone Moiety and a para-acetyl in the aryl group

We then proceeded to evaluate the reactivity of aryl azosulfone **46**, as depicted in Scheme 3.11. In this series of experiments, we maintained the *tert*-butyl substituent in the sulfonyl moiety while introducing a *para*-acyl substituent in the aryl group.

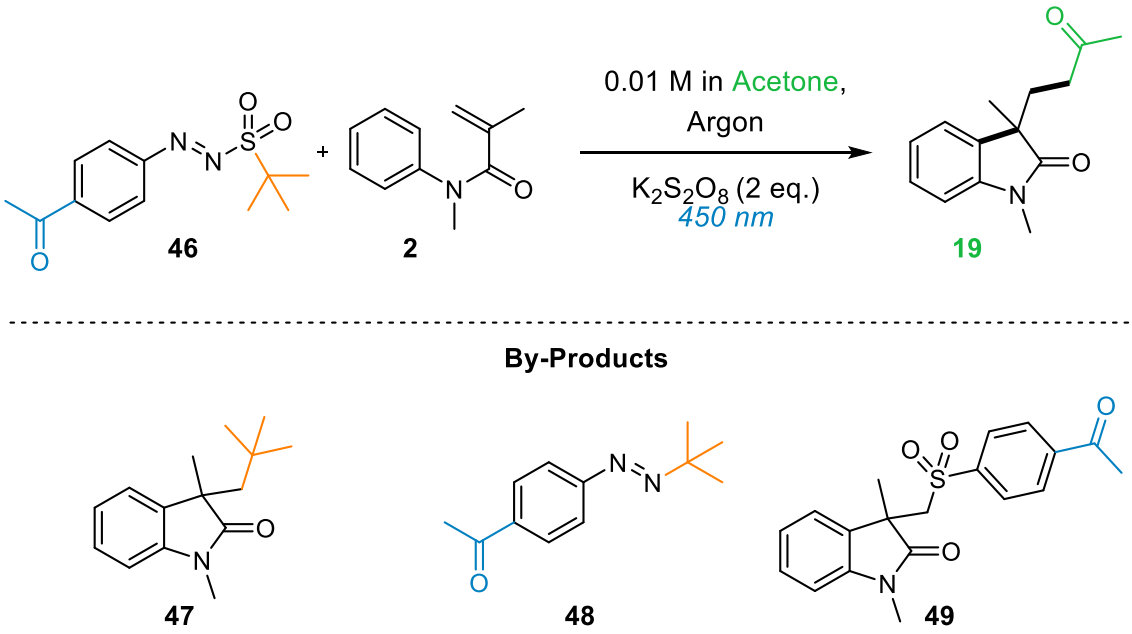

SCHEME 3.11 Scope of Aryl Azosulfone: a t-butyl in the Sulfone Moiety and a para-acetyl in the aryl group

We conducted five experiments. The first utilized 1 equivalent of aryl azosulfone **46** at room temperature. The second, performed at 35°C, also employed 1 equivalent of aryl azosulfone **46**. In the third experiment, we increased the quantity of aryl azosulfone **46** to 2 equivalents at 35°C. The last two experiments involved we slightly reduced to 1.25 equivalents the aryl azosulfone **46**, with the first conducted at room temperature and the last at 35°C.

In the initial experiment employing 1 equivalent of aryl azosulfone **46** at room temperature, the resulting crude mixture exhibited distinct signals suggesting the presence of unreacted radical trap **2**. Without further optimization, we directly tested 1 equivalent of aryl azosulfone **46** at 35°C, resulting in a satisfactory 72% yield of product **19**. Following FC purification, we isolated compounds **47** (17% yield), **48** (6% yield), and **49** (5% yield). The structures of **47** and **49** were confirmed through H^1NMR and validated using gas chromatography-mass spectrometry (GC-MS). The results of this experiment are detailed in Table 3.2, Entry 1.

Encouraged by the positive outcome, we proceeded with the solventylation reaction at 35°C, in this case using 2 equivalents of aryl azosulfone **46**. This adjustment resulted in a highly favorable 80% yield for the desired product **19**, with by-products yields of 5% for **48** and a slightly elevated 20% for **49**. Notably, there was an absence of by-product **47**. The results of this experiment are presented in Table 3.2, entry 2.

Building upon these promising results, we expanded our experiments to further explore aryl azosulfone **46** at both room temperature and 35°C, using a slightly reduced quantity of aryl azosulfone **46**, equivalent to 1.25 equivalents. Starting the reaction at room temperature with 1.25 equivalents yielded a low 30% yield for product **19**, along with 18% for by-product **48** and 8% for **49**, with no evidence of by-product **47**. Following FC purification, 42% of radical trap **2** was isolated, indicating that, under these conditions, only 58% of the radical trap had undergone reaction. The results of this experiment are detailed in Table 3.2, entry 3.

Conducting the same reaction at 35°C, however, resulted in a substantially improved yield of 77% for product **19**. Additionally, we observed a 5% yield for **47**, a reduced yield of 4% for by-product **48**, and a 17% yield for **49**. Following FC purification, only 12% of radical trap **2** remained unreacted, indicating that, in this case, 88% of radical trap **2** had undergone reaction. The results of this experiment are presented in Table 3.2, Entry 4.

Entry	Conditions	19 [%]	46 [%]	48 [%]	49 [%]
1	35°C, 1 eq of **46**	72	17	6	5
2	35°C, 2eq of **46**	80	-	5	20
3	r.t, 1.25 eq of **46**	30	-	18	8
4	35°C, 1.25 eq of **46**	77	5	4	17

Table 3.2 Experimental Outcomes with Aryl Azosulfone 48

In essence, the results obtained with aryl azosulfone **46** showed optimal conditions at 35°C using 2 equivalents of **46**, resulting in high product yields but also an increased presence of by-product **49**. We assume that elevated temperatures enhance aryl radical generation, facilitated by N_2 expulsion, influencing the production of desired product **19** and by-products **48** and **49**. Notably, at 35°C, **48** decreases in yield, suggesting in fact a limited lifetime for the intermediate containing N_2 group. The temperature-dependent enhancement is attributed to the extrusion of nitrogen as the rate-limiting step, lowering the energy barrier and promoting the formation of the reactive aryl radical essential for successful solventylation, resulting in the desired product **19** and, unfortunately, increase of also by-product **49**[68,69].

To conclude this series of experiments using the aryl azosulfone **46**, we attempted a last solventylation reaction with a different solvent, DCM, at 35°C, using 1.25 equivalents of aryl azosulfone **46**. Unfortunately, we obtained a low yield of 23% for product **21**. Additionally, most of the by-products were detected: **48** with a 7% yield, **49** with a 6% yield. What significantly impacted the results was the isolation of 66% of unreacted trap **2** after FC purification. It appears that these conditions, while effective for acetone, did not yield favorable results in DCM. The lower reactivity observed in DCM may be attributed to the higher value of C(sp^3)-H BDE measuring 97.3 kcal/mol, compared to 96.0 kcal/mol for acetonitrile and 95.9 kcal/mol for acetone.

3.2.5 Aryl Azosulfone with a phenyl in the Sulfone Moiety and a para-acetyl in the aryl group

For the final exploration within this context, we decided to investigate more the behavior of the substituent of the *para*-acyl in the aryl group using the phenyl substituent in the sulfonyl group's moiety **50** in two different solvents as depicted in Scheme 3.12. Our objective was to optimize the solventylation process in DCM.

In the initial experiment, we employed aryl azosulfone **50** and radical trap **2** in DCM. Unfortunately, despite subjecting the reaction to over 27 hours of exposure to a high-intensity blue LED at 450nm irradiation, the reaction crude displayed a ratio of radical trap **2**/product **21**/ to sulfonylated by-product **33** at **4:2:1**, respectively. The significant presence of unreacted trap **2** in the reaction crude indicated that the desired solventylation process wasn't favored using this type of aryl radical precursor under these conditions.

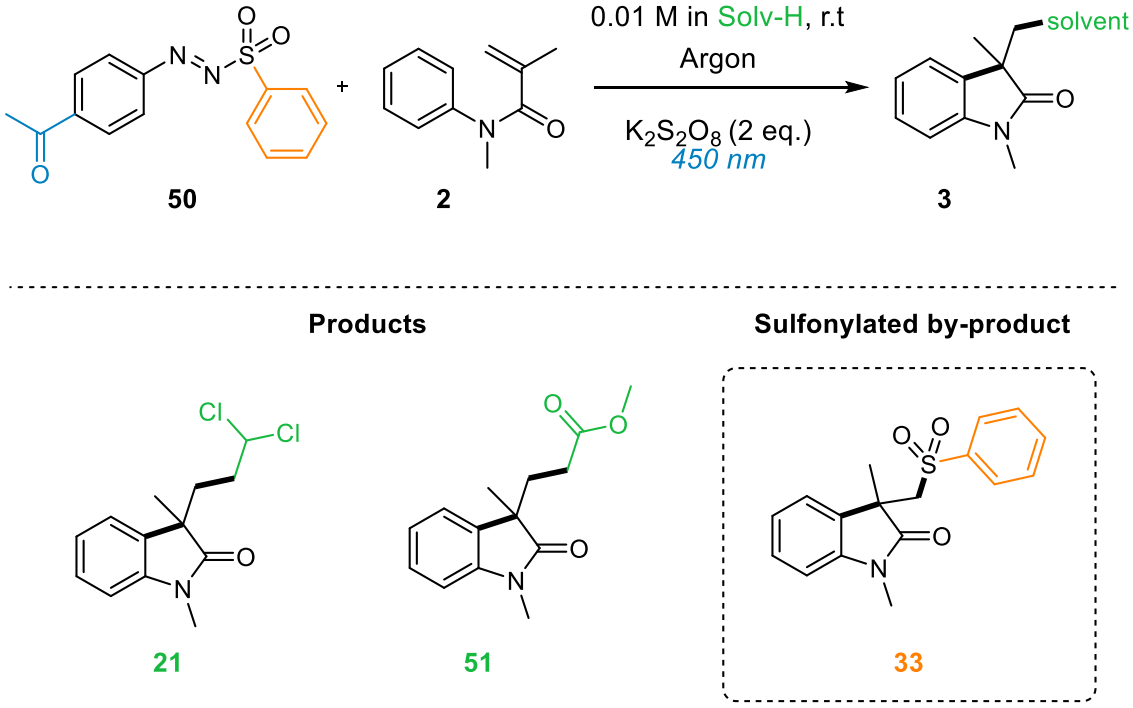

SCHEME 3.12 Scope of Aryl Azosulfone: a phenyl in the Sulfone Moiety and a para-acetyl in the aryl group

Following this, we explored the application of aryl azosulfone **50** with a different solvent, methyl acetate, to obtain product **51**. This reaction was monitored via TLC and H^1NMR. The H^1NMR analysis confirmed a significant presence of unreacted radical trap **2** in the reaction mixture, resulting in an 80% yield of unreacted trap **2** and a very low yield of 13% for the desired product **51** after FC purification, as depicted in Scheme 3.12

Additionally, fractions containing a derivative, possibly the by-product **48**, and the sulfonylated by-product **33**, were observed. Quantifying these by-products proved challenging due to impurities in the fractions and the limited amounts of these substances. These results suggest that the reactivity of aryl azosulfone **50** appears to be relatively lower, leading to the generation of aryl radicals with reduced efficiency under these conditions.

The particularity of the product **51** obtained using methyl acetate in the solventylation process is that the *para*-acetyl aryl radical **52** in scheme 3.13 generated, selectively

abstracted the protic C(sp^3)-H bond in methyl acetate, despite its higher BDE of 97.1 kcal/mol, leading to the formation of an electrophilic radical. This behavior appears to disregard the presence of the hydridic hydrogen, which has a lower BDE of 96.7 kcal/mol.

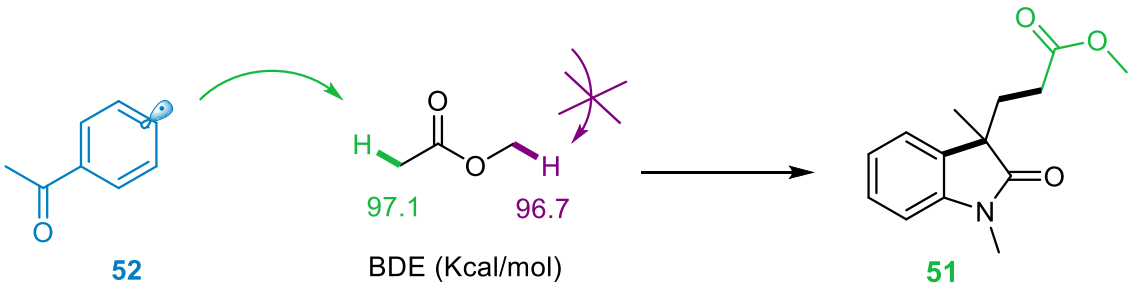

SCHEME 3.13 HAT Reactivity of para-acetyl Aryl Radical with Methyl Acetate

This las two experiments using aryl azosulfone **50** highlights the intricate interplay between the reactivity of the substituent within the sulfonyl moiety and the substituent in the aryl aromatic ring, ultimately influencing the outcome of the solventylation process using various solvents.

3.2.6 Discussion

Our investigation, focusing on the synthetic scope of six distinct aryl azosulfones employing radical trap **2**, aimed at improving the solventylation desired product while minimizing sulfonylated by-products. The experimentations explore the impact of various substituents on the sulfone moiety and aryl aromatic ring, providing insightful details into the complexities of the solventylation process. Summarizing the key outcomes, Table 3.3 presents the best results obtained with each tested aryl azosulfone at the conclusion of this chapter.

For the subsection 3.1 optimization of reaction conditions for enhanced solventylation, results obtained using aryl azosulfone **1** highlights the important role of the solvent in determining both product yield and the formation of sulfonylated by-product **22**. Acetone exhibited satisfactory performance, yielding a remarkable 72% of product **19** and a low 7.5% of sulfonylated by-product **22**. These results, being the best obtained using arylazosulfone **1** and radical trap **2**, are presented in Table 3.3, entry 1. In contrast, MeCN and DCM displayed moderate yields of 50% for products **20** and **21**, respectively, with higher sulfonylated by-product percentages (32% and 36%). Attempts to reduce sulfonylated by-product **22** formation through an additive, ethyl vinyl ether **30**, didn't demonstrate a positive impact on the outcome of the solvenylation reaction.

For the subsection of 3.2 exploring the synthetic scope of aryl azosulfones. the results observed from aryl azosulfone with a phenyl substituent **(32)** indicate us that introducing a phenyl substituent aimed at stabilizing the sulfur-centered radical, potentially reducing undesired interactions with radical trap **2**. However, yield for desired product **21** using DCM was lower compared to aryl azosulfone **1**, showcasing the delicate balance between radical stability and reaction efficiency. Table 3.3, entry 2.

Aryl azosulfone with a *para*-tolyl substituent **(34)** explorations revealed a slight increase in product yield in DCM, a successful reduction in reactivity of *para*-tolyl sulfonyl radical was obtained, minimizing the sulfonylated by-product. This observation contributes to our understanding of substituent influence on reaction dynamics. Table 3.3, entry 3.

Aryl azosulfone with a *tert*-butyl substituent **(36)** in acetone aimed at minimizing undesired by-products, but unexpected reactivity deviations occurred. Adjustment of reaction temperature proved crucial for optimizing conditions. Elevated substrate quantities adversely affected desired product **19** yield, promoting formation of by-products **42** and **44**, indicating a temperature-dependent phenomenon. Table 3.3, entry 4.

Aryl azosulfone with a *tert*-butyl and *para*-acetyl substituent **(46)** in acetone evaluation revealed favorable conditions at 35°C and 2 equivalents of **46**, yielding high product **19** yields but unfortunately with high presence of by-products (by-products **48** and **49**). The temperature-dependent enhancement highlighted the role of thermal heating in influencing solventylation, with an increased presence of by-product **49** observed at 35°C. Table 3.3, entry 5.

Aryl azosulfone **(50)** showed reduced product yield, indicating a complex interplay among substituents. Reactivity variations in different solvents highlight challenges in optimizing the solventylation process for aryazosulfones. Table 3.3, entry 6.

Entry	Aryl Azosulfone	Conditions	Desired Product Yield [%]	Yield of Major By-Products [%]
1	1	Acetone, r.t	72 (Product **19**)	7.5 (By-Product **22**)
2	32	DCM, r.t	60 (Product **21**)	16 (By-Product **33**)
3	34	DCM, r.t	63 (Product **21**)	7 (By-Product **35**)
4	36	Acetone, 35°C, 2 eq.	60 (Product **19**)	16 (By-Product **42**)
5	46	Acetone, 35°C, 2 eq.	80 (Product **19**)	20 (By-Product **49**)
6	50	Methyl acetate, r.t	13 (Product **51**)	-

Table 3.3 Best Results Obtained with Each Aryl Azosulfone Tested

3.2.7 Synthesis of the Diversely Substituted Aryl Azosulfones

This section provides an overview of how the aryl azosulfones used in Chapter 3.1 and 3.2 were synthesized during the research studies. We synthesized these aryl azosulfones from benzenediazonium tetrafluoroborate **53**, using two different salts, 4-methoxybenzenediazonium tetrafluoroborate **55** (Scheme 3.14, Entry 1-4) and the second one was 4-acetylbenzenediazonium tetrafluoroborate **56** (Entry 5-6). These functional groups leaded to the formation of the 4-methoxyphenyl radical and the 4-acetophenone radical after the N-S bond homolysis and N_2 ejection under 450 nm LED irradiation during the solventylation process.

By employing benzenediazonium tetrafluoroborate **53** with sodium sulfinate **54** having various substitutions, we synthesized a total of six aryl azosulfones for our study. We also conducted the synthesis of sodium sulfinate salts with a *tert*-butyl substituent **60** (Entry 4-5) during these studies, and the reactions series for their production are detailed briefly. The other starting materials were provided by Università degli Studi di Pavia or were synthesized by a previous PhD student.

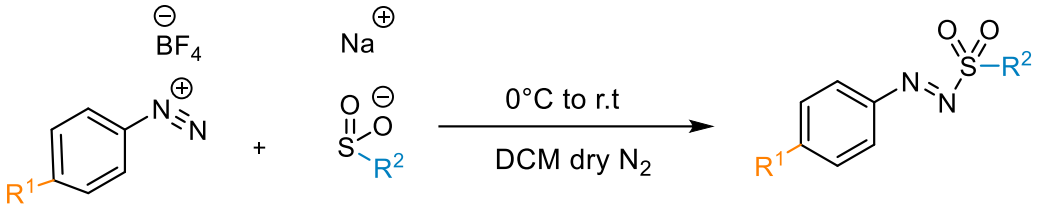

53 54

Entry						yield %
1	R^1:	OMe	*55*	R^2: Me	*57*	*73
2		OMe		Ph	*58*	53
3		OMe		*p-tolyl*	*59*	*63*
4		OMe		*t-butyl*	*60*	*67*
5		-$COCH_3$	*56*	*t-butyl*		*60*
6		-$COCH_3$		Ph		80

*SCHEME 3.14 Synthesis of Diversely Substituted Aryl Azosulfones. * A Ph.D. student contributed the reported yield for this entry.*

The synthesis of the diversly substituted aryl azosulfones started by adding substrates at 0°C and allowing the reaction to proceed at room temperature overnight. We isolated the products from the substrate salts through FC purification, resulting in moderate to good yields as illustrated in Scheme 3.14.

To obtain aryl azosulfones from entry 1 to entry 4, we employed 4-methoxybenzenediazonium tetrafluoroborate **55** obtained through the diazotization reaction of 4-methoxyaniline **61**, fluoroboric acid and sodium nitrate at -20 °C.

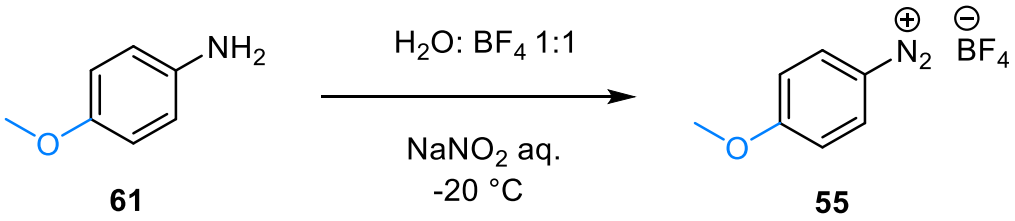

61 55

SCHEME 3.15 Diazotization Reaction

To obtain aryl azosulfones from entry 4 and 5, a multi-step synthesis process involving oxidation, chlorination, and hydrolysis reactions was employed, as outlined in Scheme 3.16. The process commenced with the oxidation of *di-tert*-butyldisulfane **62**, utilizing a 30% hydrogen peroxide solution in acetic acid at a cryocool apparatus set at 0°C. This reaction was allowed to proceed overnight, resulting in the formation of compound **63**. Following the reaction, a workup was performed involving treatment with a basic solution

containing sodium bicarbonate to neutralize any remaining acid, followed by treatment with a solution of sodium bisulfate to degrade any residual hydrogen peroxide.

Subsequently, the chlorination of **63** in dichloromethane was carried out by slowly adding sulfuryl dichloride **64**, also dissolved in DCM, at 0°C. This step led to the formation of sulfinic chloride **65**. The sodium *tert-butyl* sulfinate **66** was prepared by treating **65** in a water and ice bath, followed by the addition of an aqueous basic NaOH solution, allowing the reaction to proceed for one hour. Afterward, a filtration process using a Buchner funnel yielded a cloudy solution, and the structure of **66** was verified via H^1NMR analysis with deuterated water as the solvent.

Finally, the salt **66**, along with benzenediazonium tetrafluoroborate **55** featuring a methoxy substituent in the para position, and **56** with an acyl substituent in the para position, were utilized to obtain the desired aryl azosulfones **36** and **46**, respectively.

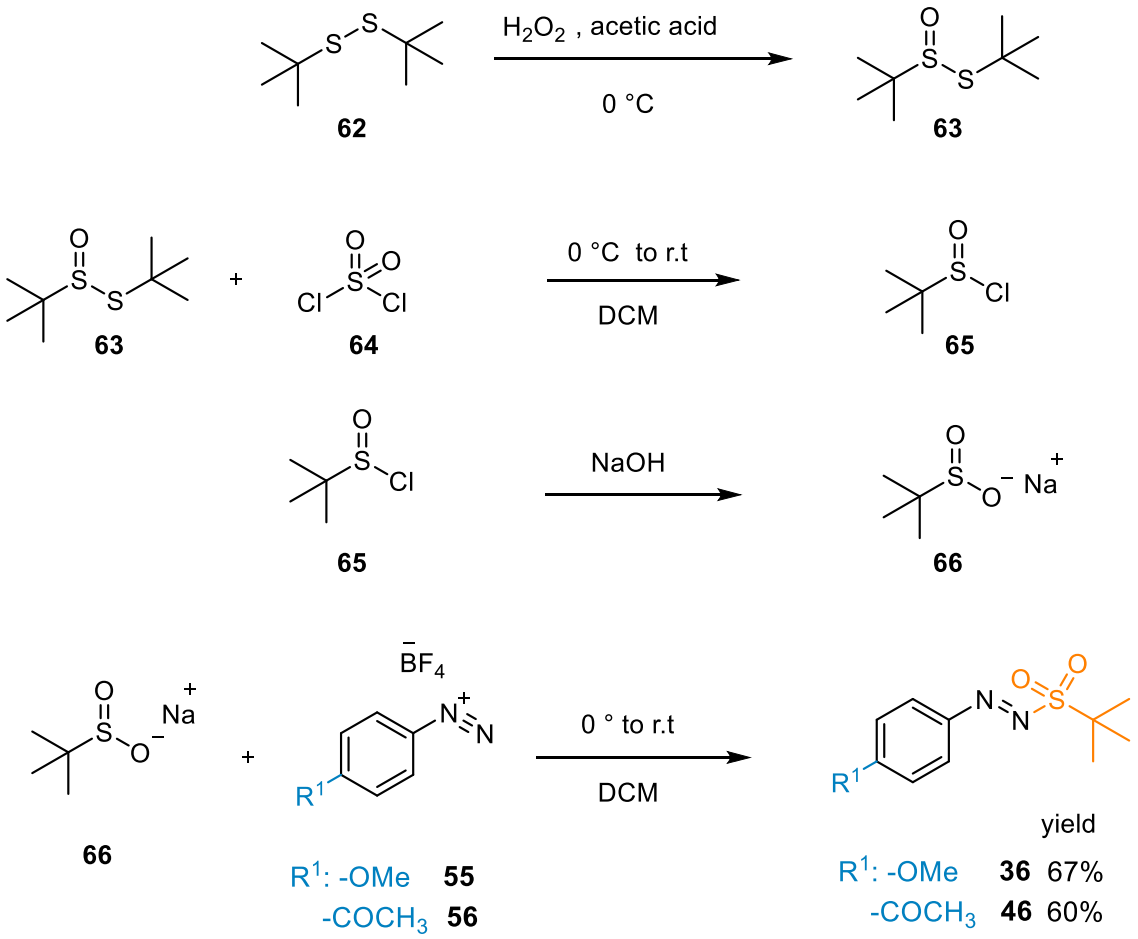

*SCHEME 3.16 Series of Reactions to Obtain Aryl Azosulfone **36** and **46***

Aryl azosulfones **36** and **46** were successfully synthesized with moderate yields, employing the corresponding benzenediazonium tetrafluoroborate and **66** in the synthesis

process. The synthesis of aryl azosulfones **36** and **47** was conducted multiple times due to the high sensitivity of reactants, particularly **64** and **65**. Notably, we achieved a 60% yield for aryl azosulfone **36** and a 67% yield for aryl azosulfone **46**. These results were obtained after a careful handling during the process, considering the inherent sensitivity of these compounds and reactions.

3.3 Exploring The Synthetic Scope of Radical Traps

In this section, we investigate the effectiveness of three distinct radical traps, evaluating their performance with various solvents. The results reveal the synthesis of novel products for each radical trap, introducing valuable contributions to scientific literature. Having thoroughly examined radical trap **2** in chapters 3.1 and 3.2, our focus shifts to three different substituent radical traps. Initially, we explore *para*-acetyl and *para*-methoxy substituents in the aromatic ring, followed by testing a radical trap with a diverse substitution group featuring a benzyl group on the nitrogen atom. Summarizing the key outcomes, Table 3.4 presents the best results obtained with each tested radical trap at the conclusion of this chapter.

All reactions detailed in this section employed arylazosulfone **1**, 2 equivalents of $K_2S_2O_8$, argon atmosphere, and at room temperature under 450 nm LED irradiation overnight. Reported yields were calculated based on the weighted compounds obtained after FC purification. All newly obtained products underwent characterization through H^1NMR, C^{13}NMR, COSY and HSQC analyses.

3.3.1 Radical Trap with a para-Methoxy Substituted Aryl Group

We started the investigation with radical trap **67**, featuring a *para*-methoxy substituent on the aryl group, outlined in scheme 3.17. In acetone, we achieved a 60% yield for product **68**, alongside a simultaneous observation of sulfonylated by-product **73** at 20%. Despite the undesirable yield for the sulfonylated by-product **73**, the absence of traces of unreacted radical trap **67** and a satisfactory product yield prompted us to extend our analysis to various solvents.

In MeCN, the desired product **69** showed a decreased yield of 43%, accompanied by a high yield of 57% for sulfonylated by-product **73**. Further investigations in DCM yielded moderate results, generating product **70** with a 63% yield and sulfonylated by-product **73** with a yield of 36%.

Continuing our solvent screening, we tested radical trap **67** in chloroform, obtaining the desired product **71** with a 68% yield and a 32% yield for sulfonylated by-product **73**. In the final trial with ethyl formate as a solvent, we obtained a low yield of 9% for product **72** and a high yield of 50% for sulfonylated by-product **73**. The low yield for product **72** was accompanied by the presence of 41% unreacted radical trap **67** suggests that its reactivity was not sufficiently high or selective for generating the desired product.

This investigation unveiled that under the given conditions for the solventylation process, radical trap **67** with arylazosulone **1** displayed a pronounced susceptibility to the addition of the sulfonyl radical, leading to higher yields of sulfonylated by-product **73** than initially anticipated.

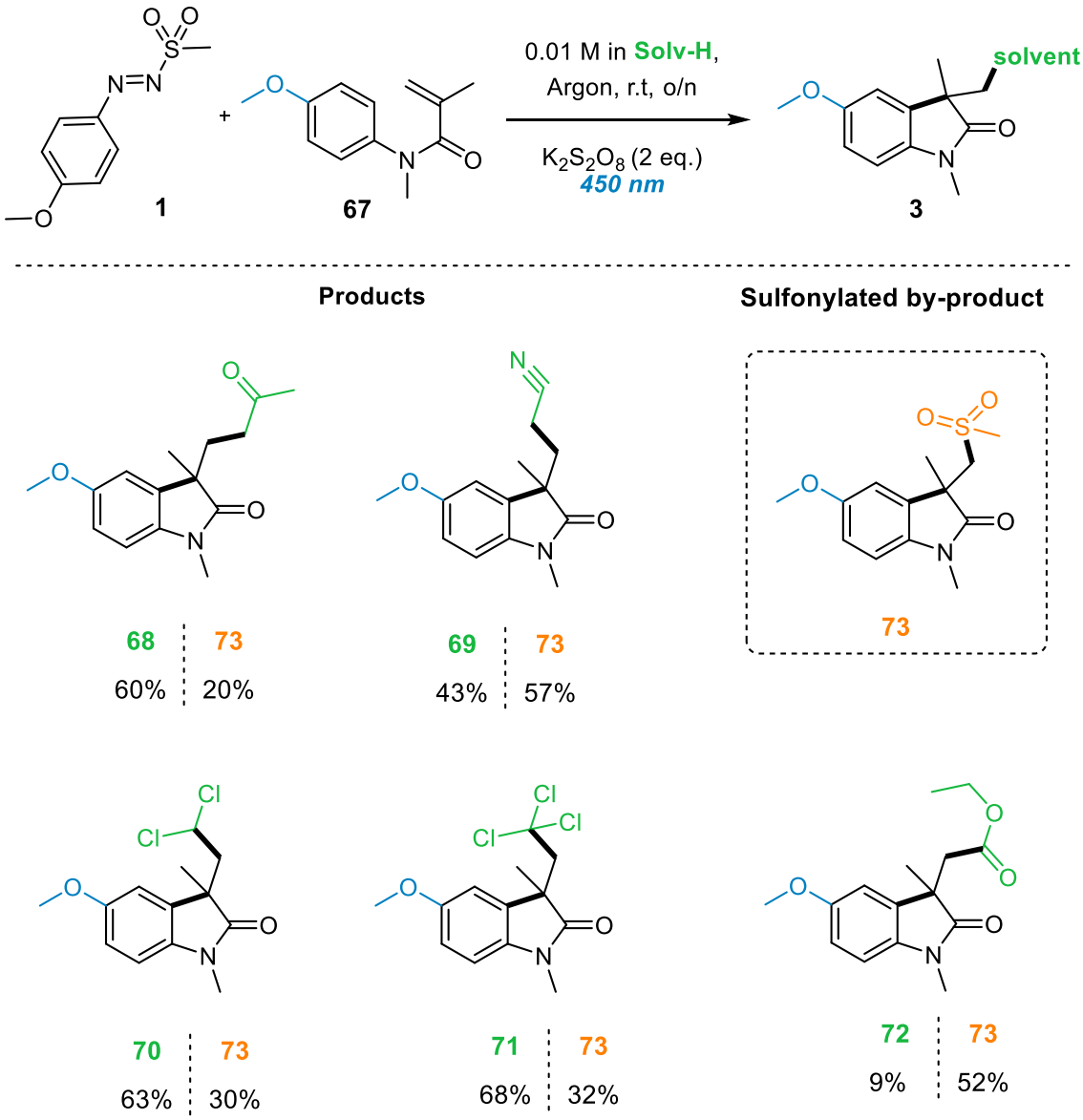

SCHEME 3.17 Scope Radical Trap with a Para-Methoxy Substituted Aryl Group

3.3.2 Radical Trap with a para-Acetyl Substituted Aryl Group

Our investigations advanced to radical trap **74**, distinguished by a *para*-acetyl substituent on the aryl group as delineated in scheme 3.18. Upon conducting three successive trials in acetone, the desired solventylation product **75** was obtained with a 44% yield, accompanied by a sulfonylated by-product **76** with 15% yield. Considering the limited reactivity of radical trap **74**, as evidenced by the low product yield in the solventylation process, we opted to proceed with an alternative radical trap for further investigation.

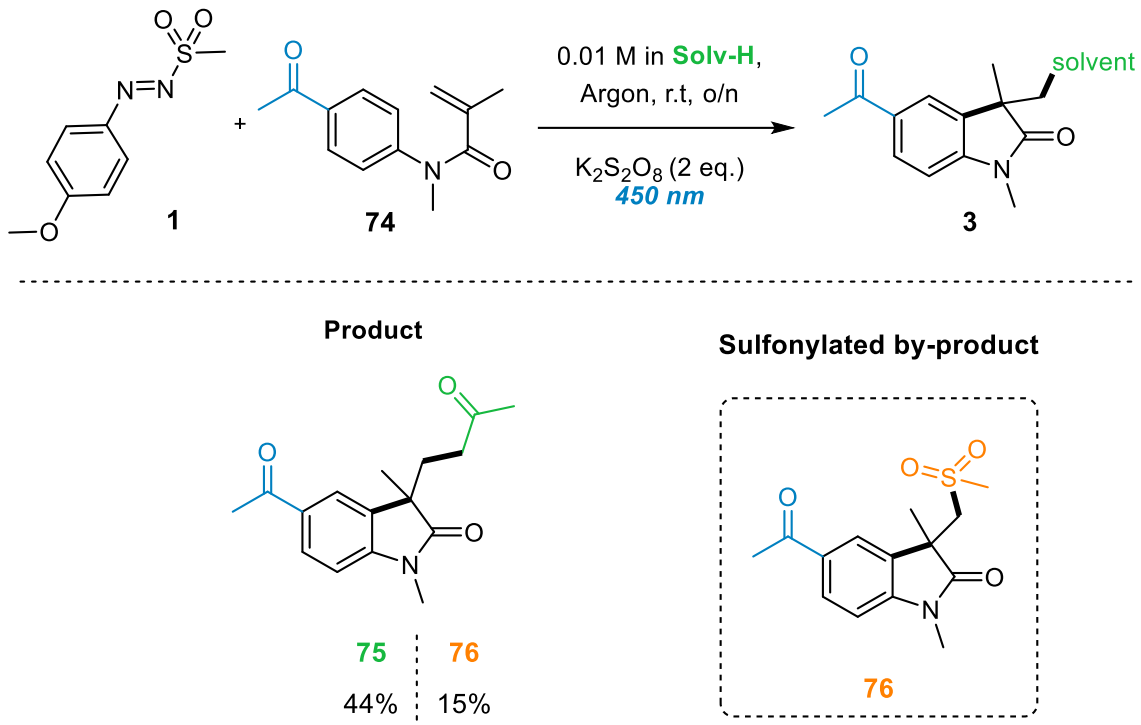

SCHEME 3.18 Scope Radical Trap with a Para-Acetyl Substituted Aryl Group

3.3.3 Radical Trap with a N-benzyl Substitution

The final investigation of radical traps involved testing N-benzyl-substituted olefin **77**, as depicted in scheme 3.19. Starting with acetone yielded product **78** with a 41% yield and a sulfonylated by-product **82** with a 10% yield. In our goal to enhance these outcomes, we extended our investigation to other solvents. Subsequent trials in MeCN resulted in product **79** with a yield of 53% and a sulfonylated by-product **82** with a 41% yield. Notably, the increased formation of the sulfonylated by-product **82** prompted us to explore DCM as a solvent, leading to product **80** with a 54% yield for the desired product and a reduced yield of the sulfonylated by-product **82** 18% compared to MeCN. In the final trial with chloroform, we successfully obtained product **81** with a 70% yield for the desired product and a sulfonylated by-product **82** with a 22% yield.

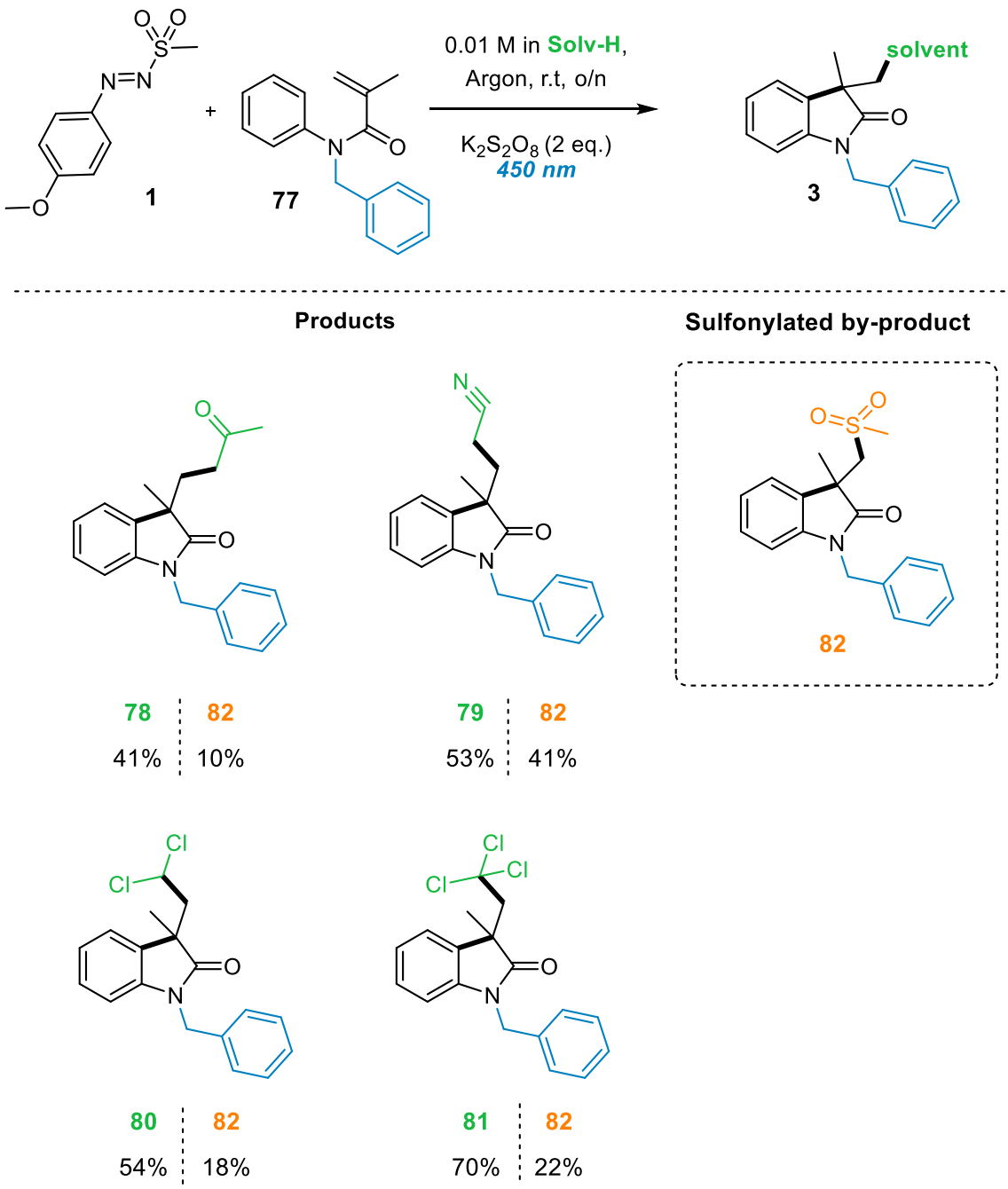

SCHEME 3.19 Radical Trap with a N-benzyl Substitution

3.3.4 Discussion

We initiated this scope with radical trap **67** in acetone, achieving a 60% yield for the desired product **68** and a sulfonylated by-product **73** at 20%. Despite the high yield for the sulfonylated by-product, the absence of unreacted radical trap **67** encouraged us to explore different solvents. The most favorable results were obtained when using chloroform, where we achieved a 68% yield for the desired product **63** and a sulfonylated by-product **73** with a 32% yield. However, the high susceptibility of radical trap **73** to sulfonylation resulted in higher yields of the sulfonylated by-product **73** than anticipated. Table 3.4, Entry 1.

Radical trap **74** featuring a *para*-acetyl substituent, exhibited rather low reactivity for the solvenylation process in acetone, with a 44% yield for the desired product **75** and a 15% yield of sulfonylated by-product **76**. Given the limited reactivity of radical trap **74** during the solventylation process, we decided to continue our scope with an alternative radical trap. Table 3.4, Entry 2.

The initial exploration with N-benzyl-substituted olefin **77** as radical trap in acetone yielded product **78** with a 41% yield and a sulfonylated by-product **82** with a 10% yield, indicating a moderate reactivity under these conditions. Subsequent trials in various solvents demonstrated varied outcomes. The most favorable results were obtained when using chloroform, where we achieved a 70% yield for the desired product **81** and a sulfonylated by-product **82** with a 22% yield. This significant improvement in product yield in chloroform suggests its reactivity as a solvent and hydrogen donor for the HAT in the solventylation process involving N-benzyl-substituted olefin **77**. Table 3.4, Entry 3.

In summary, our investigation involving diverse radical traps (**67**, **74**, and **77**) under varied solvent conditions has yielded valuable insights into the complexities of the solventylation process. These studies highlighted the intricate impact on yields for desired products and sulfonylated by-products, underscoring the intricacy of optimizing reaction outcomes.

As observed, chloroform exhibited a substantial yield of sulfonylated by-product (32% and 22%) while also proving to be a favorable solvent for achieving satisfactory yields of the desired product (68% and 70%). This observed trend may be attributed to the lower BDE of the C(sp^3)-H bond in chloroform (93.8 kcal/mol) compared to acetone (95.9 kcal/mol), acetonitrile (96.0 kcal/mol), and DCM (97.3 kcal/mol). These findings significantly enhance our comprehension and offer guidance for future enhancements in the solventylation process employing aryl azosulfones and olefins as radical traps.

Entry	Radical Trap	Solvent	Product Yield [%]	Sulfonylated By-Product [%]
1	**67**	Chloroform	68 (Product **71**)	32 (By-Product **73**)
2	**74**	Acetone	44 (Product **75**)	15 (Product **76**)
3	**77**	Chloroform	70 (Product **81**)	22 (Product **82**)

Table 3.4 Best Results Obtained with Each Radical Trap Tested

3.3.5 Synthesis of the Diversely Substituted Radical Traps

The synthetic pathway for the three radical traps employed in the experimental scope is depicted in Scheme 3.20. Initiated with methacrylic acid **83**, the addition of oxalyl chloride **84** at 0 °C, along with 6 drops of DMF as a catalyst, initiated the chlorination reaction that was then left at room temperature, yielding compound **85**.

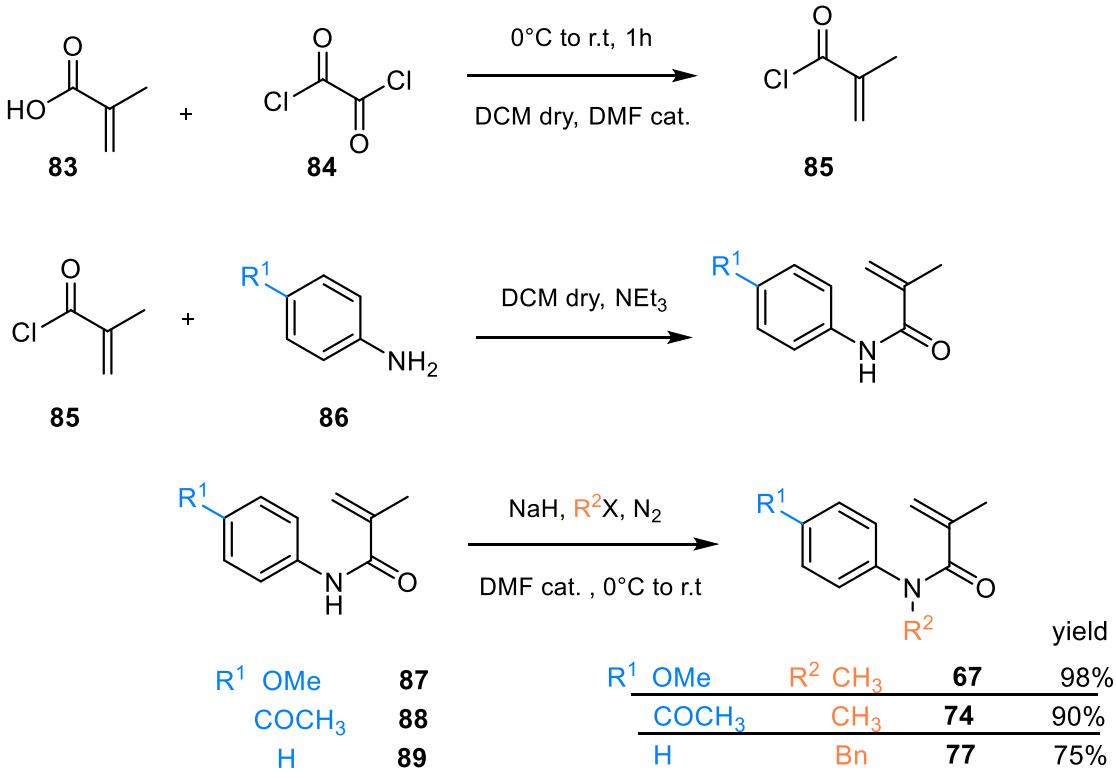

*SCHEME 3.20 Series of Reactions to Obtain Radical Traps **67, 74** and 77*

Following the reaction of **85** with an aniline derivative substituted at the *para* position containing the desired functional groups, the products obtained were **87** with a *para*-methoxy substituent, **88** with a *para*-acyl substituent, and **89** without any substituent in

the aromatic ring. The final step involved introducing a substitute in the nitrogen atom, where a methyl group was introduced to obtain radical traps **67** and **74**, while a benzyl group was incorporated to obtain radical trap **77**. The yield of this last synthetic step is outlined in Scheme 3.20.

4. Experimental Data

In this section, a comprehensive compilation of all experimental data, procedures, and analyses is presented, covering all synthesized compounds conducted throughout this thesis.

4.1 Materials and Methods

4.1.1 General remarks

NMR spectra (^{1}H, ^{13}C, COSY, and HSQC) were recorded using a Varian Mercury Plus 300 spectrometer (300 MHz for ^{1}H and 75 MHz for ^{13}C) equipped with an ATB broad band probe or a JEOL JNM-ECZR400 spectrometer (400 MHz for ^{1}H and 100 MHz for ^{13}C) with a Royal HFX probe. If not indicated otherwise, the spectra were consistently acquired using $CDCl_3$ as the solvent and at 27 °C, with tetramethylsilane (TMS, 0.00 ppm) employed as an internal standard. The chemical shifts (δ) are reported in parts per million (ppm), with tetramethylsilane (TMS, 0 ppm) as the internal standard for proton spectra and the central peak of CDC_{l3} (77.16 ppm) for carbon spectra. The spectra obtained were processed using the MestReNova software (Mestrelab Research).

GC−MS analyses were carried out on Shimadzu GC−MS-QP2010 SE with an AOC-20i Plus auto-injector mounting an Avantor Hichrom HI-5 MS column (internal diameter 0.25 mm, film thickness 0.25 mm, length 30 m). Samples were prepared upon dilution 1:100 in Et_2O of a mother solution of an estimated 1000 ppm concentration. Run parameters: V_{inj} = 6 mL, T_{inj} = 250°C, T_{ramp} = 3 min at 120°C, then 10°C/min up to 300°C, then 4 min at 300°C, total run time 25 min, He carrier gas, column flow 1 mL/min, split ratio 1:10, MS acquisition (TIC, m/z range 35−250) from 3 to 25 min.

Reactions were monitored using TLC. Silica gel plates (thickness = 0.25 mm) were employed for TLC analyses, visualized under UV light (λ = 254 nm), and developed using Hanessian stain. This involved dipping the plates into a solution containing $(NH_4)4MoO_4•4H_2O$ (21 g), $Ce(SO_4)_2•4H_2O$ (1 g) in H_2SO_4 (31 mL), and H_2O (469 mL), followed by warming.

Column chromatography was conducted using the "flash" methodology, employing 220-400 mesh silica, grade I alumina, or 60-100 mesh Florisil. Eluents and solvents for routine operations, as well as anhydrous solvents and all reagents, were obtained from commercial suppliers.

When necessary, some products were purified through preparative thin-layer chromatography (TLC). Silica gel plates supported on glass (Merck 60 F254, 0.25 mm) with dimensions of 20x20 cm were used. The compound to be purified was dissolved in the appropriate solvent and applied using a pipette with a cotton tip. After elution in the designated chamber, the bands corresponding to the product were visualized under a UV lamp, marked, and then scraped off. The removed silica was eluted with a porous plug using an appropriate solvent, followed by reducing the solution volume on a rotary evaporator.

Reagents and solvents were sourced from commercial suppliers, including Sigma-Aldrich, Tokyo Chemical Industry, Carlo Erba, Honeywell/Riedel-de-Haen, Alfa Aesar, VWR International, Acros Organics, and Merck. These materials were used in their as-received state without additional purification.

For equipment cleaning, all glassware and magnetic stir bars underwent a meticulous cleaning process after each use. Initial washing with soap and water was followed by rinsing with acetone to eliminate any organic residues. After the final wash, all glassware was dried in an oven at 105°C overnight. Volumetric glassware and Hamilton syringes were air-dried to preserve their volumes without alteration.

4.1.2 Photochemical equipment

Photochemical reactions were conducted in a dedicated apparatus designed for batch reactions. This setup comprised an aluminum cooling plate (160x100x25 mm) with 6 OSRAM® Oslon SSL 80 LDCQ7P LEDs (nominal 450 nm, royal blue) arranged in series. The LEDs were powered by a MeanWell® LPC-20-700 constant current power supply (700 mA) and positioned above a water-cooled aluminum vessel holder (170x110x38 mm). The holder, custom-built to cool both the LED plate and the vial, maintained the temperature of the sealed vials (purchased from Wicom International Co.) below 20°C. The vials were WIC43005 (5 mL crimp top vial, 38.5x22.0 mm), and WIC44510 (20 mm crimp caps with 3.0 mm PTFE septum).

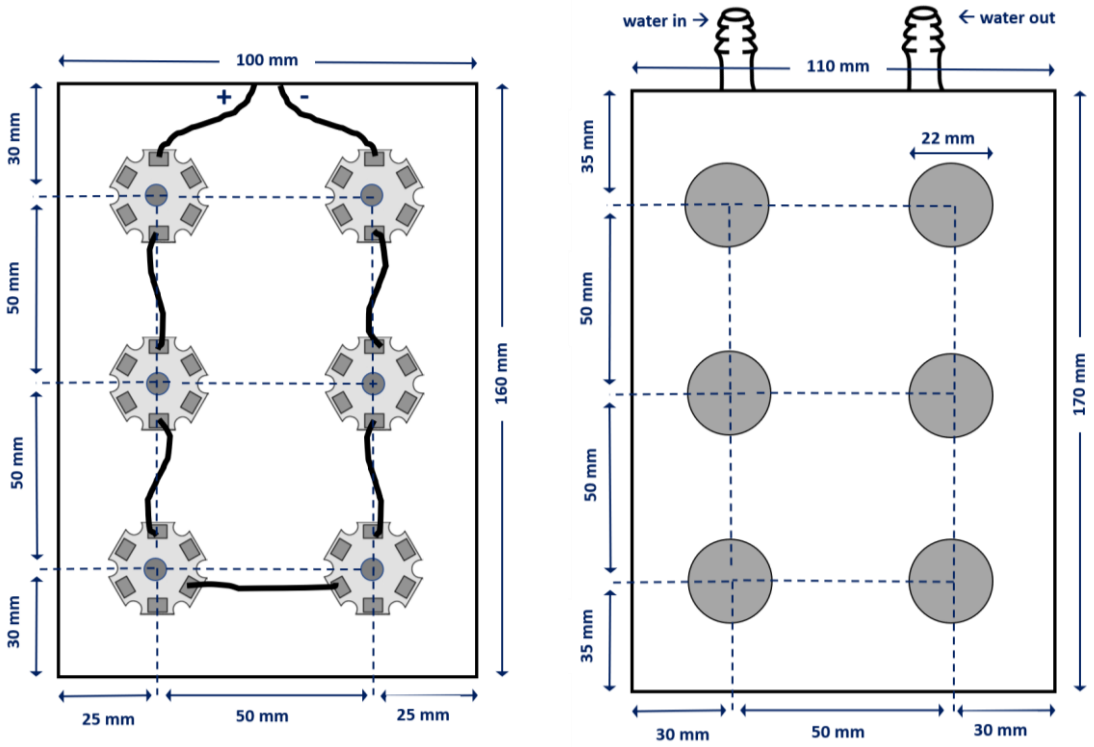

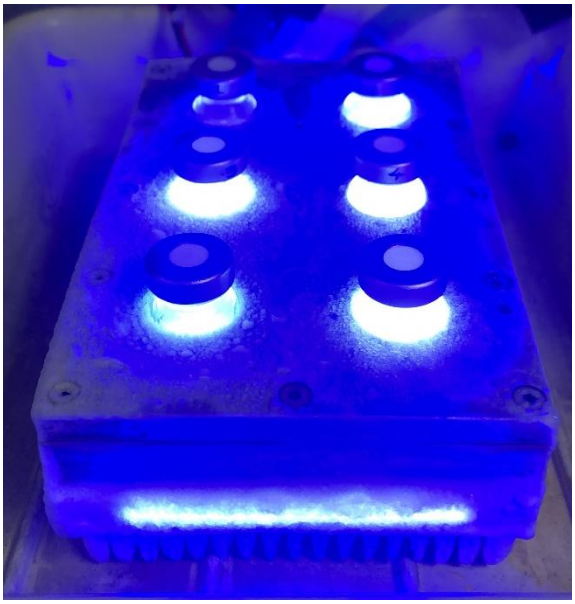

FIGURE 4.1 Example of the dedicated apparatus designed for batch reactions at -15°C.

Experiments were also conducted using an alternative apparatus equipped with an irradiation system featuring 12 OSRAM® Oslon SSL 80 LDCQ7P LEDs (nominal 450 nm, royal blue) arranged in series and powered by an EA Elektro-Automatik EA-PS 2042-06 B Digital Bench Power Supply. The solution was positioned approximately 35 mm from the irradiation source and shielded with aluminum foil to prevent unintended light exposure. The irradiation system comprised four aluminum LED plates connected

in series and mounted on a 200x200 mm wooden support. Each aluminum cooling plate (HWD 130x40x25 mm) accommodated three blue LEDs (40 mm apart) and was positioned in the middle of each side of the square wooden support. To ensure efficient heat dispersion from the LED plates, an 80 mm fan (powered independently with a 12V DC power supply) was strategically placed in the center of the wooden support within a hollow cavity to facilitate air circulation. Additionally, a magnetic agitator was placed under the system.

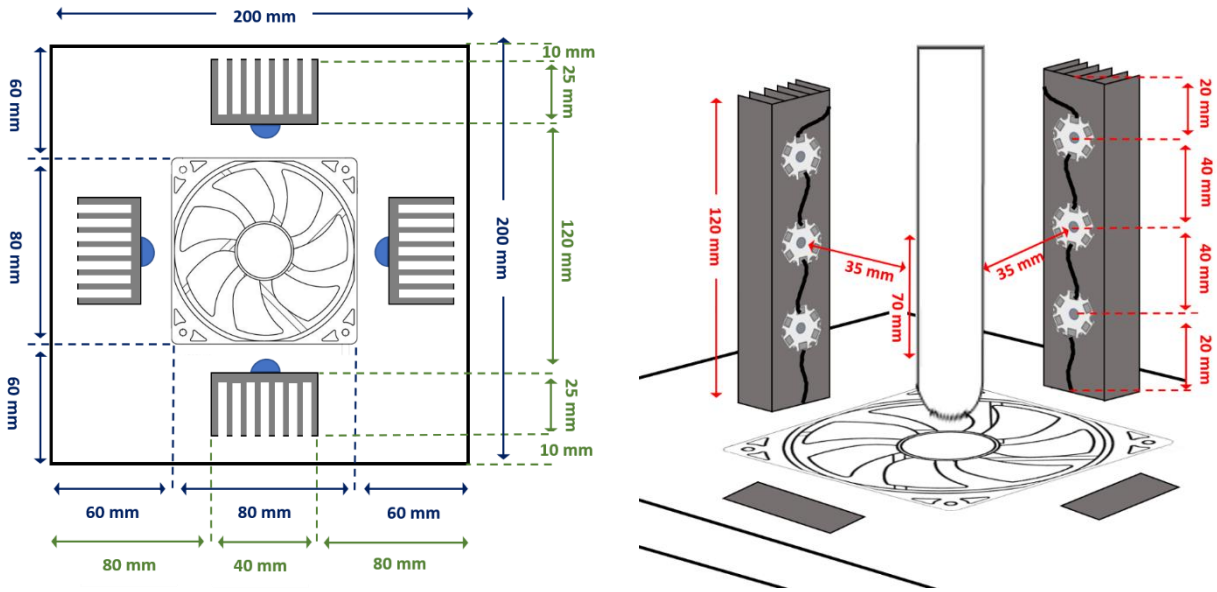

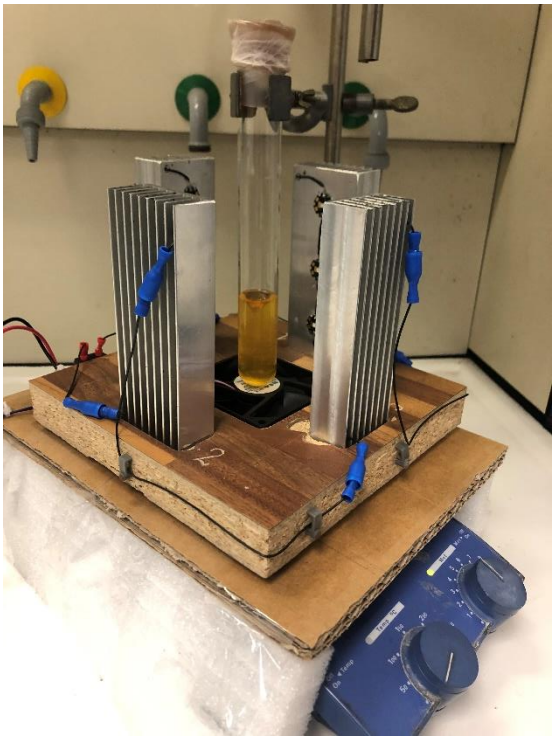

FIGURE 4.2 Example of the Alternative Apparatus System

4.2 Experimental Data

General procedure for photoinduced solventylation reactions

Note that the volume depends on the irradiation system employed. In the Osram vial system, the volume per vial was 8 mL, with typically two experiments conducted, resulting in a total solution volume of 16 mL. Conversely, when utilizing the alternative system, the standard volume was 20 mL.

The standard procedure for the solventylation reaction utilizing 1 equivalent of aryl azosulfone is as follows: the desired radical precursor, aryl azosulfone (0.2 mmol, 1 eq.), was accurately weighed and placed into a 20 mL reaction vessel containing a magnetic stir bar. Subsequently, the olefin, which serves as the radical trap (0.2 mmol, 1 eq.), and the external oxidant, sodium persulfate (0.4 mmol, 2 eq.), were also precisely weighed and added to the vessel. The vial was sealed with a rubber septum and purged of air by argon degassing (10 minutes) through a needle. Then, 20 mL of solvent, degassed with argon (10 minutes), was added. Finally, the solution was purged of oxygen impurities one last time by argon sparging (1 minute). The solution was then irradiated with high-power blue LEDs at 450 nm. Following irradiation, solid residues were removed by filtration through cotton. The reaction crude was monitored by TLC using PE:EtOAc (3:1) as the eluent and analyzed by H^1NMR ($CDCl_3$). Purification via flash chromatography (FC) was conducted using a PE:EtOAc mixture as the eluent, with the ratio adjusted based on the product's polarity. After purification, all substances underwent H^1NMR analysis.

4.2.1 Experimental Data of the Optimization of Reaction Conditions for the Solvenylation

(E)-1-(4-methoxyphenyl)-2-(methylsulfonyl)diazene (1)

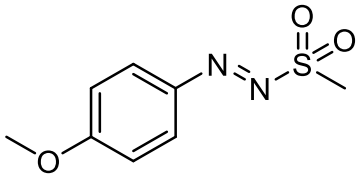

Procedure* The diazonium salt, 4-methoxybenzenediazonium tetrafluoroborate (6.0 mmol, 1 eq.) was suspended in dry DCM (20 mL) at 0°C in an ice bath. Subsequently, sodium methanesulfinate (6.3 mmol, 1.05 eq.) was added in a single portion under vigorous stirring. The reaction exhibited a yellow color. The solution was left to react in the dark overnight, allowing the temperature to reach room temperature. The residual salt waste was then separated through Büchner filtration. The collected yellow-orange solution was concentrated to the minimum volume using a rotary evaporator, and the pure product was precipitated by the addition of iced heptane (-24°C), recovering the product as a yellow solid through filtration. *The specific diazosulfone described herein was

synthesized by a previous PhD researcher before the initiation of this thesis. Nevertheless, it plays an important role in this study.
Yield 73%* reported yield.
PM 214.04 g/mol ($C_8H_{10}N_2O_3S$)
TLC R_f 0.22 (PE:EtOAc 3:1) UV + Hanessian stain
^{1}H NMR (400 MHz, Chloroform-*d*, 27 °C) δ 7.97–7.06 (m, 4H, Ar), 3.96 (s, 3H, CH_3O), 3.21 (s, 3H, CH_3SO_2). *Reported spectra by the PhD researcher
UV λ 342.0 nm
The data aligns with the scientific literature[70].

N-methyl-N-phenylmethacrylamide (2)

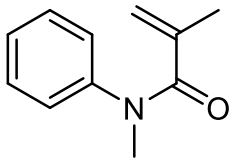

Procedure* A solution was prepared by combining N-methylaniline (10 mmol, 1 eq.) and triethylamine (10 mmol, 1 eq.) in dry DCM (20 mL) under an inert atmosphere. The mixture was cooled to 0°C in an ice bath. Subsequently, a solution of commercially available methacryloyl chloride (10 mmol, 1 eq.) in DCM (15 mL) was added dropwise using a syringe. The reaction was allowed to proceed overnight at room temperature. After monitoring the reaction through TLC (PE:EtOAc 4:1, UV+Hanessian stain), the resulting crude product was transferred to a funnel and subjected to a series of washes with HCl 0.1M (25 mL), water (25 mL), and brine (25 mL). Each aqueous layer underwent a single extraction with 15 mL of fresh DCM. The combined organic layers were dried using anhydrous Na_2SO_4, followed by evaporation under reduced pressure. Purification was achieved through FC starting with PE:EtOAc 5:1 as eluents until PE:EtOAc 3:1, with further purification by precipitation from diethyl ether (Et_2O) (500 mg product / 1 mL) overnight at -24°C. *The specific radical trap described herein was synthesized by a preceding PhD researcher before the commencement of this thesis. Nevertheless, it represents a fundamental compound for this thesis.
Yield 79%* reported yield.
PM 175.23 g/mol ($C_{11}H_{13}NO$)
TLC R_f 0.65 (PE:EtOAc 3:1) UV + Hanessian stain
^{1}H NMR (400 MHz, Chloroform-*d*, 27 °C) δ 7.38 – 7.29 (m, 2H, Ar), 7.28 – 7.23 (m, 1H, Ar), 7.16 – 7.10 (m, 2H, Ar), 5.01 (m, 2H, CH_2), 3.35 (s, 3H, CH_3N), 1.76 (s, 3H, CH_3).
The data aligns with the scientific literature[52].

1,3-dimethyl-3-(3-oxobutyl)indolin-2-one (19)

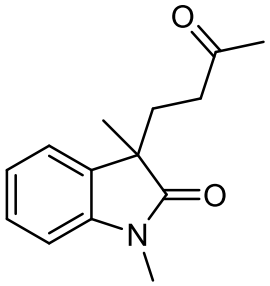

Procedure See general procedure for photoinduced solventylation reactions.
Yield 72%
PM 231.30 g/mol ($C_{14}H_{17}NO_2$)
TLC R_f 0.28 (PE:EtOAc 3:1) UV + Hanessian stain
^{1}H NMR (400 MHz, Chloroform-*d*, 27 °C) δ 7.33 – 7.27 (m, 1H, Ar), 7.16 (d, *J* = 7.4 Hz, 1H, Ar), 7.08 (m, 1H, Ar), 6.86 (d, *J* = 7.8, 1H, Ar), 3.23 (s, 3H, CH_3N), 2.27 – 187 (m, 4H, CH_2CH_2), 1.98 (s, 3H, CH_3CO), 1.38 (s, 3H, CH_3).
The data aligns with the scientific literature[71].

3-(1,3-dimethyl-2-oxoindolin-3-yl)propanenitrile (20)

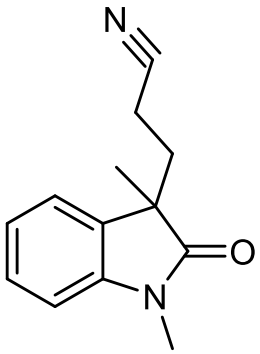

Procedure See general procedure for photoinduced solventylation reactions.
Yield 50%
PM 214.27 g/mol ($C_{13}H_{14}N_2O$)
TLC R_f 0.33 (PE:EtOAc 3:1) UV+Hanessian stain
^{1}H NMR (400 MHz, Chloroform-*d*, 27 °C) δ 7.33 (td, *J* = 7.7, 1.3 Hz, 1H, Ar), 7.20 (d, *J* = 7.3 Hz, 1 H, Ar), 7.12 (m, 1H, Ar), 6.88 (d, *J* = 7.9 Hz, 1H, Ar), 3.23 (s, 3 H, CH_3N), 2.39-2.26 (m, 1 H, CH_2), 2.12–2.05 (m, 2H, CH_2CH_2), 2.03-1.96 (m, 1H, CH_2) 1.41 (s, 3 H, CH_3).
The data aligns with the scientific literature[72].

3-(2,2-dichloroethyl)-1,3-dimethylindolin-2-one (21)

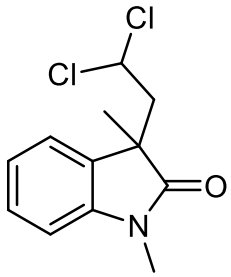

Procedure See general procedure for photoinduced solventylation reactions.
Yield 63%
PM 258.14 g/mol ($C_{12}H_{13}Cl_2O$)
TLC R_f 0.68 (PE:EtOAc 3:1) UV+Hanessian stain
^{1}H NMR (400 MHz, Chloroform-*d*, 27 °C) δ 7.33 (td, *J* = 7.7, 1.3 Hz, 1H, Ar), 7.20 (d, *J* = 7.3 Hz, 1H, Ar), 7.11 (m, Hz, 1H, Ar), 6.88 (d, *J* = 7.8 Hz, 1H, Ar), 5.38 (dd, *J* = 9.3, 4.1 Hz, 1H, $CHCl_2$), 3.21 (s, 3H, CH_3N), 3.04 (dd, *J* = 14.8, 9.3 Hz, 1H, CH_2), 2.71 (dd, *J* = 14.8, 4.2 Hz, 1H, CH'_2), 1.40 (s, 3H, CH_3).
The data aligns with the scientific literature[73].

1,3-dimethyl-3-((methylsulfonyl)methyl)indolin-2-one (22)

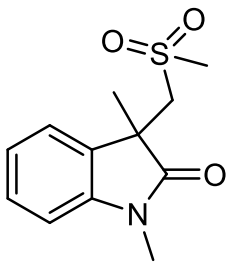

Procedure See general procedure for photoinduced solventylation reactions.
Yield 36%
PM 253.32 g/mol ($C_{12}H_{15}NO_3S$)
TLC R_f 0.07 (PE:EtOAc 3:1) UV+Hanessian stain
^{1}H NMR (400 MHz, Chloroform-*d*, 27 °C) δ 7.41 – 7.31 (m, 2H, Ar), 7.13 (m, 1H, Ar), 6.92 (d, *J* = 8.2, 1H, Ar), 3.72 (d, *J* = 14.6 Hz, 1H, CH_2SO_2), 3.57 (d, *J* = 14.6 Hz, 1H, CH'_2SO_2), 3.27 (s, 3H, CH_3N), 2.62 (s, 3H, CH_3SO_2), 1.47 (s, 3H, CH_3C).
The data aligns with the scientific literature[74].

4.2.2 Experimental Data of the Synthetic Scope of Aryl Diazosulfones

(E)-1-(4-methoxyphenyl)-2-(phenylsulfonyl)diazene (32)

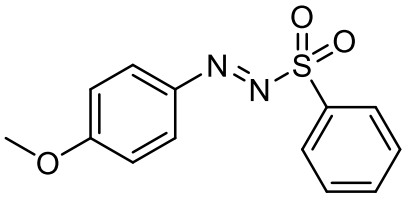

Procedure The diazonium salt, 4-methoxybenzenediazonium tetrafluoroborate (1.126 mmol, 1 eq.), was weighed, added to a flask and it was then suspended in dry DCM (4 mL) in an ice bath at 0°C. Sodium benzenesulfinate (1.126 mmol, 1 eq.) was added under vigorous stirring, resulting in a rapid development of a vibrant yellow color. The reaction proceeded overnight in the dark, allowing the temperature to reach room temperature. Residual salt waste was efficiently separated by cotton filtration. The resulting yellow-orange solution was concentrated to its minimum volume using a rotary evaporator, followed by FC purification.
Yield 53%
PM 276.31 g/mol ($C_{13}H_{12}N_2O_3S$)
TLC R_f 0.07 (PE:EtOAc 3:1) UV+Hanessian stain
^{1}H NMR (400 MHz, Chloroform-*d*, 27 °C) δ 7.99 (m, 2H, Ar), 7.83 (dd, *J* = 9.0, 3.1 Hz, 2H, Ar), 7.70 (tt, *J* = 7.6, 1.9 Hz, 1H, Ar), 7.59 (tt, *J* = 7.8, 1.5 Hz, 2H, Ar), 6.97 (dd, *J* = 9.1, 3.2 Hz, 2H, Ar), 3.90 (s, 3H, CH_3O).
^{13}C NMR (100 MHz, Chloroform-*d*, 27 °C) δ 165.6 (Cq, Ar), 143.5 (Cq, Ar), 134.5 (1C, Ar), 134.0 (Cq, Ar), 130.3 (2C, Ar), 129.8 (2C, Ar), 127.5 (2C, Ar), 114.8 (2C, Ar), 56.0 (1C, CH_3O).
UV λ 347.9 nm

1,3-dimethyl-3-((phenylsulfonyl)methyl)indolin-2-one (33)

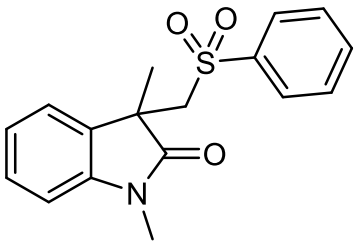

Procedure See general procedure for photoinduced solventylation reactions.
Yield 27%
PM 315.39 g/mol ($C_{17}H_{17}NO_3S$)
TLC R_f 0.01 (PE:EtOAc 3:1) UV+Hanessian stain

^{1}H NMR (400 MHz, Chloroform-*d*, 27 °C) δ 7.58 – 7.47 (m, 3H, Ar), 7.38 (t, *J* = 7.5 Hz, 2H, Ar), 7.30 (dd, *J* = 7.8, 1.3 Hz, 1H, Ar), 7.05 (d, *J* = 7.2 Hz, 1H, Ar), 6.90 (t, *J* = 7.5 Hz, 1H), 6.85 (d, *J* = 7.7 Hz, 1H, Ar), 3.89 (d, *J* = 14.6 Hz, 1H, CH_2SO_2), 3.69 (d, *J* = 14.5 Hz, 1H, CH'_2SO_2), 3.17 (s, 3H, CH_3N), 1.39 (s, 3H, CH_3C).
^{13}C NMR (100 MHz, Chloroform-*d*, 27 °C) δ 177.7 (C=O), 143.3 (Cq, Ar), 140.0 (Cq, Ar), 133.5 (1C, CH, Ar), 129.5 (Cq, Ar), 129.0 (2C, CH, Ar), 128.7 (1C, CH, Ar), 127.9 (2C, CH, Ar), 124.1 (1C, CH, Ar), 122.6 (1C, CH, Ar), 108.5 (1C, CH, Ar), 61.9 (1C, CH_2), 45.7 (Cq, aliphatic), 26.7 (1C, CH_3N), 25.6 (1C, CH_3) .
The data aligns with the scientific literature[75].

(E)-1-(4-methoxyphenyl)-2-tosyldiazene (34)

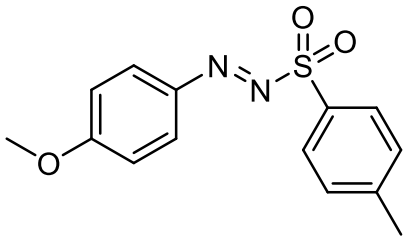

Procedure The diazonium salt, 4-methoxybenzenediazonium tetrafluoroborate (1.126 mmol, 1 eq.), was weighed in a flask, and was suspended in dry DCM (4 mL) within an ice bath at 0°C. Sodium 4-methylbenzenesulfinate (1.126 mmol, 1 eq.) was then added in a single portion with vigorous stirring, resulting in the rapid formation of a vibrant yellow color solution. The reaction proceeded overnight in darkness, allowing the system to reach room temperature. Residual salt waste was efficiently removed through cotton filtration. The resulting yellow solution was concentrated to its minimum volume using a rotary evaporator. The obtained yellow solid underwent precipitation-based purification by dissolving it in ice-cold DCM (-20 °C) and gradually adding ice-cold hexane (-20 °C, 8 mL), leading to the formation of an orange precipitate. After allowing the solution to sit at -20 °C overnight, filtration using a Büchner flask yielded the collected orange solid. The residual mother liquor was then reduced in volume using a rotary evaporator. This purification process was repeated twice.
Yield 63%
PM 290.34 g/mol ($C_{14}H_{14}N_2O_3S$)
^{1}H NMR (400 MHz, Chloroform-*d*, 27 °C) δ 7.90 – 7.79 (m, 4H, Ar), 7.38 (d, *J* = 8.3 Hz, 2H, Ar), 6.97 (dd, *J* = 9.2, 5.3 Hz, 2H, Ar), 3.89 (s, 3H, CH_3O), 2.47 (s, 3H, CH_3).
^{13}C NMR (100 MHz, Chloroform-*d*, 27 °C) δ 165.5 (Cq, Ar), 145.7 (Cq, Ar), 143.5 (Cq, Ar), 130.8 (Cq, Ar), 130.3 (2C, CH, Ar), 129.9 (2C, CH, Ar), 127.4 (2C, CH, Ar), 114.8 (2C, CH, Ar), 56.0 (1C, CH_3O), 21.9 (1C, CH_3).
UV λ 347.9 nm
The data aligns with the scientific literature[76].

1,3-dimethyl-3-(tosylmethyl)indolin-2-one (35)

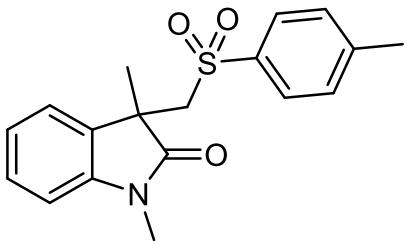

Procedure See general procedure for photoinduced solventylation reactions.
Yield 7%
PM 329.11 g/mol ($C_{18}H_{19}NO_3S$)
TLC R_f 0.03 (PE:EtOAc 7:2) UV+Hanessian stain
^{1}H NMR (400 MHz, Chloroform-*d*, 27 °C) δ 7.39 (dd, *J* = 8.4, 3.8 Hz, 2H, Ar), 7.30 (td, *J* = 7.7, 1.3 Hz, 1H, Ar), 7.17 (d, *J* = 8.1 Hz, 2H, Ar), 7.10 (d, *J* = 7.4 Hz, 1H, Ar), 6.93 (td, *J* = 7.5, 1.0 Hz, 1H), 6.85 (d, *J* = 7.8 Hz, 1H, Ar), 3.86 (d, *J* = 14.5 Hz, 1H, CH_2SO_2), 3.66 (d, *J* = 14.5 Hz, 1H, CH'_2SO_2), 3.16 (s, 3H, CH_3N), 2.40 (s, 3H, CH_3C aromatic), 1.39 (s, 3H, CH_3C aliphatic).
The data aligns with the scientific literature[77].

(E)-1-(tert-butylsulfonyl)-2-(4-methoxyphenyl)diazene (36)

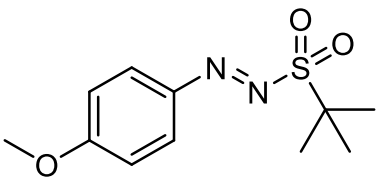

Procedure The sodium 2-methylpropane-2-sulfinate obtained (2.61 mmol, 1 eq.) was weighed in a flask and was suspended in dry DCM (8 mL) within an ice bath at 0°C. The diazonium salt, 4-methoxybenzenediazonium tetrafluoroborate (2.61 mmol, 1 eq.), was then added in a single portion with vigorous stirring, resulting in the rapid formation of a yellow-beige color solution; after 1 hour, the reaction turned orange. The reaction proceeded overnight in darkness, allowing the system to reach room temperature. Residual salt waste was efficiently removed through funnel filtration. The resulting solution was concentrated to its minimum volume using a rotary evaporator. The obtained solid underwent precipitation-based purification by dissolving it in ice-cold DCM (-20 °C, 7 mL) and gradually adding ice-cold hexane (-20 °C, 5 mL), leading to the formation of an orange precipitate. Filtration using a Büchner flask yielded the collected orange solid. The residual mother liquor was then reduced in volume using a rotary evaporator. This purification process was iterated five times until no further precipitation was observed.
Yield 67%

PM 256.32 g/mol ($C_{11}H_{16}N_2O_3S$)
TLC R_f 0.35 (PE:EtOAc 3:1) UV+Hanessian stain
^{1}H NMR (400 MHz, Chloroform-*d*, 27 °C) δ 7.98 (dd, *J* = 8.7, 1.4 Hz, 2H, Ar), 7.03 (dd, *J* = 9.0, 1.7 Hz, 2H, Ar), 3.93 (s, 3H, CH_3O), 1.60 (s, 9H, $3CH_3$)
^{13}C NMR (100 MHz, Chloroform-*d*, 27 °C) δ 165.6 (Cq, Ar), 144.4 (Cq, Ar) 127.4 (2C, Ar), 114.9 (2C, Ar), 59.8 (Cq, aliphatic), 56.1 (CH_3O), 24.4 (3C, $3CH_3$).
UV λ 347.9 nm

(E)-1-(tert-butyl)-2-(4-methoxyphenyl)diazene (42)

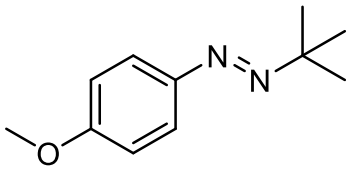

PROCEDURE See general procedure for photoinduced solventylation reactions.
Yield 48%
PM 192.26 g/mol ($C_{11}H_{16}N_2O$)
TLC R_f 0.76 (PE:EtOAc 10:1) UV+Hanessian stain
^{1}H NMR (400 MHz, Chloroform-*d*, 27 °C) δ 7.66 (dd, *J* = 9.2, 3.1 Hz, 2H, Ar), 6.94 (dd, *J* = 9.1, 3.3 Hz, 2H, Ar), 3.85 (s, 3H, CH_3O), 1.32 (s, 9H, $3CH_3$)
^{13}C NMR (100 MHz, Chloroform-*d*, 27 °C) δ 161.2 (Cq, Ar), 146.6 (Cq, Ar), 123.7 (2C, Ar), 114.0 (2C, Ar), 67.0 (Cq, aliphatic), 55.6 (1C, CH_3O), 27.2 (3C, $3CH_3$).
The data aligns with the scientific literature[78].

3-(((4-methoxyphenyl)sulfonyl)methyl)-1,3-dimethylindolin-2-one (43)

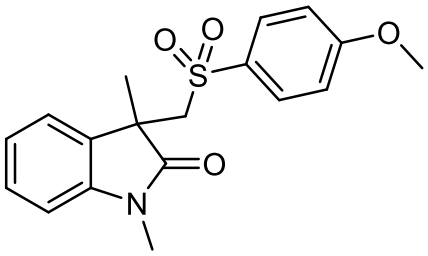

PM 345.41 g/mol ($C_{18}H_{19}NO_4S$)
TLC R_f 0.06 (PE:EtOAc 3:1) UV+Hanessian stain
^{1}H NMR (400 MHz, Chloroform-*d*, 27 °C) δ 7.41 (dd, *J* = 8.8, 2.0 Hz, 2H, Ar), 7.29 (td, *J* = 7.8, 1.3 Hz, 1H, Ar), 7.11 (d, *J* = 7.8 Hz, 1H, Ar), 6.96 (m, 1H, Ar), 6.84 (m, 3H, Ar), 3.86 (d, *J* = 14.5 Hz, 1H, CH_2SO_2), 3.85 (s, 3H, CH_3O), 3.65 (d, *J* = 14.5 Hz, 1H, CH'_2SO_2), 3.16 (s, 3H, CH_3N), 1.39 (s, 3H, CH_3C).
The data aligns with the scientific literature[79].

(E)-1-(4-((tert-butylsulfonyl)diazenyl)phenyl)ethan-1-one (46)

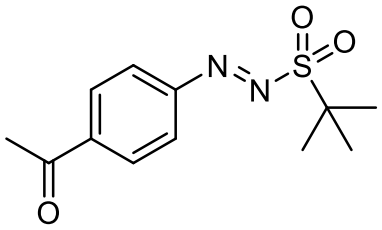

Procedure The sodium 2-methylpropane-2-sulfinate obtained (2.61 mmol, 1 eq.) was weighed in a flask and was suspended in dry DCM (8.7 mL) within an ice bath at 0°C. The diazonium salt, 4-acetylbenzenediazonium tetrafluoroborate (2.61 mmol, 1 eq.), was then added in a single portion with vigorous stirring, resulting in the rapid formation of a red solution. The reaction proceeded overnight in darkness, allowing the system to reach room temperature. Residual salt waste was efficiently removed through funnel filtration. The resulting solution was concentrated to its minimum volume using a rotary evaporator. The obtained solid underwent precipitation-based purification by dissolving it in ice-cold DCM (-20 °C, 7 mL) and gradually adding ice-cold hexane (-20 °C, 5 mL), leading to the formation of a red precipitate. Filtration using a Büchner flask yielded the collected red solid. The residual mother liquor was then reduced in volume using a rotary evaporator. This purification process was repeated twice.
Yield 60%
PM 268.33 g/mol ($C_{12}H_{16}N_2O_3S$)
TLC R_f 0.26 (PE:EtOAc 3:1) UV+Hanessian stain
^{1}H NMR (400 MHz, Chloroform-*d*, 27 °C) δ 8.14 (dd, *J* = 8.8, 1.9 Hz, 2H, Ar), 8.03 (dd, *J* = 8.8, 2.1 Hz, 2H, Ar), 2.69 (s, 3H, CH_3CO), 1.66 (s, 9H, $3CH_3$).
^{13}C NMR (100 MHz, Chloroform-*d*, 27 °C) δ 197.0 (C=O), 152.1 (Cq, Ar), 141.2 (Cq, Ar), 129.7 (2C, CH, Ar), 124.5 (2C, CH, Ar), 60.3 (Cq, aliphatic), 27.1 (1C, CH_3), 24.3 (3C, CH_3).
UV λ 345.0 nm

1,3-dimethyl-3-neopentylindolin-2-one (47)

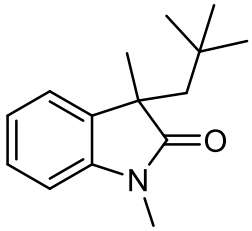

Procedure See general procedure for photoinduced solventylation reactions.
Yield 17%
PM 231.34 g/mol ($C_{15}H_{21}NO$)
TLC R_f 0.52 (PE:EtOAc 3:1) UV+Hanessian stain

^{1}H NMR (400 MHz, Chloroform-*d*, 27 °C) δ 7.30 – 7.23 (m, 1H, Ar, it overlaps with the chloroform residual peak at δ 7.26), 7.20 (d, *J* = 7.3 Hz, 1H, Ar), 7.04 (m, 1H, Ar), 6.85 (d, *J* = 7.7 Hz, 1H, Ar), 3.23 (s, 3H, CH_3N), 2.17 (d, *J* = 14.5 Hz, 1H, CH_2), 1.86 (d, *J* = 14.4 Hz, 1H, CH'_2), 1.30 (s, 3H, CH_3C), 0.61 (s, 9H, $3CH_3$).
^{13}C NMR (100 MHz, Chloroform-*d*, 27 °C) δ 181.2 (C=O), 143.0 (Cq, Ar), 134.3 (Cq, Ar), 127.6 (1C, CH, Ar), 124.0 (1C, CH, Ar), 122.1 (1C, CH, Ar), 108.1 (1C, CH, Ar), 50.9 (1C, CH_2), 47.5 (Cq, aliphatic), 31.9 (Cq, aliphatic), 30.9 (3C, $3CH_3$), 28.4 (1C, CH_3), 26.3 (1C, CH_3).
GC-MS: t_R = 8,382, *m/z* (%): molecular ion 231,15 relative intensity 64,54.
The data aligns with the scientific literature[80].

(E)-1-(4-(tert-butyldiazenyl)phenyl)ethan-1-one (48)

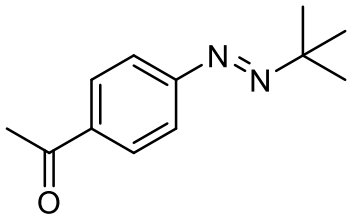

Procedure See general procedure for photoinduced solventylation reactions.
Yield 18%
PM 204.13 g/mol ($C_{12}H_{16}N_2O$)
TLC R_f 0.70 (PE:EtOAc 3:1) UV+Hanessian stain
^{1}H NMR (400 MHz, Chloroform-*d*, 27 °C) δ 8.05 (dd, *J* = 8.6, 2.0 Hz, 2H, Ar), 7.68 (dd, *J* = 8.5, 1.9 Hz, 2H, Ar), 2.64 (s, 3H, CH_3O), 1.36 (s, 9H, $3CH_3$).
^{13}C NMR (100 MHz, Chloroform-*d*, 27 °C) δ 197.7 (C=O), 155.1 (Cq, Ar), 137.8 (Cq, Ar), 129.4 (2C, CH, Ar), 122.1 (2C, CH, Ar), 31.1 (Cq, aliphatic), 27.0 (3C, $3CH_3$).

3-(((4-acetylphenyl)sulfonyl)methyl)-1,3-dimethylindolin-2-one (49)

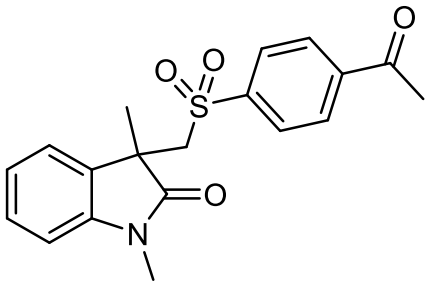

Procedure See general procedure for photoinduced solventylation reactions.
Yield 20%
PM 357.42 g/mol ($C_{19}H_{19}NO_4S$)
TLC R_f 0.06 (PE:EtOAc 3:1) UV+Hanessian stain
^{1}H NMR (400 MHz, Chloroform-*d*, 27 °C) δ 7.92 (d, *J* = 8.7 Hz, 2H, Ar), 7.58 (d, *J* = 8.7 Hz, 2H, Ar), 7.30 (td, *J* = 7.7, 1.2 Hz, 1H, Ar), 6.98 (d, *J* = 7.4 Hz, 1H, Ar), 6.90 –

6.84 (m, 2H, Ar), 3.92 (d, *J* = 14.6 Hz, 1H, CH_2SO_2), 3.71 (d, *J* = 14.6 Hz, 1H, CH'_2SO_2), 3.19 (s, 3H, CH_3N), 2.64 (s, 3H, CH_3CO),1.40 (s, 3H, CH_3C).

^{13}C NMR (100 MHz, Chloroform-*d*, 27 °C) δ 196.9 (C=O), 177.6 (C=O), 143.7 (Cq, Ar), 143.4 (Cq, Ar), 140.5 (Cq, Ar), 131.1 (Cq, Ar), 128.9 (2C, CH, Ar) , 128.7 (2C, CH, Ar), 128.3 (1C, CH, Ar), 124.0 (1C, CH, Ar), 122.6 (1C, CH, Ar), 108.7 (1C, CH, Ar), 62.0 (1C, CH_2), 45.7 (Cq, aliphatic), 27.1 (1C, CH_3), 26.7 (1C, CH_3), 25.5 (1C, CH_3).
GC-MS: t_R = 14,659, *m/z* (%): molecular ion 357,15, relative intensity 100,00.
The data aligns with the scientific literature[77].

(E)-1-(4-((phenylsulfonyl)diazenyl)phenyl)ethan-1-one (50)

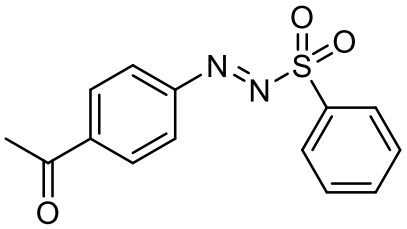

Procedure The diazonium salt, 4-acetylbenzenediazonium tetrafluoroborate (1.068 mmol, 1 eq.), was weighed in a flask and was suspended in dry DCM (4 mL) within an ice bath at 0°C. Sodium benzenesulfinate (1.068 mmol, 1 eq.) was then added in a single portion with vigorous stirring, resulting in the rapid formation of an orange color solution. The reaction proceeded overnight in darkness, allowing the system to reach room temperature. Residual salt waste was efficiently removed through cotton filtration. The resulting orange solution was concentrated to its minimum volume using a rotary evaporator. The obtained yellow solid underwent precipitation-based purification by dissolving it in ice-cold DCM (-20 °C, 7mL) and gradually adding ice-cold hexane (-20 °C, 5 mL), leading to the formation of an orange precipitate. After allowing the solution to sit at -20 °C overnight, filtration using a Büchner flask yielded the collected orange solid. The residual mother liquor was then reduced in volume using a rotary evaporator. This purification process was iterated five times until no further precipitation was observed.
Yield 80%
PM 288.32 g/mol ($C_{14}H_{12}N_2O_3S$)
TLC Rf 0.05 (PE:EtOAc 3:1) UV+Hanessian stain
^{1}H NMR (400 MHz, Chloroform-*d*, 27 °C) δ 8.07 (dd, *J* = 8.5, 1.8 Hz, 2H, Ar), 8.01 (m, 2H, Ar), 7.89 (dd, *J* = 8.5, 1.8 Hz, 2H, Ar), 7.76 (tt, *J* = 7.7, 1.1 Hz, 1H, Ar), 7.63 (t, *J* = 8.0 Hz, 1H, Ar), 2.65 (s, 3H, CH_3CO).
^{13}C NMR (100 MHz, Chloroform-*d*, 27 °C) δ 197.0 (C=O), 151.4 (Cq, Ar), 141.3 (Cq, Ar), 135.1 (1C, Ar), 132.7 (Cq, Ar), 130.6 (2C, Ar), 129.6 (2C, Ar), 129.4 (2C, Ar), 124.7 (2C, Ar), 27.1 (1C, CH_3).
UV λ 299.0 nm
The data aligns with the scientific literature[77].

ethyl 3-(1,3-dimethyl-2-oxoindolin-3-yl)propanoate (51)

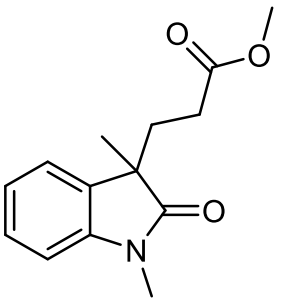

Procedure See general procedure for photoinduced solventylation reactions.
Yield 13%
PM 247.12 g/mol ($C_{14}H_{17}NO_3$)
TLC R_f 0.38 (PE:EtOAc 7:2) UV+Hanessian stain
^{1}H NMR (400 MHz, Chloroform-*d*, 27 °C) δ 7.25 – 7.17 (m, 1H, Ar), 7.11 (d, *J* = 7.3 Hz, 1H, Ar), 7.04 – 6.96 (m, 1H, Ar), 6.78 (d, *J* = 7.7 Hz, 1H, Ar), 3.47 (s, 3H, CH_3O), 3.15 (s, 3H, CH_3N), 2.22 – 1.93 (m, 3H, CH_2CH_2), 1.88-1.74 (m, 1H, CH_2CH_2), 1.38 (s, 3H, CH_3C).
The data aligns with the scientific literature[81].

4.2.3 Experimental Data of the Synthesis of Aryl Azosulfones

4-methoxybenzenediazonium tetrafluoroborate (55)

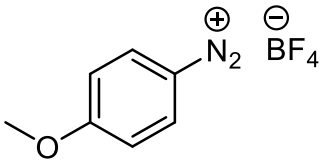

Procedure The commercially available 4-metoxyaniline (20.3 mmol, 1 eq.) was dissolved in 15 ml of a 25% w/w aqueous HBF4 solution. Subsequently, a cold (-20 °C) solution of sodium nitrite (22.3 mmol, 1.1 equiv.) in 2.5 mL of water was added dropwise. After 30 minutes of vigorous stirring, the resulting precipitate was separated using a Büchner funnel. The crude product underwent purification through crystallization, dissolving the salt in the minimum amount of acetone, followed by the addition of cold (-20°C) Et_2O. The purified solid product was collected via filtration and dried under high vacuum.
Yield 92%
PM 221.95 g/mol ($C_7H_7BF_4N_2O$)
TLC N/A
^{1}H NMR (400 MHz, DMSO-d_6) δ 8.66 – 8.57 (m, 2H), 7.53 – 7.44 (m, 2H), 4.04 (s, 3H, CH_3O).
The data aligns with the scientific literature[46].

sodium 2-methylpropane-2-sulfinate (60)

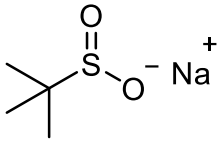

Procedure In a vial, acetic acid (2.8 mL) and the commercially available, di-tert-butyl disulfide (2.61 mmol, 1 eq.) were added and cooled to 0°C. H_2O_2 (30%, 7.01 mmol, 1.25 eq.) was added, and the reaction proceeded for 22 hours. Water (6 mL) was introduced, and the organic phase underwent extraction with DCM twice (8 mL each) and washing with $NaHSO_3$ (4 mL), $NaHCO_3$ (4 mL), and water (4 mL). The resulting organic phase was dried with Na_2SO_2 and reduced in volume using a rotary evaporator. The resulting S-(tert-butyl) 2-methylpropane-2-sulfinothioate (2.85 mmol, 1 eq) was then treated with sulfuryl chloride added dropwise (2.85 mmol, 1 eq.) in DCM (2M, 1.3 mL) in an ice bath. The resulting yellow solution was stirred for 1 hour at room temperature. The obtained solution of 2-methylpropane-2-sulfinic chloride (2.02 mmol, 1 eq.) was reduced in volume using a rotary evaporator and treated with NaOH (1M, 4.1 mL, 4.04 mmol, 2 eq.) added slowly in an ice bath, forming an instant precipitate. The precipitate was separated by decantation, and the remaining solid was washed with deionized water twice (5 mL in total). The remaining aqueous solution was concentrated under the rotary evaporator.
Yield 153% (The overestimated yield is likely attributed to the formation of NaCl)
PM 144.18 g/mol ($C_4H_9NaO_2S$)
TLC N/A
^{1}H NMR (400 MHz, Deuterium Oxide) δ 0.92 (s, 9H).
^{13}C NMR (100 MHz, Deuterium Oxide) δ 54.3, 23.3.
The data aligns with the scientific literature[82].

4.2.4 Experimental Data of the Synthetic Scope of Radical Traps

N-(4-methoxyphenyl)-N-methylmethacrylamide (67)

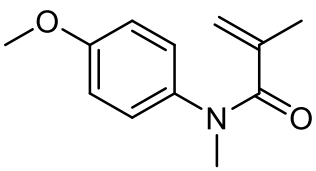

Procedure The obtained N-(4-methoxyphenyl)methacrylamide **87** (3.00 mmol, 1 eq.) was weighed. Under an inert atmosphere, dimethylformamide (DMF) (0.4M, 7 mL) was added, and sodium hydride (NaH) (60%, 3.90 mmol, 1.3 eq.) was added in portions at

0°C, resulting in a yellow solution. The mixture was stirred for 15 minutes at 0°C and then left at room temperature for an additional 15 minutes obtaining a dark brown solution. Methyl iodide (MeI) (4.20 mmol, 1.4 eq.) was added at 0°C, and the reaction was allowed to proceed at room temperature overnight. The reaction was monitored via TLC (ETP:EtOAc 3:1). Following this, water was added to the reaction mixture, and organic phase was extracted with EtOAc three times (20 mL in total). The organic phase was further washed with lithium chloride and brine until no DMF was observed via TLC. Each aqueous layer was extracted with EtOAc (25 mL in total). The combined organic layers were dried over anhydrous sodium sulfate, evaporated under reduced pressure, and purified by FC using eluents PE:EtOAc 3:1 as eluent.
Yield 98%
PM 205.26 g/mol ($C_{12}H_{15}NO_2$)
TLC R_f 0.44 (PE:EtOAc 3:2) UV+Hanessian stain
^{1}H NMR (400 MHz, Chloroform-*d*, 27 °C) δ 7.05 (dd, *J* = 8.9, 3.2, Hz, 2H, Ar), 6.85 (dd, *J* = 8.9, 3.3, Hz, 2H, Ar), 5.01 (d, *J* = 13.1, 2H, CH_2=C), 3.81 (s, 3H, CH_3O), 3.31 (s, 3H, CH_3N), 1.74 (s, 3H, CH_3C).
^{13}C NMR (100 MHz, Chloroform-*d*, 27 °C) δ 172.3 (C=O), 158.4 (Cq, Ar), 141.0 (Cq, Ar), 137.5 (Cq, aliphatic), 127.9 (2C, CH, Ar), 119.1 (1C, CH_2), 114.4 (2C, CH, Ar), 55.5 (1C, CH_3O), 37.9 (1C, CH_3N), 20.5 (1C, CH_3).
The data aligns with the scientific literature[83].

5-methoxy-1,3-dimethyl-3-(3-oxobutyl)indolin-2-one (68)

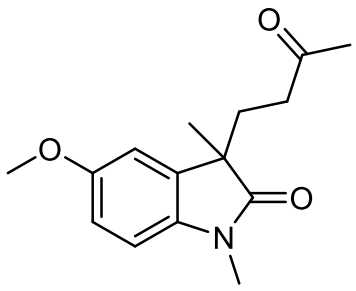

Procedure See general procedure for photoinduced solventylation reactions.
Yield 60%
PM 261.32 g/mol ($C_{15}H_{19}NO_3$)
TLC R_f 0.77 (PE:EtOAc 3:2) UV+Hanessian stain
^{1}H NMR (400 MHz, Chloroform-*d*, 27 °C) δ 6.84 – 6.73 (m, 3H, Ar), 3.80 (s, 3H, CH_3O), 3.21 (s, 3H, CH_3N), 2.27 – 2.01 (m, 4H, aliphatic), 1.99 (s, 3H, CH_3CO). 1.37 (s, 3H, s, 3H, CH_3C).
^{13}C NMR (100 MHz, Chloroform-*d*, 27 °C) δ 207.8 (C=O), 179.8 (C=O), 156.3 (Cq, Ar), 136.7 (Cq, Ar), 134.7 (Cq, Ar), 112.2 (1C, CH, Ar), 110.2 (1C, CH, Ar), 108.4 (1C, CH, Ar), 55.9 (1C, CH_3O), 47.9 (Cq, aliphatic), 38.6 (2C, CH_2), 29.7 (1C, CH_3), 26.3 (1C, CH_3N), 23.8 (1C, CH_3).
The data aligns with the scientific literature[84].

3-(5-methoxy-1,3-dimethyl-2-oxoindolin-3-yl)propanenitrile (69)

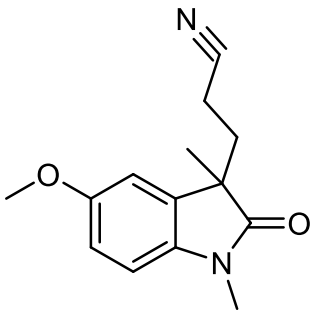

Procedure See general procedure for photoinduced solventylation reactions.
Yield 43%
PM 244.29 g/mol ($C_{14}H_{16}N_2O_2$)
TLC R_f 0.28 (PE:EtOAc 3:2) UV+Hanessian stain
^{1}H NMR (400 MHz, Chloroform-*d*, 27 °C) δ 6.87 – 6.75 (m, 3H, Ar), 3.82 (s, 3H, CH_3O), 3.20 (s, 3H, CH_3N), 2.37 – 2.27 (m, 1H, CH_2), 2.17 – 1.95 (m, 3H, CH_2), 1.39 (s, 3H, CH_3C).
^{13}C NMR (100 MHz, Chloroform-*d*, 27 °C) δ 178.6 (C=O), 156.5 (Cq, Ar), 136.6 (Cq, Ar), 133.1 (Cq, Ar), 118.9 (Cq, CN), 112.6 (1C, CH, Ar), 110.4 (1C, CH, Ar), 108.9 (1C, CH, Ar), 55.9 (1C, CH_3O), 47.9 (Cq, aliphatic), 33.6 (1C, CH_2), 26.3 (1C, CH_3N), 23.6 (1C, CH_3), 12.9 (1C, CH_2).
The data aligns with the scientific literature[72].

3-(2,2-dichloroethyl)-5-methoxy-1,3-dimethylindolin-2-one (70)

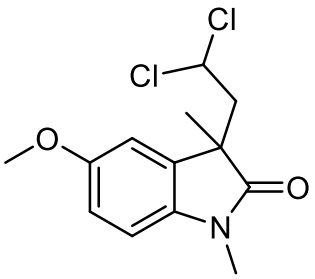

Procedure See general procedure for photoinduced solventylation reactions.
Yield 63%
PM 388.17 g/mol ($C_{13}H_{15}Cl_2NO_2$)
TLC R_f 0.64 (PE:EtOAc 3:2) UV+Hanessian stain
^{1}H NMR (400 MHz, Chloroform-*d*, 27 °C) δ 6.87 – 6.74 (m, 3H, Ar), 5.42 (dd, *J* = 9.2, 4.2 Hz, 1H, $CHCl_2$), 3.82 (s, 3H, CH_3O), 3.19 (s, 3H, CH_3N), 3.00 (dd, *J* = 14.7, 5.6 Hz, 1H, CH_2), 2.68 (dd, *J* = 14.7, 4.3 Hz, 1H, CH'$_2$), 1.39 (s, 3H, CH_3C).
^{13}C NMR (100 MHz, Chloroform-*d*, 27 °C) δ 178.7 (C=O), 156.2 (Cq, Ar), 137.0 (Cq, Ar), 132.6 (Cq, Ar), 112.4 (1C, CH, Ar), 110.6 (1C, CH, Ar), 109.0 (1C, CH, Ar), 69.7

(1C, $CHCl_2$), 55.9 (1C, CH_3O), 50.2 (1C, CH_2), 47.7 (Cq, aliphatic), 26.6 (1C, CH_3N), 25.6 (1C, CH_3).
The data aligns with the scientific literature[73].

5-methoxy-1,3-dimethyl-3-(2,2,2-trichloroethyl)indolin-2-one (71)

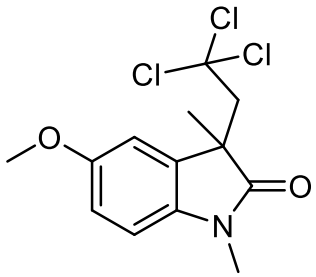

Procedure See general procedure for photoinduced solventylation reactions.
Yield 68%
PM 322.61 g/mol ($C_{13}H_{14}Cl_3NO_2$)
TLC R_f 0.60 (PE:EtOAc 3:2) UV+Hanessian stain
^{1}H NMR (400 MHz, Chloroform-*d*, 27 °C) δ 6.97 (d, *J* = 2.4 Hz, 1H, CH, Ar), 6.84 (dd, *J* = 8.5, 2.5 Hz, 1H, CH, Ar), 6.78 (d, *J* = 8.4 Hz, 1H, CH, Ar), 3.80 (s, 3H, CH_3O), 3.69 (d, *J* = 15.3 Hz, 1H, CH_2), 3.32 (d, *J* = 15.3 Hz, 1H, CH'_2), 3.22 (s, 3H, CH_3N), 1.39 (s, 3H, CH_3C).
^{13}C NMR (100 MHz, Chloroform-*d*, 27 °C) δ 178.3 (C=O), 155.6 (Cq, Ar), 136.9 (Cq, Ar), 131.0 (Cq, Ar), 113.3 (1C,Ar), 112.8 (1C, Ar), 108.7 (1C, Ar), 96.2 (Cq, aliphatic, CCl_3), 59.8 (1C, CH_2), 55.9 (1C, CH_3O), 48.4 (Cq, aliphatic), 27.0 (1C, CH_3), 26.7 (1C, CH_3N).
The data aligns with the scientific literature[85].

ethyl 2-(5-methoxy-1,3-dimethyl-2-oxoindolin-3-yl)acetate (72)

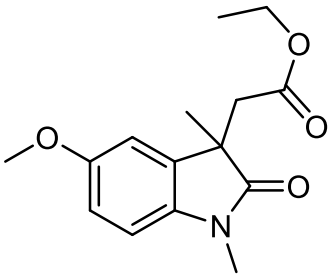

Procedure See general procedure for photoinduced solventylation reactions.
Yield 9%
PM 277.32 g/mol ($C_{15}H_{19}NO_4$)
TLC R_f 0.33 (PE:EtOAc 3:2) UV+Hanessian stain
^{1}H NMR (400 MHz, Chloroform-*d*, 27 °C) δ 6.83 (d, *J* = 2.3 Hz, 1H, CH, Ar), 6.81 – 6.77 (m, 1H, CH, Ar) 6.75 (d, *J* = 8.4 Hz, 1H, CH, Ar), 3.97 – 3.83 (m, 2H, CH_2O), 3.79 (s, 3H, CH_3O), 3.23 (s, 3H, CH_3N), 3.02 (d, *J* = 16.2 Hz, 1H, CH_2), 2.80 (d, *J* = 16.4 Hz, 1H, CH'_2), 1.36 (s, 3H, CH_3C), 1.02 (t, *J* = 7.1 Hz, 3H, CH_3).

^{13}C NMR (100 MHz, Chloroform-*d*, 27 °C) δ 179.7 (C=O), 169.9 (C=O), 156.0 (Cq, Ar), 137.3 (Cq, Ar), 134.5 (Cq, Ar), 112.0 (1C, Ar), 110.3 (1C, Ar), 108.4 (1C, Ar), 60.5 (1CH, CH_2O), 55.9 (1C, CH_3O), 46.0 (Cq, aliphatic), 41.7 (1C, CH_2), 26.5 (1C, CH_3N), 24.6 (1C, CH_3), 14.0 (1C, CH_3).

5-methoxy-1,3-dimethyl-3-((methylsulfonyl)methyl)indolin-2-one (73)

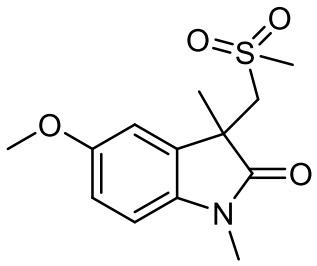

Procedure See general procedure for photoinduced solventylation reactions.
Yield 57%
PM 283.34 g/mol ($C_{13}H_{17}NO_4S$)
TLC R_f 0.04 (PE:EtOAc 3:2) UV+Hanessian stain
^{1}H NMR (400 MHz, Chloroform-*d*, 27 °C) δ 6.98 (d, *J* = 2.3 Hz, 1H, CH, Ar), 6.86 (dd, *J* = 8.5, 2.4 Hz, 1H, CH, Ar), 6.81 (d, *J* = 8.5 Hz, 1H, CH, Ar), 3.81 (s, 3H, CH_3O), 3.69 (dd, *J* = 14.7 Hz, 1H, CH_2), 3.54 (d, *J* = 14.8 Hz, 1H, CH'_2), 3.24 (s, 3H, CH_3N), 2.68 (s, 3H, CH_3SO_2), 1.46 (s, 3H, CH_3C).
^{13}C NMR (100 MHz, Chloroform-*d*, 27 °C) δ 177.5 (C=O), 156.2 (Cq, Ar), 136.8 (Cq, Ar), 131.7 (Cq, Ar), 113.1 (1C, Ar), 111.3 (1C, Ar), 109.3 (1C, Ar), 60.8 (1C, CH_2), 55.9 (1C, CH_3O), 46.2 (Cq, aliphatic), 43.5 (1C, CH_3SO_2), 26.8 (1C, CH_3N), 25.1 (1C, CH_3).

N-(4-acetylphenyl)-N-methylmethacrylamide (74)

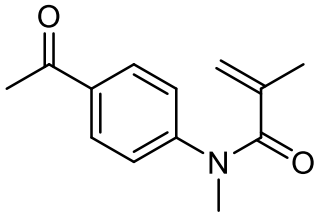

Procedure The obtained N-(4-acetylphenyl)methacrylamide **88** (1.6 mmol, 1 eq.) was weighed in a flask. Under an inert atmosphere, DMF (0.2M, 6 mL) was added, and NaH (60%, 2.1 mmol, 1.3 eq.) was added in portions at 0°C, resulting in a yellow solution. The mixture was stirred for 15 minutes at 0°C and then left at room temperature for an additional 15 minutes. MeI (2.2 mmol, 1.4 eq.) was added at 0°C, and the reaction was allowed to proceed at room temperature overnight. The reaction was monitored via TLC (ETP:EtOAc 3:1). Following this, water was added to the reaction mixture, and organic phase was extracted with EtOAc three times (20 mL in total). The organic phase was further washed with lithium chloride, and brine five times until no DMF was observed via TLC. Each aqueous layer was extracted with EtOAc (25 mL in total). The combined

organic layers were dried over anhydrous sodium sulfate, evaporated under reduced pressure, and purified by FC using eluents from PE:EtOAc 3:2 to PE:EtOAc 1:1.
Yield 90%
PM 217.27 g/mol ($C_{13}H_{15}NO_2$)
TLC R_f 0.20 (PE:EtOAc 3:1) UV+Hanessian stain
^{1}H NMR (400 MHz, Chloroform-*d*, 27 °C) δ 7.95 (dd, *J* = 8.3, 4.2 Hz, 2H, Ar), 7.23 (dd, *J* = 8.4, 4.1 Hz, 2H, Ar), 5.10 (m, 1H, CH_2), 5.00 (m, 1H, CH'_2), 3.39 (s, 3H, CH_3N), 2.61 (s, 3H, CH_3CO), 1.82 (s, 3H, CH_3).
^{13}C NMR (100 MHz, Chloroform-*d*, 27 °C) δ 196.8 (C=O), 171.7 (C=O), 148.8 (Cq, Ar), 140.2 (Cq, Ar), 135.0 (Cq, aliphatic), 129.4 (2C, Ar), 125.9 (2C, Ar), 120.1 (1C, CH_2), 37.3 (1C, CH_3N), 26.5 (1C, CH_3CO), 20.1 (1C, CH_3).
The data aligns with the scientific literature[83].

5-acetyl-1,3-dimethyl-3-(3-oxobutyl)indolin-2-one (75)

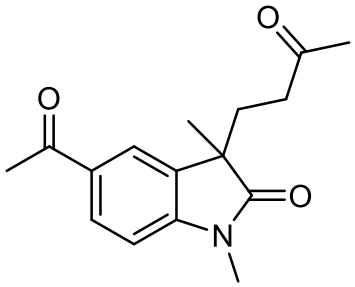

Procedure See general procedure for photoinduced solventylation reactions.
Yield 44%
PM 273.33 g/mol ($C_{16}H_{19}NO_3$)
TLC R_f 0.44 (PE:EtOAc 3:2) UV+Hanessian stain
^{1}H NMR (400 MHz, Chloroform-*d*, 27 °C) δ 7.96 (dd, *J* = 8.2, 1.8 Hz, 1H, Ar), 7.80 (d, *J* = 1.7 Hz, 1H, Ar), 6.91 (d, *J* = 8.2 Hz, 1H, Ar), 3.27 (s, 3H, CH_3N), 2.60 (s, 3H, CH_3CO), 2.28 – 2.02 (m, 4H, CH_2CH_2). 2.01 (s, 3H, CH_3CO), 1.41 (s, 3H, CH_3C).
^{13}C NMR (100 MHz, Chloroform-*d*, 27 °C) δ 207.4 (C=O), 197.0 (C=O), 180.5 (C=O), 147.6 (Cq, Ar), 133.8 (Cq, Ar), 132.4 (Cq, Ar), 130.2 (1C, CH, Ar), 122.7 (1C, CH, Ar), 107.7 (1C, CH, Ar), 47.3 (Cq, aliphatic), 38.5 (1C, CH_2), 31.7 (1C, CH_2), 29.9 (1C, CH_3N), 26.5 (2C, CH_3CO), 23.6 (1C, CH_3).
The data aligns with the scientific literature[84].

5-acetyl-1,3-dimethyl-3-((methylsulfonyl)methyl)indolin-2-one (76)

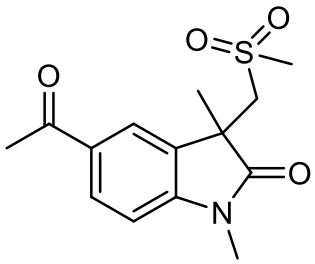

Procedure See general procedure for photoinduced solventylation reactions.
Yield 15%
PM 295.35 g/mol ($C_{14}H_{17}NO_4S$)
TLC R_f 0.04 (PE:EtOAc 3:2) UV+Hanessian stain
^{1}H NMR (400 MHz, Chloroform-*d*, 27 °C) δ 8.03 – 7.97 (m, 2H Ar), 6.96 (dd, *J* = 8.7, 3.3 Hz, 1H, Ar), 3.77 (d, *J* = 14.7 Hz, 1H, CH_2), 3.64 (d, *J* = 14.7 Hz, 1H, CH'_2), 3.31 (s, 3H, CH_3N), 2.69 (s, 3H, CH_3SO_2), 2.61 (s, 3H, CH_3CO), 1.48 (s, 3H, CH_3C).
^{13}C NMR (100 MHz, Chloroform-*d*, 27 °C) δ 196.8 (C=O), 178.3 (C=O), 147.8 (Cq, Ar), 132.3 (Cq, Ar), 131.1 (1C, Ar), 130.8 (Cq, Ar), 123.4 (1C, Ar), 108.4 (1C, Ar), 60.6 (1C, CH_2SO_2), 45.5 (Cq, aliphatic), 43.6 (1C, CH_3SO_2), 27.0 (1C, CH_3N), 26.5 (1C, CH_3CO), 25.2 (1C, CH_3).

N-benzyl-N-phenylmethacrylamide (77)

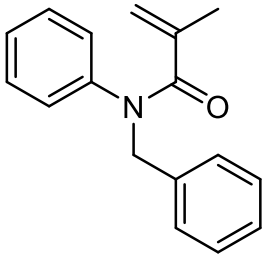

Procedure The N-phenylmethacrylamide **89** (1.24 mmol, 1 eq.) obtained was weighed in a flask. Under an inert atmosphere, DMF (0.2M, 5 mL) was added, with NaH (60%, 1.62 mmol, 1.3 eq.) introduced in portions at 0°C, resulting in a yellow solution. The mixture was stirred for 10 minutes at 0°C and then allowed to reach room temperature for an additional 10 minutes, yielding a yellow turbid solution. After 20 minutes, benzyl bromide (1.74 mmol, 1.4 eq.) was added at 0°C, and the reaction proceeded at room temperature overnight. Monitoring via TLC (ETP:EtOAc 3:1) confirmed the reaction progress. Subsequently, water was introduced to the reaction mixture, and the organic phase underwent extraction with ethyl acetate (EtOAc) three times (20 mL in total). The organic phase was washed with lithium chloride and brine five times until no DMF was observed via TLC. Each aqueous layer was further extracted with EtOAc (25 mL in total). The combined organic layers were dried over anhydrous sodium sulfate, evaporated under

reduced pressure, and subjected to purification by FC using eluents from PE:EtOAc 3:1 to PE:EtOAc 3:1. The compound obtained is known, and it synthesis aligns with established procedures found in the literature.

Yield 75%

PM 251.33 g/mol ($C_{17}H_{17}NO$)

TLC R_f 0.28 (PE:EtOAc 3:1) UV+Hanessian stain

^{1}H NMR (400 MHz, Chloroform-*d*, 27 °C) δ 7.32 – 7.16 (m, 8H, Ar), 6.97 (d, *J* = 7.0 Hz, 2H, Ar), 5.03 (d, *J* = 8.6 Hz, 2H, CH_2), 4.97 (s, 2H, CH_2), 1.78 (s, 3H, CH_3).

^{13}C NMR (100 MHz, Chloroform-*d*, 27 °C) δ 172.0 (C=O), 143.3 (Cq, Ar), 140.8 (Cq, Ar), 137.6 (Cq, aliphatic), 129.1 (2C, CH, Ar), 128.5 (4C, CH, Ar), 127.6 (2C, CH, Ar), 127.4 (1C, CH, Ar), 127.2 (1C, CH, Ar), 119.6 (1C, CH_2), 53.2 (1C, CH_2N), 20.5 (1C, CH_3).

The data aligns with the scientific literature[86].

1-benzyl-3-methyl-3-(3-oxobutyl)indolin-2-one (78)

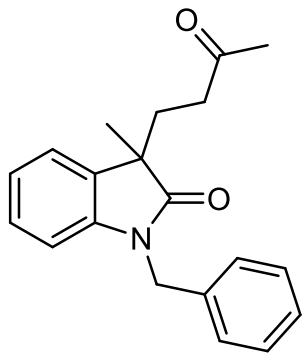

Procedure See general procedure for photoinduced solventylation reactions.

Yield 41%

PM 307.39 g/mol ($C_{20}H_{21}NO_2$)

TLC R_f 0.35 (PE:EtOAc 1:1) UV+Hanessian stain

^{1}H NMR (400 MHz, Chloroform-*d*, 27 °C) δ 7.37 – 7.22 (m, 5H, CH, Ar), 7.22 – 7.13 (m, 2H, CH, Ar), 7.04 (m, 1H, CH, Ar), 6.78 (d, *J* = 7.5 Hz, 1H, CH, Ar), 4.92 (dd, *J* = 23.3, 15.7 Hz, CH_2), 2.29 – 1.96 (m, 4H), 1.95 (s, 3H, CH_3C) 1.43 (s, 3H, CH_3).

^{13}C NMR (100 MHz, Chloroform-*d*, 27 °C) δ 207.8 (C=O), 180.3 (C=O), 142.3 (Cq, Ar), 136.2 (Cq, Ar), 133.3 (Cq, Ar), 128.9 (2C, CH, Ar), 128.0 (1C, CH, Ar), 127.8 (2C, CH, Ar), 127.5 (1C, CH, Ar), 122.9 (1C, CH, Ar), 122.8 (1C, CH, Ar), 109.2 (1C, CH, Ar), 47.4 (Cq, aliphatic), 43.7 (1C, CH_2), 38.7 (1C, CH_2), 31.9 (1C, CH_2), 30.0 (1C, CH_3), 24.0 (1C, CH_3).

The data aligns with the scientific literature[87].

3-(1-benzyl-3-methyl-2-oxoindolin-3-yl)propanenitrile (79)

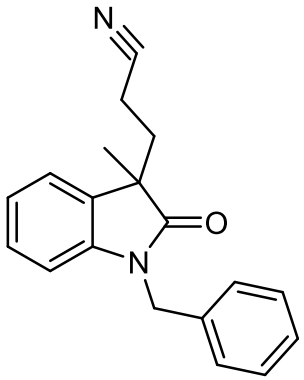

Procedure See general procedure for photoinduced solventylation reactions.
Yield 53%
PM 290.37 g/mol ($C_{19}H_{18}N_2O$)
TLC R_f 0.35 (PE:EtOAc 1:1) UV+Hanessian stain
^{1}H NMR (400 MHz, Chloroform-*d*, 27 °C) δ 7.36 – 7.25 (m, 5H, Ar), 7.21 (m, 2H, Ar), 7.08 (m, Hz, 1H, Ar), 6.80 (d, *J* = 7.5 Hz, 1H, Ar), 4.91 (dd, *J* = 22.1, 15.6 Hz, 2H, CH_2), 2.44 – 2.33 (m, 1H), 2.20 – 1.94 (m, 3H), 1.46 (s, 3H, CH_3).
^{13}C NMR (100 MHz, Chloroform-*d*, 27 °C) δ 179.14 (C=O), 142.3 (Cq, Ar), 135.8 (Cq, Ar), 131.7 (Cq, Ar), 129.0 (2C, CH, Ar), 128.7 (1C, CH, Ar), 127.9 (1C, CH, Ar), 127.4 (2C, CH, Ar), 123.2 (1C, CH, Ar), 122.8 (1C, CH, Ar), 119.0 (Cq, CN), 109.6 (1C, CH, Ar), 47.4 (Cq, aliphatic), 43.9 (1C, CH_2), 33.6 (1C, CH_2), 23.9 (1C, CH_3), 13.0 (1C, CH_2). The data aligns with the scientific literature[72].

1-benzyl-3-(2,2-dichloroethyl)-3-methylindolin-2-one (80)

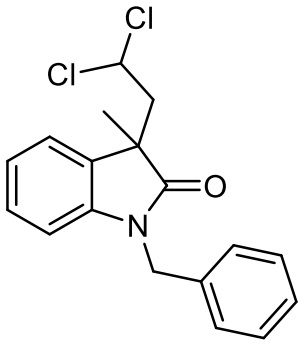

Procedure See general procedure for photoinduced solventylation reactions.
Yield 54%
PM 334.07 g/mol ($C_{18}H_{17}Cl_2NO$)
TLC R_f 0.89 (PE:EtOAc 3:2) UV+Hanessian stain
^{1}H NMR (400 MHz, Chloroform-*d*, 27 °C) δ 7.35 – 7.17 (m, 7H, CH, Ar), 7.07 (m, 1H, CH, Ar), 6.79 (dd, *J* = 8.2, 1.0 Hz, 1H, CH, Ar), 5.45 (dd, *J* = 9.0, 4.4 Hz, 1H, $CHCl_2$),

5.01 (d, *J* = 15.5 Hz, 1H, CH_2), 4.81 (d, *J* = 15.5 Hz, 1H, CH'_2), 3.10 (dd, *J* = 14.8, 9.0 Hz, 1H,CH_2), 2.76 (dd, *J* = 14.8, 4.4 Hz, 1H, CH'_2), 1.45 (s, 3H, CH_3).
^{13}C NMR (100 MHz, Chloroform-*d*, 27 °C) δ 179.2 (C=O), 142.7 (Cq, Ar), 135.8 (Cq, Ar), 131.2 (Cq, Ar), 128.8 (2C, CH, Ar), 128.6 (1C, CH, Ar), 127.8 (1C, CH, Ar), 127.6 (2C, CH, Ar), 122.8 (2C, CH, Ar), 109.8 (1C, CH, Ar), 69.7 (1C, $CHCl_2$), 50.0 (1C, CH_2), 47.3 (Cq, aliphatic), 44.2 (1C, CH_2), 26.2 (1C, CH_3).
The data aligns with the scientific literature[73].

1-benzyl-3-methyl-3-(2,2,2-trichloroethyl)indolin-2-one (81)

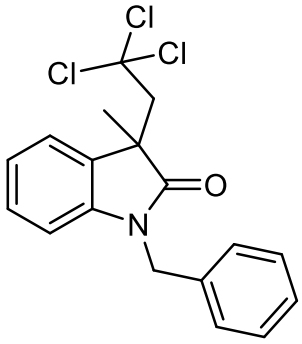

Procedure See general procedure for photoinduced solventylation reactions.
Yield 70%
PM 368.68 g/mol ($C_{18}H_{16}Cl_3NO$)
TLC R_f 0.80 (PE:EtOAc 3:2) UV+Hanessian stain
^{1}H NMR (400 MHz, Chloroform-*d*, 27 °C) δ 7.39 – 7.16 (m, 7H, Ar), 7.03 (m, 1H, Ar), 6.82 (d, *J* = 7.8 Hz, 1H, Ar), 4.98 (d, *J* = 15.5 Hz, 1H, CH_2), 4.88 (d, *J* = 15.5 Hz, 1H, CH'_2), 3.75 (d, *J* = 15.3 Hz, 1H, CH_2), 3.38 (d, *J* = 15.3 Hz, 1H, CH'_2), 1.44 (s, 3H, CH_3).
^{13}C NMR (100 MHz, Chloroform-*d*, 27 °C) δ 178.7 (C=O), 142.5 (Cq, Ar), 135.7 (Cq, Ar), 129.7 (Cq, Ar), 128.8 (2C, CH, Ar), 128.4 (1C, CH, Ar), 127.8 (2C, CH, Ar), 127.8 (1C, CH, Ar), 125.9 (1C, CH, Ar), 122.13 (1C, CH, Ar), 109.5 (1C, CH, Ar), 96.2 (Cq, aliphatic), 59.7 (1C, CH_2), 48.1 (Cq, aliphatic), 44.3 (1C, CH_2), 27.6 (1C, CH_3).
The data aligns with the scientific literature[85].

1-benzyl-3-methyl-3-((methylsulfonyl)methyl)indolin-2-one (82)

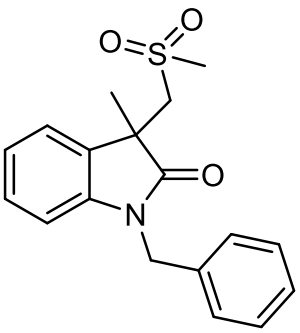

Procedure See general procedure for photoinduced solventylation reactions.
Yield 41%
PM 321.41 g/mol ($C_{18}H_{19}NO_3S$)
TLC R_f 0.21 (PE:EtOAc 1:1) UV+Hanessian stain
^{1}H NMR (400 MHz, Chloroform-*d*, 27 °C) δ 7.39 – 7.27 (m, 6H, CH, Ar), 7.22 (m, 1H, Ar), 7.08 (m, 1H, Ar), 6.77 (d, *J* = 7.8 Hz, 1H, Ar), 5.05 (d, *J* = 15.8 Hz, 1H, CH_2), 4.89 (d, *J* = 15.8 Hz, 1H, CH'_2), 3.78 (dd, *J* = 14.7, 0.9 Hz, 1H, CH_2), 3.62 (d, *J* = 14.7 Hz, 1H, CH'_2), 2.66 (s, 3H, CH_3SO_2), 1.52 (s, 3H, CH_3).
^{13}C NMR (100 MHz, Chloroform-*d*, 27 °C) δ 177.9 (C=O), 142.6 (Cq, Ar), 135.7 (Cq, Ar), 130.3 (Cq, Ar), 129.1 (1C, CH, Ar), 128.9 (2C, CH, Ar), 127.8 (1C, CH, Ar), 127.4 (2C, CH, Ar), 123.6 (1C, CH, Ar), 122.8 (1C, CH, Ar), 110.1 (1C, CH, Ar), 60.6 (1C, CH_2), 45.8 (Cq, aliphatic), 44.3 (1C, CH_2), 43.4 (1C, CH_2), 25.8 (1C, CH_3).

4.2.5 Experimental Data of the Synthesis of the Acrylamides Employed for the Synthesis of the Radical Traps

N-(4-methoxyphenyl)methacrylamide (87)

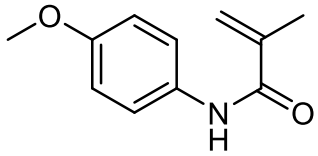

Procedure In the initial synthetic step, commercially available methacrylic acid (7.56 mmol, 1 eq) and dry DCM (0.3M, 25 mL) were combined in a flask under an inert atmosphere. Subsequently, commercially available oxalyl chloride (8.32 mmol, 1.1 eq.) was added to the flask at 0 °C, and six drops of DMF were added as a catalyst. The reaction proceeded for 2h, and the resulting crude product was concentrated in a rotary evaporator, yielding methacryloyl chloride with a yellow oil appearance.
For the second synthetic step, 4-methoxyaniline (5.97 mmol, 1 eq.) was dissolved in dry DCM (8 mL) under an inert atmosphere and cooled to 0 °C. Triethylamine (7.16 mmol, 1.2 eq.) was added, followed by the dropwise addition of the methacryloyl chloride obtained (7.16 mmol, 1.2 eq), assisted by dry DCM (8 mL) 0.4M. The reaction was left overnight, resulting in a light brown solution. The solution was treated with $NaHCO_3$ (20 mL) and extracted with DCM (3 extractions with 25 mL each). The combined organic phases underwent washing with 2N HCl (2 times with 20 mL each), water (2 times with 20 mL each), and brine (2 times with 15 mL each). The obtained organic phases were dried over Na_2SO_4, and volatiles were removed using a rotary evaporator. Purification by FC with eluent ETP/EtOAc 3:4 resulted in N-(4-methoxyphenyl)methacrylamide. This was used for the synthes of the radical trap **60**. all compounds in the synthesis are known, and their synthesis aligns with established procedures found in the literature[88].
Yield 63%
PM 191.23 g/mol ($C_{11}H_{13}NO_2$)

TLC R_f 0.31 (PE:EtOAc 3:1) UV+Hanessian stain
^{1}H NMR (400 MHz, Chloroform-*d*, 27 °C) δ 7.46 (dd, *J* = 9.0, 3.4 Hz, 2H, Ar), 7.38 (sb, NH), 6.88 (dd, *J* = 9.0, 3.4 Hz, 2H, Ar), 5.78 (m, 1H, CH_2), 5.44 (m, 1H, CH'_2), 3.80 (s, 3H, CH_3O), 2.06 (s, 3H, CH_3).
The data aligns with the scientific literature[88].

N-(4-acetylphenyl)methacrylamide (88)

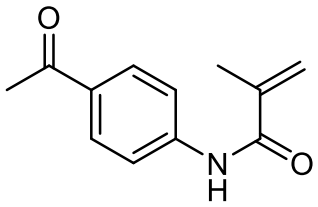

Procedure In the initial synthetic step, commercially available methacrylic acid (10 mmol, 1 eq) and dry DCM (0.4M, 25 mL) were combined in a flask under an inert atmosphere. Subsequently, commercially available oxalyl chloride (11 mmol, 1.1 eq.) was added to the flask at 0 °C, and six drops of DMF were added as a catalyst. The reaction proceeded for 2h, and the resulting crude product was concentrated in a rotary evaporator, yielding methacryloyl chloride with a yellow oil appearance.
For the second synthetic step, *p*-anisidine (4.15 mmol, 1 eq.) was dissolved in dry DCM (8 mL) under an inert atmosphere and cooled to 0 °C. Triethylamine (5.0 mmol, 1.2 eq.) was added, followed by the dropwise addition of the methacryloyl chloride (10 mmol, 1.2 eq), assisted by dry DCM (8 mL) 0.2M. The reaction was left overnight, resulting in a light brown solution. The solution was treated with $NaHCO_3$ (20 mL) and extracted with DCM (3 extractions with 25 mL each). The combined organic phases underwent washing with 2N HCl (2 times with 20 mL each), water (2 times with 20 mL each), and brine (2 times with 15 mL each). The obtained organic phases were dried over Na_2SO_4, and volatiles were removed using a rotary evaporator. Purification by FC with eluent ETP/EtOAc 3:1 resulted in N-(4-acetylphenyl)methacrylamide. This was used for the synthesis of the radical trap **67**. all compounds in the synthesis are known, and their synthesis aligns with established procedures found in the literature.
Yield 40%
PM 203.24 g/mol ($C_{12}H_{13}NO_2$)
TLC R_f 0.20 (PE:EtOAc 3:1) UV+Hanessian stain
^{1}H NMR (400 MHz, Chloroform-*d*, 27 °C) δ 7.96 (d, *J* = 8.3 Hz, 2H, Ar), 7.68 (d, *J* = 8.3 Hz, 2H, Ar), 5.82 (m, 1H, CH_2), 5.53 (m, 1H, CH'_2), 2.59 (s, 3H, CH_3O), 2.08 (s, 3H, CH_3).
The data aligns with the scientific literature[89].

N-phenylmethacrylamide (89)

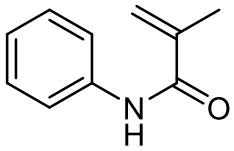

Procedure In the initial synthetic step, commercially available methacrylic acid (7.56 mmol, 1 eq.) and dry DCM (0.3M, 25 mL) were combined in a flask under an inert atmosphere. Subsequently, commercially available oxalyl chloride (8.32 mmol, 1.1 eq.) was added to the flask at 0 °C, and six drops of DMF were added as a catalyst. The reaction proceeded for 2h, and the resulting crude product was concentrated in a rotary evaporator, yielding methacryloyl chloride with a yellow oil appearance.
For the second synthetic step, aniline (6.30 mmol, 1 eq.) was dissolved in dry DCM (8 mL) under an inert atmosphere and cooled to 0 °C. Triethylamine (7.56 mmol, 1.2 eq.) was added, followed by the dropwise addition of the methacryloyl chloride obtained (7.56 mmol, 1.2 eq.), assisted by dry DCM (8 mL) in total 16 mL 0.4M. The reaction was left overnight, resulting in a light brown solution. The solution was treated with $NaHCO_3$ (20 mL) and extracted with DCM (3 extractions with 25 mL each). The combined organic phases underwent washing with 2N HCl (2 times with 20 mL each), water (2 times with 20 mL each), and brine (2 times with 15 mL each). The obtained organic phases were dried over Na_2SO_4, and volatiles were removed using a rotary evaporator. Purification by FC with eluent ETP/EtOAc resulted in N-phenylmethacrylamide. This was used for the synthesis of the radical trap **70**. all compounds in the synthesis are known, and their synthesis aligns with established procedures found in the literature[90].
Yield 70%
PM 161.20 g/mol ($C_{10}H_{11}NO$)
TLC R_f 0.50 (PE:EtOAc 3:1) UV+Hanessian stain
^{1}H NMR (400 MHz, Chloroform-*d*, 27 °C) δ 7.78 (bs, NH), 7.56 (m, 2H, Ar), 7.31 (t, *J* = 7.4 Hz, 2H, Ar), 7.10 (d, *J* = 7.1 Hz, 1H, Ar), 5.77 (m, 1H, CH_2), 5.42 (m, 1H', CH'_2), 2.03 (s, 3H, CH_3).
The data aligns with the scientific literature [90].

5. Abbreviations

HAT	Hydrogen Atom Transfer
Hz	Hertz
LEDs	Light-Emitting Diodes
Cpd I	Compound I
PCET	Proton Coupled Electron Transfer
cPCET	Concerted Proton Coupled Electron Transfer
VB	Valence Bond
BDE	Bond Dissociation Energy
PCA	Principal Component Analysis
SET	Single Electron Transfer
TS	Transitional State
PRC	Polarity Reversal Catalysis
TBADT	TetraButylAmmonium DecaTungstate
XAT	Halogen Atom Transfer
SOMO	Singly Occupied Molecular Orbital
ISC	InterSystem Crossing
FC	Flash Chromatography
qH^1NMR	Quantitatively Proton Nuclear Magnetic Resonance
MeCN	Acetonitrile
TLC	Thin Layer Chromatography
DCM	Dichloromethane
H^1NMR	Proton Nuclear Magnetic Resonance
GC-MS	Gas Chromatography-Mass Spectrometry
PE	Petroleum Ether
EtOAc	Ethyl Acetate
UV	Ultraviolet Light
Et_2O	Diethyl Ether
DMF	Dimethylformamide
NaH	Sodium Hydride

6. References

1. Neville, J. J., Palmieri, T. & Young, A. R. Physical Determinants of Vitamin D Photosynthesis: A Review. *JBMR Plus* **5**, (2021).
2. Roth, H. D. The Beginnings of Organic Photochemistry. *Angewandte Chemie International Edition in English* **28**, 1193–1207 (1989).
3. Hermann Trommsdorff. Ueber Santonin. *Ann. der Pharm.* **11**, 190–207 (1834).
4. Giacomo Ciamician, P. S. Chemische Lichtwirkungen. *Berichte der deutschen chemischen Gesellschaft* **41**, 1928–1935 (1901).
5. Skoog, D. A. ; W. D. M. ; H. F. J. ; C. S. R. *Fundamentals of Analytical Chemistry*. (2014).
6. Percuoco, R. Plain Radiographic Imaging. in *Clinical Imaging: With Skeletal, Chest, & Abdominal Pattern Differentials: Third Edition* 1–43 (Elsevier Inc., 2013).
7. Bonfield, H. E. *et al.* Photons as a 21st Century Reagent. *Nat Commun* **11**, (2020).
8. Schweizer, T., Kubach, H. & Koch, T. Investigations to Characterize the Interactions of Light Radiation, Engine Operating Media and Fluorescence Tracers for the Use of Qualitative Light-Induced Fluorescence in Engine Systems. *Automotive and Engine Technology* **6**, 275–287 (2021).
9. Qiu, D., Lian, C., Mao, J., Fagnoni, M. & Protti, S. Dyedauxiliary Groups, an Emerging Approach in Organic Chemistry. The Case of Arylazo Sulfones. *Journal of Organic Chemistry* **85**, 12813–12822 (2020).
10. Kärkäs, M. D., Porco, J. A. & Stephenson, C. R. J. Photochemical Approaches to Complex Chemotypes: Applications in Natural Product Synthesis. *Chem Rev* **116**, 9683–9747 (2016).
11. Shaw, M. H., Twilton, J. & MacMillan, D. W. C. Photoredox Catalysis in Organic Chemistry. *Journal of Organic Chemistry* **81**, 6898–6926 (2016).
12. Tavakolian, M. & Hosseini-Sarvari, M. Catalyst-Free Organic Transformations under Visible-Light. *ACS Sustain Chem Eng* **9**, 4296–4323 (2021).
13. Darcy, J. W., Koronkiewicz, B., Parada, G. A. & Mayer, J. M. A Continuum of Proton-Coupled Electron Transfer Reactivity. *Acc Chem Res* **51**, 2391–2399 (2018).
14. Capaldo, L. & Ravelli, D. Hydrogen Atom Transfer (HAT): A Versatile Strategy for Substrate Activation in Photocatalyzed Organic Synthesis. *European J Org Chem* **2017**, 2056–2071 (2017).
15. Ji, L. & Schüürmann, G. Model and Mechanism: N-hydroxylation of Primary Aromatic Amines by Cytochrome P450. *Angewandte Chemie - International Edition* **52**, 744–748 (2013).
16. Ortiz De Montellano, P. R. Hydrocarbon Hydroxylation by Cytochrome P450 Enzymes. *Chem Rev* **110**, 932–948 (2010).

17. Guengerich, F. P. Common and Uncommon Cytochrome P450 Reactions Related to Metabolism and Chemical Toxicity. *Chem Res Toxicol* **14**, 611–650 (2001).
18. Lai, W., Li, C., Chen, H. & Shaik, S. Hydrogen-Abstraction Reactivity Patterns from A to Y: The Valence Bond Way. *Angewandte Chemie - International Edition* **51**, 5556–5578 (2012).
19. Usharani, D., C. Lacy, D., S. Borovik, A. & Shaik, S. Dichotomous Hydrogen Atom Transfer vs Proton-Coupled Electron Transfer During Activation of X–H Bonds (X = C, N, O) by Nonheme Iron–Oxo Complexes of Variable Basicity. *J Am Chem Soc* **135**, 17090–17104 (2013).
20. Hammes-Schiffer, S. & Soudackov, A. V. Proton-coupled Electron Transfer in Solution, Proteins, and Electrochemistry. *Journal of Physical Chemistry B* **112**, 14108–14123 (2008).
21. Capaldo, L., Quadri, L. L. & Ravelli, D. Photocatalytic Hydrogen Atom Transfer: The Philosopher's Stone for Late-Stage Functionalization? *Green Chemistry* **22**, 3376–3396 (2020).
22. Capaldo, L., Ravelli, D. & Fagnoni, M. Direct Photocatalyzed Hydrogen Atom Transfer (HAT) for Aliphatic C-H Bonds Elaboration. *Chem Rev* **122**, 1875–1924 (2022).
23. Goldman, A. S. & Goldberg, K. I. *Organometallic C-H Bond Activation: An Introduction*. vol. 885 (2004).
24. Sambiagio, C. *et al.* A comprehensive Overview of Directing Groups Applied in Metal-Catalysed C-H Functionalisation Chemistry. *Chem Soc Rev* **47**, 6603–6743 (2018).
25. Cernak, T., Dykstra, K. D., Tyagarajan, S., Vachal, P. & Krska, S. W. The Medicinal Chemist's Toolbox for Late Stage Functionalization of Drug-Like Molecules. *Chem Soc Rev* **45**, 546–576 (2016).
26. Eyring, H., Evans, M. G. & Polanyi, M. Inertia and Driving Force of Chemical Reactions. *Trans. Faraday Soc.* **34**, 11–24 (1938).
27. M. Mayer, J. Understanding Hydrogen Atom Transfer: From Bond Strengths to Marcus Theory. *Acc Chem Res* **44**, 36–46 (2010).
28. Shaik, S., Kumar, D. & De Visser, S. P. A Valence Bond Modeling of Trends in Hydrogen Abstraction Barriers and Transition States of Hydroxylation Reactions Catalyzed by Cytochrome P450 Enzymes. *J Am Chem Soc* **130**, 10128–10140 (2008).
29. Luo & Yu-Ran. *Comprehensive Handbook of Chemical Bond Energies*. (CRC press, 2007).
30. K. Ingold, C. Principles of an Electronic Theory of Organic Reactions. *Chem Rev* **15**, 225–274 (2002).
31. Parsaee, F. *et al.* Radical philicity and its Role in Selective Organic Transformations. *Nat Rev Chem* **5**, 486–499 (2021).
32. De Vleeschouwer, F., Van Speybroeck, V., Waroquier, M., Geerlings, P. & De Proft, F. Electrophilicity and Nucleophilicity Index for Radicals. *Org Lett* **9**, 2720–2724 (2007).

33. Okada, M. *et al.* Sunlight Photocatalyzed Regioselective β-Alkylation and Acylation of Cyclopentanones. *Chem Sci* **5**, 2893–2898 (2014).
34. Le, C., Liang, Y., Evans, R. W., Li, X. & MacMillan, D. W. C. Selective sp 3 C-H Alkylation Via Polarity-Match-Based Cross-Coupling. *Nature* **547**, 79–83 (2017).
35. Cole, S. J., Kirwan, J. N., Roberts, B. P. & Willis, C. R. Radical Chain Reduction of Alkyl Halides, Dialkyl Sulphides and 0-Alkyl S-Methyl Dithiocarbonates t o Alkanes by Trialkylsilanes. *J. Chem. Soc. Perkin Trans* **1**, 103–112 (1991).
36. Peter Griess. Ueber eine neue Klasse organischer Verbindungen, in denen Wasserstoff durch Stickstoff vertreten ist. *Annalen der chemie und pharmacie* **137**, (1866).
37. Traugott Sandmeyer. Ueber die Ersetzung der Amidgruppe durch Chlor in den aromatischen Substanzen. **17**, 1633–1635 (1884).
38. Robert Pschorr. Neue Synthese des Phenanthrens und seiner Derivate. *Mittheilungen* **29**, 496–501 (1896).
39. Gomberg, M. & Bachmann, W. E. The Synthesis of Biaryl Compounds by Means of the Diazo Reaction. *J. Am. Chem. Soc* **46**, 2339–2343 (1924).
40. Meerwein Mitarb Aromatische Diazoverbindungen usw, H., Hans Meerwein, V., Biiohner, E. & van Emster, K. Uber die Einwirkung aromatischer Diazoverbindungen aaf a, p-unges'eittigte Carbonylverbindungen l). *dtsch. chem. Ges* **47**, 2274 (1914).
41. Pratsch, G. & Heinrich, M. R. Modern Developments in Aryl Radical Chemistry. *Top Curr Chem* **320**, 33–59 (2012).
42. Bugaenko, D. I., Volkov, A. A., Karchava, A. V. & Yurovskaya, M. A. Generation of Aryl Radicals by Redox Processes. Recent Progress in the Arylation Methodology. *Russian Chemical Reviews* **90**, 116–170 (2021).
43. Albini, A. & Fagnoni, M. Green Chemistry and Photochemistry were Born at the Same Time. *Green Chemistry* **6**, 1–6 (2004).
44. Albini, A. & Fagnoni, M. *Handbook of Synthetic Photochemistry*. (2009).
45. Zarei, A., Hajipour, A. R., Khazdooz, L. & Aghaei, H. Fast, Efficient, and Convenient Method for the Preparation of Arylazo Aryl Sulfones Using Stable Aryldiazonium Silica Sulfates Under Mild Conditions. *Synlett* **2010**, 1201–1204 (2009).
46. Liu, J. B., Chen, F. J., Liu, E., Li, J. H. & Qiu, G. Copper-Catalyzed Synthesis of Aryldiazo Sulfones from Arylhydrazines and Sulfonyl Chlorides under Mild Conditions. *New Journal of Chemistry* **39**, 7773–7776 (2015).
47. Rosenthal, D. J., Overbergek G, Arnold Rosextiixl, B. J. & Overberger, C. G. Azo Compounds. XXXII.l Kinetics of the Thermal Decomposition of Phenylphenylsulfonyl Diimide. *J. Am. Chem. Soc* **82**, 108–117 (1960).
48. Kamigata, N. & Kobayashi, M. Azosulfones: Versatile Precursors for Aryl Radicals, Aryl Cations, Aryl Anions, Carbenes, and Benzynes. *Sulfur reports* **2**, 87–128 (1982).

49. Müller, C. & Jacobson, K. A. Xanthines as Adenosine Receptor Antagonists. *Handb Exp Pharmacol* **200**, 99–151 (2011).
50. Capurro, P. *et al.* Visible-Light-Driven Solventylation Strategy for Olefin Functionalization. *ACS Omega* **7**, 48564–48571 (2022).
51. Crespi, S. & Fagnoni, M. Generation of Alkyl Radicals: From the Tyranny of Tin to the Photon Democracy. *Chem Rev* **120**, 9790–9833 (2020).
52. Sarkar, S., Cheung, K. P. S. & Gevorgyan, V. C-H Functionalization Reactions Enabled by Hydrogen Atom Transfer to Carbon-Centered Radicals. *Chem Sci* **11**, 12974–12993 (2020).
53. Yu, Y., Zhuang, S., Liu, P. & Sun, P. Cyanomethylation and Cyclization of Aryl Alkynoates with Acetonitrile under Transition-Metal-Free Conditions: Synthesis of 3-Cyanomethylated Coumarins. *Journal of Organic Chemistry* **81**, 11489–11495 (2016).
54. Lu, P. H. *et al.* Coumarin Derivatives Inhibit ADP-Induced Platelet Activation and Aggregation. *Molecules* **27**, (2022).
55. Li, X. *et al.* Cascade Arylalkylation of Activated Alkenes: Synthesis of Chloro- and Cyano-Containing Oxindoles. *Journal of Organic Chemistry* **80**, 2621–2626 (2015).
56. Singh, G. S. & Desta, Z. Y. Isatins as Privileged Molecules in Design and Synthesis of Spiro-Fused Cyclic Frameworks. *Chem Rev* **112**, 6104–6155 (2012).
57. Zhao, Y. *et al.* Microwave-Assisted Copper-Catalyzed Oxidative Cyclization of Acrylamides with Non-Activated Ketones. *Chemistry - A European Journal* **22**, 5878–5882 (2016).
58. Li, Z., Zhang, Y., Zhang, L. & Liu, Z. Q. Free-radical cascade Alkylarylation of Alkenes with simple Alkanes: Highly efficient access to Oxindoles via selective (sp3)C-H and (sp 2)C-H Bond functionalization. *Org Lett* **16**, 382–385 (2014).
59. Anselmo, M., Basso, A., Protti, S. & Ravelli, D. Photoredox-Catalyzed Generation of Acetonyl Radical in Flow: Theoretical Investigation and Synthetic Applications. *ACS Catal* **9**, 2493–2500 (2019).
60. Anselmo, M. *et al.* Photocatalyzed Synthesis of Ssochromanones and Isobenzofuranones under Batch and Flow Conditions. *Beilstein Journal of Organic Chemistry* **13**, 1456–1462 (2017).
61. Huang, A., Kodanko, J. J. & Overman, L. E. Asymmetric Synthesis of Pyrrolidinoindolines. Application for the Practical Total Synthesis of (-)-Phenserine. *J Am Chem Soc* **126**, 14043–14053 (2004).
62. Hell, S. M. *et al.* Hydrosulfonylation of Alkenes with Sulfonyl Chlorides under Visible Light Activation. *Angewandte Chemie - International Edition* **59**, 11620–11626 (2020).
63. Mandal, S., Bera, T., Dubey, G., Saha, J. & Laha, J. K. Uses of K2S2O8 in Metal-Catalyzed and Metal-Free Oxidative Transformations. *ACS Catal* **8**, 5085–5144 (2018).

64. Dogliotti, L. & Hayon, E. Flash Photolysis of Persulfate Ions in Aqueous Solutions. Study of the Sulfate and Ozonide Radical Anions. *J. Phys. Chem* **71**, 2511–2516 (1967).
65. Gao, Y. qiong, Gao, N. yun, Deng, Y., Yang, Y. qiong & Ma, Y. Ultraviolet (UV) Light-Activated Persulfate Oxidation of Sulfamethazine in Water. *Chemical Engineering Journal* **195–196**, 248–253 (2012).
66. Chen, F., Wan, J., Guan, C., Yang, J. & Zhang, H. Tetrabutylammonium peroxydisulfate in organic synthesis; III1. An efficient procedure for the selective oxidation of sulfides to sulfoxides by tetrabutylammonium peroxydisulfate. *Synth Commun* **26**, 253–260 (1996).
67. Tokmakov, I. V., Kim, G. S., Kislov, V. V., Mebel, A. M. & Lin, M. C. The Reaction of Phenyl Radical with Molecular Oxygen: A G2M Study of the Potential Energy Surface. *Journal of Physical Chemistry A* **109**, 6114–6127 (2005).
68. Hui, C., Wang, S. & Xu, C. Dinitrogen Extrusion from Diazene in Organic Synthesis. *Chinese Chemical Letters* **33**, 3695–3700 (2022).
69. Engel, P. S., Hayes, L. R. A., Keifer, L. L., Szilagyi, S. & Timberlake, J. W. Extrusion of Nitrogen from Cyclic and Bicyclic Azo Compounds. *J Am Chem Soc* **100**, (1978).
70. Liu, J. *et al.* Metal-Free Synthesis of Unsymmetrical Aryl Selenides and Tellurides via Visible Light-Driven Activation of Arylazo Sulfones. *European J Org Chem* **2020**, 7358–7367 (2020).
71. Wang, H., Guo, L. N. & Duan, X. H. Silver-Catalyzed Oxidative Coupling/Cyclization of Acrylamides with 1,3-Dicarbonyl Compounds. *Chemical Communications* **49**, 10370–10372 (2013).
72. Li, J., Wang, Z., Wu, N., Gao, G. & You, J. Radical Cascade Cyanomethylation of Activated Alkenes to Construct Cyanomethylation of Activated Alkenes to Construct Cyano Substituted Oxindoles. *Chem. Commun.* **50**, 15049–150151 (2014).
73. Dai, Y., Cui, M., Li, X., Chen, H. & Xu, X. Polychlorinated Alkylation Annulation of N-arylacrylamide Under Electrochemical Conditions. *New. J. Chem.* **47**, 5780–5785 (2023).
74. Shen, T., Yuan, Y., Song, S. & Jiao, N. Iron-Catalyzed Aerobic Difunctionalization of Alkenes: a Highly Efficient Approach to Construct Oxindoles by C–S and C–C Bond Formation. *Chem. Commun.* **50**, 4115–4118 (2014).
75. Jiang, Y.-Q. *et al.* Ethylene Glycol: A Green Solvent for Visible Light-Promoted Aerobic Transition Metal-Free Cascade Sulfonation/Cyclization Reaction. *Adnvanced Synthesis & Catalysis* **365**, 2609–2614 (2020).
76. Ito, M., Tanaka, A., Higuchi, K. & Sugiyama, S. Rhodium(II)-Catalyzed Synthesis of N-Aryl-N′-tosyldiazenes from Primary Aromatic Amines Using (Tosylimino)aryliodinane: A Potent Stable Surrogate for Diazonium Salts. *European J Org Chem* **2017**, 1272–1276 (2017).

77. Wei, W. *et al.* Catalyst-Free Direct Arylsulfonylation of N-Arylacrylamides with Sulfinic Acids: A Convenient and Efficient Route to Sulfonated Oxindoles. *Green Chem* **16**, 2988–2991 (2014).
78. Zhang, J. *et al.* A variation of the Fischer Indolization Involving condensation of Quinone Monoketals and Aliphatic Hydrazines. *Angewandte Chemie - International Edition* **52**, 1753–1757 (2013).
79. Tian, Q., He, P. & Kuang, C. Copper-catalyzed Arylsulfonylation of N-arylsulfonyl-Acrylamides with Arylsulfonohydrazides: Synthesis of Sulfonated Oxindoles. *Org. Biomol. Chem* **12**, 6349–6353 (2014).
80. Bag, S., Ojha, S., Venugopalan, S. & Sahoo, B. Photocatalytic Alkylation/Arylative Cyclization of N-Acrylamides of N-Heteroarenes and Arylamines with Dihydroquinazolinones from Unactivated Ketones. *J. Org. Chem.* **88**, 12121–12130 (2023).
81. Wang, S. *et al.* A Metal-Free Synthesis of Oxindoles by a Radical Addition-Cyclization onto N-arylacrylamides with Xanthates. *Tetrahedron* **71**, 1869–1875 (2015).
82. King, J. F. *et al.* tert-Butyl Cation Formation in the Hydrolysis of 2-Methyl-2-propanesulfonyl Chloride, the Simplest Tertiary Alkanesulfonyl Chloride. *J. Org. Chem.* **60**, 2831–2834 (1995).
83. Fabry, D. C., Stodulski, M., Hoerner, S. & Gulder, T. Metal-Free Synthesis of 3,3-Disubstituted Oxoindoles by Iodine(III)-Catalyzed Bromocarbocyclizations. *Chemistry - A European Journal* **18**, 10834–10838 (2012).
84. Xia, X. F. *et al.* Acid-Catalyzed Cascade Radical Addition/Cyclization of Arylacrylamides with Ketones. *Tetrahedron* **71**, 6099–6103 (2015).
85. Lu, M. Z. & Loh, T. P. Iron-Catalyzed Cascade Carbochloromethylation of Activated Alkenes: Highly Efficient Access to Chloro-Containing Oxindoles. *Org Lett* **16**, 4698–4701 (2014).
86. Sun, X. *et al.* Metal-free Visible-Light-Driven Cascade Cyclization Reaction to Synthesize 2-oxindoles via Benzoyl and Phenylsulfinyl Radicals with Acrylamide Derivatives. *Org. Biomol. Chem.*, **20**, 8042–8048 (2022).
87. Fan, X., Lei, T., Chen, B., Tung, C. H. & Wu, L. Z. Photocatalytic C-C Bond Activation of Oxime Ester for Acyl Radical Generation and Application. *Org Lett* **21**, 4153–4158 (2019).
88. Zhang, J. & Loh, T.-P. Ruthenium-and Rhodium-Catalyzed Cross-Coupling Reaction of Acrylamides with Alkenes: Efficient Access to (Z, E)-Dienamides. *Chem. Commun.* **48**, 11232–11234 (2012).
89. Nishio, T., Koyama, H., Sasaki, D. & Sakamoto, M. A Novel Intramolecular Photocyclization of N-(2-Bromoalkanoyl) Derivatives of 2-Acylanilines via 1,8-Hydrogen Abstraction. *Helv Chim Acta* **88**, 996–1003 (2005).
90. Liu, Z. *et al.* In Silico, Synthesis and Anticancer Evaluation of Benzamide Tryptamine Derivatives as Novel eEF2K Inhibitors. *Bioorg Med Chem Lett* **67**, (2022).